THE EFFECT OF NANOPARTICLES ON THE FUNCTION OF IMMUNE CELLS OF THE SKIN

A thesis submitted in fulfilment of the requirements for the degree of
Doctor of Philosophy

Cenchao Shen

B.Sc. M.Sc.

School of Medical Sciences
College of Science, Engineering and Health
RMIT University

February 2014

Author's Declaration

I certify that except where due acknowledgement has been made, the work is that of the author alone; the work has not been submitted previously, in whole or in part, to qualify for any other academic award; the content of the thesis is the result of work which has been carried out since the official commencement date of the approved research program; any editorial work, paid or unpaid, carried out by a third party is acknowledged; and, ethics procedures and guidelines have been followed.

Cenchao Shen

February 2014

Dedication

To my parents

To my wife

To my friends

I dedicate this work

Acknowledgements

I would like to express my sincere thanks and deepest gratitude to my supervisors Associate Professor Paul Wright and Dr. Bryce Feltis for offering knowledgeable advice on all aspects of academic life and providing the encouragement and intellectual support that made my research possible. Their profound knowledge, rigorous academic style, and innovative spirit will be the model of my life.

I would also like to thank Professor Terence Turney from Monash University, for providing nanoparticles and offering advice on my project. I thank Associate Professor Terry Piva, for the advice on UV radiation and encouragement on my project.

I would like to acknowledge the scholarship provided by the National Health and Medical Research Council (NHMRC), and Advanced Manufacturing Cooperative Research Centre (AMCRC) top-up scholarship. I would also like to acknowledge the fee waiver scholarship for international student tuition fees from the RMIT College of Science, Engineering & Health.

I would like to thank Victoria Coleman and the National Measurement Institute (NMI) for assistance with disc centrifugation assay. I would like to thank Simon James and Bryce Feltis for the assistance of XFM beamline work at the Australian Synchrotron, Victoria, Australia. I would also like to thank Lynne Waddington and Andrew Hastings at the CSIRO for support with the cryo-TEM work. Thanks also to Bryce

Feltis and Mingdeng Luo at Monash University for assistance with ICP-MS. I would like to acknowledge Mindeng Luo for surface modification of ZnO nanoparticles and characterization.

I am very grateful to the other members in the nanosafety research group, Dr Visalini Muthusamy, Dr Andrew Hastings, Dr Abdulkareem Elbaz, Sean O'Keefe, Nikolas Patsikatheodorou, Griffin D'Costa, Christian Aloe, and Mingdeng Luo, whose help within the group made my learning and growing during my graduate education possible.

Publications/Presentations including Research from this Thesis

Refereed papers

Shen C, James SA, deJonge MD, Turney TW, Wright PFA, Feltis BN. Relating cytotoxicity, zinc ions and reactive oxygen in ZnO nanoparticle exposed human immune cells. *Toxicological Sciences*, 2013, 136(1):120 -130.

Shen C, Turney TW, Piva TJ, Feltis BN, Wright PFA. Comparison of UVA-induced ROS and sunscreen nanoparticle-generated ROS in human immune cells. *Photochem. Photobiol. Sci.*, 2014, 13: 781-788.

Luo M, **Shen C**, Feltis BN, James SA, Martin LL, Hughes AE, Wright PFA, Turney TW. Reducing ZnO Nanoparticle Cytotoxicity by Surface Modification. *Nanoscale*, 2014, 6(11):5791-5798.

Book Chapter

Shen C, Zhang Z. An Overview on Nanoparticle-Assisted Polymerase Chain Reaction Technology, in Bio-Nanotechnology: A Revolution in Food, Biomedical and Health Sciences. 2013. Wiley-Blackwell. ISBN: 978-0-470-67037-8.

Refereed Technical Reports

Wright PFA, Feltis BN, Muthusamy V, Patsikatheodorou N, **Shen C**, Hastings A, O'Keefe SJ, Piva TJ, Turney TW. Australian Consortium - RMIT Report for OECD ZnO Nanomaterial Testing using *in vitro* toxicology assays in human cells. OECD WPMN safety testing program for nanomaterials. NANOhub, EU Joint Research Centre, 2012, 18 pages.

Wright PFA, Feltis BN, Muthusamy V, Patsikatheodorou N, **Shen C**, Hastings A, O'Keefe SJ, Piva TJ, Turney TW. Australian Consortium - RMIT Report for OECD Ceria Nanomaterial Testing using *in vitro* toxicology assays in human cells. OECD WPMN safety testing program for nanomaterials. NANOhub, EU Joint Research Centre, 2012, 17 pages.

Conference presentations

As presenter:

Shen C, Wright PFA, Turney TW, Feltis BN. ZnO Nanoparticle-Induced Cytotoxicity Requires Particle-Cell Contact and Intracellular Zinc Ion Release. *Australian Health & Medical Research Congress (AH&MRC)*. Adelaide, Nov., 2012. **(Oral presentation)**

Shen C, Wright PFA, Turney TW, Feltis BN. Induction of Reactive Oxygen Species by Sunscreen Nanoparticles and UVA Radiation and its Effects on Human Immune Cells. *Proceeding of 2011 MEPSA Annual Scientific Meeting*. Brisbane, Nov., 2011. **(Oral presentation)**

As co-author:

Luo M, **Shen C**, Feltis BN, James SA, Martin LL, Hughes AE, Wright PFA, Turney TW. Fate of ZnO nanoparticles in human immune cells: focus on surface chemistry effects. *NANOTOX 2014, 7th International Nanotoxicology Congress.* Antalya, Turkey, Apr., 2014.

Wright PFA, **Shen C**, Turney TW, Feltis BN. Comparison of ROS Generation by UVA and Sunscreen Nanoparticles in Human Immune Cells. *The 2014*

International Conference on Nanoscience and Nanotechnology. Adelaide, Feb., 2014. (Oral presentation)

Wright PFA, Feltis BN, **Shen C**, James SA, Turney TW. Importance of Intracellular Dissolution to the Cytotoxicity of Zinc Oxide Nanoparticles. *6th International Symposium on Nanotechnology, Occupational and Environmental Health.* Oct., 2013 in Nagoya, Japan. (Oral presentation)

Luo M, Turney TW, Martin LL, **Shen C**, Feltis BN, Wright PFA. Probing ZnO Nanoparticle Cytotoxicity Using Tunable Surfaces. *Inorganic Chemistry Symposium.* Melbourne, Nov., 2012. (Poster)

Feltis BN, **Shen C**, Elbaz AK, Turney TW, Wright PFA. Mode of Action of ZnO Nanoparticle Induced Immune Cell Cytotoxicity. *The 2012 International Conference on Nanoscience and Nanotechnology*. Perth, Feb., 2012. (Invited oral presentation)

Muthusamy V, O'Keefe SJ, **Shen C**, Feltis BN, Piva TJ, Turney TW, Wright PFA. In vitro effects of nanoceria in human skin and immune cells. *The 2012 International Conference on Nanoscience and Nanotechnology*. Perth, Feb., 2012. (Poster-ICONN Prize winner)

O'Keefe SJ, **Shen C**, Feltis BN, Turney TW, Piva TJ, Wright PFA. *In Vitro* Cytotoxicity of OECD Zinc Oxide Nanoparticles in Human THP-1 Monocytes and Macrophages. *The 2012 International Conference on Nanoscience and Nanotechnology*. Perth, Feb., 2012. (Poster)

Table of Contents

List of Figures

List of Tables

Abstract

The effect of nanoparticles (NPs) of photoactive zinc and titanium oxides on innate immunity is unknown, despite the advent of new transparent sunscreens containing these nanomaterials. This is particularly important as tissue resident immune cells in the skin are the first point of contact where sunscreen NPs can be actively sequestered by cells. In preparing sunscreen formulations, NPs are also being coated with various surfactants – affecting their solubility, bioavailability and dermal penetration, which may also alter their potential immune effects. Widespread use of such materials in sunscreens is crucial to public health practices to reduce skin cancer in Australia, so their safety needs to be investigated. Therefore, in this project I investigated the effect that these NPs have on the function of cellular elements of the innate immune system, including monocytes, macrophages, and Langerhans cells (LCs). Specific emphasis was placed on the role of intracellular zinc ions, reactive oxygen species (ROS), and altered immune functions following exposure to these NPs.

Although zinc oxide (ZnO) NPs are widely used in sunscreens, the relationship between ROS generation, zinc ion release and the cytotoxicity caused by these particles, is not clearly understood. The first part of this project explored whether these factors could be accurately quantified and related. This study demonstrated a strong correlation between ZnO NP-induced cytotoxicity and free intracellular zinc concentration (R^2=0.945) in human immune cells, indicating a requirement for NP dissolution to precede cytotoxicity. While direct exposure to ZnO NPs was found to induce cytotoxicity at relatively high concentrations, indirect exposure (via dialysis) was not cytotoxic, even at extremely high concentrations – highlighting a requirement

for NP-to-cell contact. The elevated ROS levels present in NP-exposed cells also correlated to both cytotoxicity and intracellular free zinc. Although the addition of antioxidants (ascorbate or α-tocopherol) was able to reduce ROS, cytotoxicity to ZnO NPs was unaffected – this suggested that ROS may be, in part, a result of cytotoxicity rather than solely as a causal factor for cytotoxicity. This study highlights both the requirement and role of the intracellular dissolution of zinc nanomaterials in eliciting a cytotoxic response. Therefore, modification of NP uptake and their intracellular solubility are key components in modulating the bioactivity of ZnO NPs.

The second part of this project compared the ROS generation by UVA and sunscreen NPs in human immune cells. Although it is known that ROS generation occurs in cells exposed to ZnO and TiO_2 NPs, it is unknown to what extent this ROS generation is altered with UVA co-exposure, which is more relevant to actual sunscreen usage. Furthermore, ZnO and TiO_2 NPs in sunscreens themselves attenuate the oxidative damage to cells and tissues from free radicals induced by UVA irradiation. In order to determine the relative hazard potential of UVA co-exposure with nanosunscreen NPs, ROS generation was investigated in human THP-1 monocyte immune cells co-exposed to UVA and NPs. Whilst the applied UVA dose (6.7 J/cm^2) did not affect the viability of THP-1 monocytes, it induced significant ROS production in these cells. However, co-exposure to UVA and NPs generated the same or less ROS than with UVA alone, with the exception of the highly photocatalytic anatase form of TiO_2, which significantly increased ROS levels. This study indicates that ROS generation from nanosunscreens is, in most cases, an insignificant contributor to the overall hazard associated with oxidative stress from UVA exposure itself.

In the third part of this project, the effect of ZnO NPs on the function of LCs was investigated, as these dendritic cells are present in the epidermis and constitute the first immunological barrier against NPs. This study found that ZnO NPs can simultaneously cause pro-inflammatory and anti-inflammatory effects in these antigen presenting cells. In addition, ZnO NPs altered the release of bioactive molecules (cytokines) from immune cells, suppressed antigen processing and presentation, and stimulated lymphocyte proliferation. This study indicates that ZnO NPs may modulate antigen presentation processes that can lead to allergic reactions.

In conclusion, sunscreen ZnO and TiO_2 NPs are well tolerated by skin immune cells, with ZnO only causing cytotoxicity at very high concentrations. Also, ZnO NPs possess immunomodulatory effects that provide further evidence of the mode of action in the therapeutic topical use of zinc.

List of Abbreviations

μXFM	micro X-ray fluorescence microscopy
8-OHdG	8-hydroxydeoxyguanosine
APCs	antigen presenting cells
APTES	3-aminopropyltriethoxysilane
Au	gold
CdTe	cadmium telluride
CeO_2	cerium dioxide
CHS	contact hypersensitivity
CPDs	cyclobutane pyrimidine dimers
cryo-TEM	cryogenic transmission electron microscopy
DCFDA	2-Dichlorofluorescin diacetate
DCs	dendritic cells
DLS	dynamic light scattering
EC_{20}	effective concentration causing 20% response
EC_{50}	effective concentration causing 50% response
ELISA	enzyme-linked immunosorbant assay
FBS	fetal bovine serum
FTIR	Fourier transform infrared
GSH	reduced glutathione
GSSG	oxidised glutathione
GST	glutathione S-transferase
H_2O_2	hydrogen peroxide
HBSS	Hank's Balanced Salt Solution
HCA	high-content screening assay
HO-1	heme oxygenase 1
ICP	inductively coupled plasma
IEP	isoelectric point
IL	interleukin
JNK	Jun Kinase
LCs	Langerhans cells
LPS	lipopolysaccharide

MED	minimal erythemal dose
MHC	major histocompatibility complex
MS	mass spectrometry
ND	nanodiamond
nm	nanometer
NPs	nanoparticles
NQO1	NADPH quinone oxidoreductase 1
Nrf2	Nuclear factor erythroid-2-related factor 2
O_2	dioxygen
$O_2^{\cdot -}$	superoxide radicals
PBS	phosphate buffered saline
PEG	polyethylene glycol
PI	propidium iodide
PMA	phorbol-12-myristate-13-acetate
QDs	quantum dots
ROS	reactive oxygen species
SEM	scanning electron microscopy
SOD	superoxide dismutase
sZnO	surfactant-dispersed form of ZnO
TCM	THP-1 culture media
TEM	transmission electron microscopy
TESPIC	3-(triethoxysilyl) propyl isocyanate
TGA	thermal gravimetric analysis
TiO_2	titanium dioxide
TLR	Toll-like receptor
TNF	tumour necrosis factor
TOF	Time of Flight
Treg	regulatory T cells
UCA	urocanic acid
UV	ultraviolet
XRD	X-ray diffraction
$ZnCl_2$	zinc chloride
ZnO	zinc oxide

Chapter 1. Introduction and Literature Review

1.1 Nanoparticles and Nanotechnology

Nanotechnology is a fast growing field that has the potential to offer significant advances to society. Currently, nanotechnology is widely used in our daily life, such as nanoparticle-based cosmetics, nano-emissive displays, nanofabric clothes, nanoparticle-lined refrigerators, and so on. It is estimated that nanotechnology will become a $1 trillion market by 2015 (Nel *et al*., 2006).

1.1.1 Nanotechnology

Nanotechnology is a technological development at the length scale of between approximately 1 - 100 nanometers (nm), following the definition used by the National Nanotechnology Initiative (NNI) in the USA (NNI, 2013). NPs are often defined as particles having all dimensions that are between 1-100 nm (ISO, 2010).

Materials at the nano-scale can show very different properties compared to the same material at larger scales. For example, gold which is normally chemically inert, can serve as a catalyst of oxidation reactions at the nano-scale (Goodman, 2008). Actually, NPs are not new to us and have been around for a long time. For instance, some NPs are naturally-occurring biological structures like viruses, or chemical by-products, such as those formed in ashes from volcanoes and fires. Other NPs come from man-made processes, such as welding fumes and car exhausts. It is, however, engineered NPs, which are deliberately manufactured to a specific size, shape and structure that have attracted the interest of scientific and industrial research. These engineered NPs are relatively new and have potential applications across a range of industries. It should also be noted that larger engineered materials often contain

incidental NPs. For example, nanosized ZnO NPs are found in the manufacture of bulk ZnO material using standard procedures.

1.1.2 NPs in cosmetics and personal care products

NPs have been used in almost every type of cosmetics and personal care products on the market, including deodorant, soap, toothpaste, shampoo, hair conditioner, sunscreen, anti-wrinkle cream, moisturizer, foundation, face powder, lipstick, blush, eye shadow, nail polish, perfume and after-shave lotion (FoE, 2006). For example, due to the strong antibacterial property of nanosilver, it has been formulated into soap. Nanosized silica is also used in skin cream products. It is also reported that nanoencapsulation techniques are employed in perfumes for time-controlled and prolonged release of scents (Paget *et al*., 2006).

The use of nano-sized metal oxides such as titanium dioxide (TiO_2) and zinc oxide (ZnO) in sunscreens are two of the largest uses of NPs in cosmetics and personal care products. As TiO_2 and ZnO are very efficient in filtering harmful ultraviolet (UV) light, these two materials are widely-formulated as UV filters in sunscreens and other personal care products. Micron-sized TiO_2 and ZnO are white, and when used in sunscreens will appear as a thick white paste on the skin. However, when formulated at the nano-scale, these materials become transparent while still retaining their UV-filtering capability. Therefore, most TiO_2 and ZnO sunscreens that are transparent (and not white) are indicative of the presence of nano-scale material (Figure 1.1).

Figure 1.1: Visual comparison of the skin application of sunscreen containing either bulk (right) or nano-sized (left) metal oxide particles. [Adapted from http://www.nanoandme.org/images/cosmetics_surfer.jpg]

1.2 Nanosafety issues

The novel properties of NPs have made nanotechnology applications very popular today. Although nanotechnology benefits society and the economy, increased exposure to NPs of workers and consumers may have the potential to cause adverse health effects. Current guidelines regard NPs as generalized hazardous chemicals, which means their deposition and use may have an impact on the environment and on humans. It is reported that exposures to certain NPs have been associated with many adverse health effects, such as pulmonary inflammation (Shvedova *et al.*, 2005, 2008 & 2009; Rossi *et al.*, 2010), genotoxicity (Lindberg *et al.*, 2009), carcinogenicity (Takagi *et al.*, 2008; Sakamoto *et al.*, 2009) and circulatory effects (Nurkiewicz *et al.*, 2004; Nurkiewicz *et al.*, 2006). Rossi *et al.* reported that inhalational exposure to silica-coated TiO_2 NPs induces pulmonary neutrophilia in mice (Rossi *et al.*, 2010). Similar airway exposure studies with single-walled carbon nanotubes have shown pulmonary inflammatory in mice (Shvedova *et al.*, 2005, 2008 & 2009). It was found that carbon nanotubes and graphite nanofibres can induce DNA damage and

micronuclei in human bronchial epithelial cells (Lindberg *et al.*, 2009). It is also reported that multi-walled carbon nanotubes can induce mesothelioma in mice (Takagi *et al.*, 2008, Sakamoto *et al*., 2009). However, it should be noted that not all NP types are biologically hazardous, and even for one NP type that demonstrates a cytotoxic response, there is a threshold dose for such cytotoxicity.

Materials that are considered safe to use at larger particle scales may be not necessarily being as safe at the nano-scale. The novel physicochemical properties of NPs also raise concerns about potential negative effects on biological systems. However, very little is known about the risks of exposure to NPs. The research field of nanosafety has lagged far behind the advancement of nanotechnology due to several experimental challenges and issues faced when designing appropriate studies involving the toxicological assessment of NPs (Dhawan *et al*., 2009). One of the most important challenges of nanosafety research is the diverse physicochemical properties of NPs, including different particle sizes, surface chemistry and coating, solubility, shapes, and aggregation. So even the same NP material, with or without a surface coating, may lead to potentially different nanotoxicological outcomes. Safe Work Australia (Jackson, *et al.*, 2010) has outlined the difficulty in monitoring NPs as they can form unpredictable structures in different solutions, which may alter their toxicological profiles. This is why at the present state, a case-by-case approach continues to be important to nanosafety research (Kisin *et al*., 2007; Zhu *et al*., 2007; Colognato *et al*., 2008; Karlsson *et al*., 2008; Muller *et al*., 2008; Pacurari *et al*., 2008).

1.2.1 Physicochemical properties of NPs

The physicochemical properties of NPs are very important to their bioactivity, and should be considered when talking about nanosafety issues. The unusual physicochemical properties of

NPs are attributable to the numerous particle characteristics stated above (Nel *et al*., 2006). NPs with different physicochemical characteristics may have different biological effects, which in turn can result in different cytotoxicity endpoints and profiles.

Size and surface area are important characteristics of NPs. The number of atoms on the particle surface determines the reactivity of the material. As NPs decrease in size, their relative surface area increases, with an increasing proportion of the atoms displayed on the surface. For example, in a 30 nm particle, about 10% of its atoms are displayed on the surface, and as the particle size decreases to 10 and 3 nm, the percentage of atoms displayed on the surface increases to 20% and 50% respectively (Figure 1.2) (Oberdorster *et al*., 2005). Such surface atoms have elongated electron orbitals, resulting in the increased reactivity of nanomaterials. Secondly, size shrinkage of a material may also bring together discontinuous crystal planes and disrupt the electronic configuration of the material, which can result in altered electronic properties (Donaldson and Tran, 2002; Oberdorster *et al*., 2005). For example, electron capture can turn dioxygen (O_2) interacting with the NP surface into superoxide radicals ($O_2^{\cdot-}$), which may potentially increase oxidative stress in biological systems exposed to such NPs.

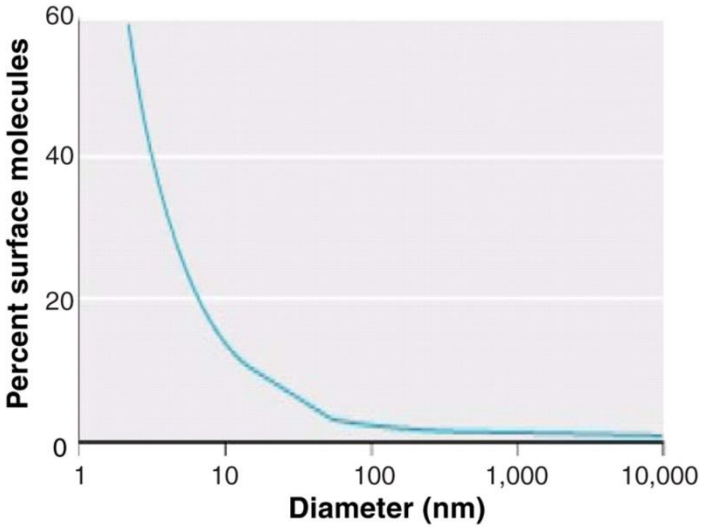

Figure 1.2: Relationship between diminishing particle size and the increase in the percentage of surface molecules. [Adapted from (Oberdorster *et al*., 2005)]

Particle shape is also a very important physicochemical property of NPs. Sometimes even for the same material, alteration of the NP shape will result in different properties. For example, TiO_2 NPs that are widely-used in sunscreens as a UV filter have two common crystalline shapes, anatase and rutile; the latter is less photocatalytic and therefore more desirable for use in sunscreens (Tran and Salmon, 2011).

Other physicochemical properties such as surface coatings, solubility and aggregation will also affect the potential toxicity of NPs. For example, ZnO and TiO_2 are two NPs with very different solubilities in aqueous systems; ZnO NPs have a much higher water solubility than TiO_2 NPs. It is therefore possible that in certain systems, dissolved Zn^{2+}contributes more to the cytotoxic properties of ZnO NPs than the particulate form itself (Xia *et al*., 2008). Surface coatings and aggregation of NPs may also lead to different biological effects, with the possibility of either negating or amplifying the nano-scale size effects. For example, the dispersants used for surface modification of NPs can affect many particulate properties – e.g. reactive surface area or particle-membrane interactions.

1.2.2 Different routes of exposure to NPs

There are 3 main routes of exposure to NPs, like any other chemical, *i.e.* inhalation, oral and dermal exposure (Figure 1.3). Inhalation of airborne NPs, such as exhaust fumes, may be deposited in the respiratory tract and also enter the blood stream and translocate to other organs (Semmler-Behnke *et al*., 2008; Furuyama *et al*., 2009). Some NPs are used in food as food colorants, preservatives, and so on. Ingestion of these NPs may travel to other organ systems, such as the liver, brain, and heart (Oberdorster *et al*., 2005). In addition to the general physiological pH of 7.4, various organ systems can also exhibit different pH environments, including acidic environments that NPs such as ZnO would not survive. This again emphasises the concept that "all NPs are not the same".

Dermal exposure to NPs occurs when applying NP-containing cosmetics and personal care products on the skin. These NPs are usually metal oxides, and there is much evidence showing that these NPs do not penetrate beyond the stratum corneum of healthy skin (Elder *et al*., 2009; Sadrieh *et al*., 2010; Therapeutic Goods Administration, 2013). However, Gulson and coworkers found that very small amounts of Zn ions from sunscreens containing ZnO in bulk or NP form can enter the body (Gulson *et al*. 2010). Also, in a "worst case" scenario such as wound or UV-burned skin, it is highly possible that the NPs in the sunscreens may penetrate the epidermis and encounter immune cells. This project will focus on the safety of these metal oxides formulated in sunscreens and so, following the worst case scenario, human immune cells directly exposed to sunscreen NPs were investigated in this project. It should be noted that the immune responses measured in this study are also applicable to the potential immune effects from inhalational exposure to such NPs.

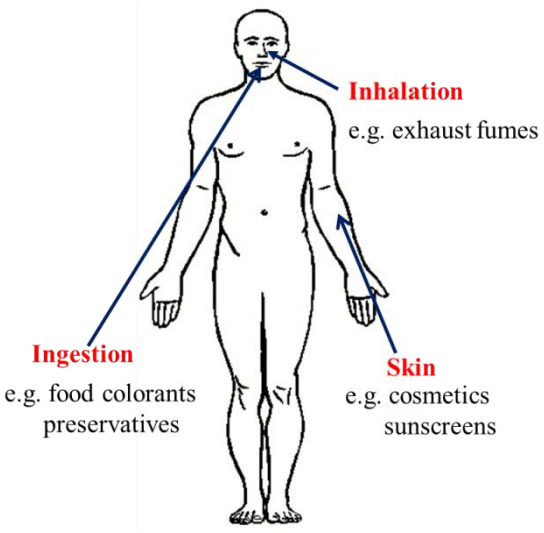

Figure 1.3: Potential routes of exposure to NPs.

1.2.3 Approaches for toxicity assessment of NPs

Several lines of investigations have been reported to measure the safety parameters of NPs. In general, the risk assessment for NPs can include evaluation of data from both *in vitro* and *in vivo* approaches (Table 1.1).

1.2.3.1 *In vitro* assays

The primary endpoint of interest for *in vitro* toxicology is cytotoxicity. In the *in vitro* assays, cytotoxicity is usually assessed by a decrease the viability of different cell types after exposure to NPs. These approaches include the trypan blue exclusion assay, tetrazolium dye-based (MTT and MTS) assays, and the neutral red assay (Wang *et al*., 2007; Vevers and Jha, 2008; Feltis *et al*., 2012). In addition to cytotoxicity, other common *in vitro* toxicological endpoints for nanotoxicology include: oxidative stress and reactive oxygen species (ROS) generation; genotoxicity; mode of cell death; intra- and intercellular signalling; and so on.

Table 1.1: Examples of the approaches for toxicity assessment of NPs.

	Nanoparticle	Cell types/ subjects	Toxicity assay/ study	Citation
In vitro	SiO_2 NP	WIL2-NS human lymphoblastoid cells	MTT assay; trypan blue staining.	(Wang *et al*., 2007)
	ZnO NP	THP-1 Human acute monocytic leukaemia cell line	MTS assay	(Feltis, *et al*., 2012)
	TiO_2 NP	RTG-2 fish cells	Neutral red assay	(Vevers and Jha, 2008)
	CdTe QDs, Au NP	NG108-15 murine neuroblastoma cells and HepG2 human hepatocellular carcinoma cells	High-content screening assay	(Jan *et al*., 2008)
In vivo	TiO_2 NP	Male rats (Fischer 344)	Subchronic inhalation study	(Oberdorster *et al*., 1994)
	Carbon NP	Human subjects	Subchronic inhalation study	(Nemmar *et al*., 2002)
	Single-walled carbon nanotubes	Male mice (B6C3F1, 2 months old)	Intratracheal Instillation study	(Lam *et al*., 2004)
	ZnO NP	Human subjects	Direct dermal exposure study	(Gulson *et al*., 2010)

The choice of cell type for such *in vitro* assays is determined by the target organ/cell under investigation, the assay procedure and requirements, or the specific endpoints selected. As discussed before, there are different routes of exposure to NPs, so the appropriate cell type selected for a nanotoxicology study should match the route of exposure or target organ of specific interest to the test NPs. Epithelial cells are good candidate cells as they are the first contact barrier for NPs in all exposure routes. For the inhalation exposure route, human bronchial epithelial cells, such as A549 or BEAS-2B cell lines, are good cell candidates for screening cell responses in inhalation-related *in vitro* studies. For the dermal exposure route, primary keratinocytes harvested from human donors or immortalised keratinocyte cell lines, such as HaCaT cells, are frequently used. Thus, *in vitro* assays usually employ immortalised cell lines or primary cells. Immortalised cell lines are commonly used because their responses

are highly reproducible and they are easy to handle and culture compared to primary cells. However, some important cellular processes of primary cells may be altered or lost as a result of immortalisation, and this aspect must be taken into account when interpreting findings from such *in vitro* studies.

Jan and coworkers (Jan *et al*., 2008) demonstrated the use of a high-content screening assay (HCA) as a universal tool to probe the cytotoxicity of NPs, specifically cadmium telluride quantum dots (CdTe QDs) and gold NPs (Au NPs). They proposed that the cellular morphology of neurons is suitable for automated HCA screening. They found that the CdTe QDs induced primarily an apoptotic response in a time- and dose-dependent manner, and also produced different toxicological profiles and responses in undifferentiated and differentiated neural cells. In contrast, the Au NPs were found to inhibit the proliferation and intracellular calcium release of HepG2 cells. In another study, Shaw *et al.* reported the development of *in vitro* assays that correlated with *in vivo* activity (Shaw *et al*., 2008). They assessed NP effects in a multidimensional manner, using multiple cell types and assays that reflect different aspects of cellular physiology. Hierarchical clustering of this data identified nanomaterials with similar patterns of biological activity across a broad sampling of cellular contexts. A subset of NPs was then tested in mice, and they found that NPs with similar activity profiles *in vitro* exerted similar effects on monocyte number following *in vivo* exposure. A shortcoming of the study is that the selected NPs were still very similar in nature, suggesting that their approach was efficient in characterizing similar NPs, but has not been validated as being suitable for different forms of nanomaterials.

1.2.3.2 *In vivo* assays

Rodents such as rats or mice are usually employed for *in vivo* toxicity studies of NPs. However, there are many issues and difficulties surrounding the design of appropriate *in vivo* dose ranges, reproducible NP sample preparation, and uniform repeated dosing of monodisperse NPs or their agglomerates, especially for inhalational studies. Human subjects have even been studied in such assays, with this data being the most valued according to the standard "weight of evidence" approach to evaluating findings in toxicological studies.

1.2.3.2.1 Subchronic inhalation assay

Oberdörster and coworkers reported a subchronic inhalation experiment on male Fischer 344 rats (Oberdorster *et al.*, 1994). Their study used whole body exposure of the rats to either 20 or 200 nm TiO_2 with similar concentrations, for 6 hours per day, 5 days per week for 12 weeks. Control animals were sham-exposed to filtered air. Upon aerosolisation, both TiO_2 particle types formed agglomerates with mass median aerodynamic diameters of 0.71 μm (20 nm) and 0.78 μm (200 nm), which were almost the same aerodynamic diameters for both TiO_2 particulates, so the compartmental deposition in the respiratory tract of the animals was expected to be very similar. Rats were killed and sampled at 29 and 64 weeks after cessation of exposure. It was found that the 20 nm particles caused a persistently higher inflammatory reaction in rat lungs compared to the 200 nm particles. The authors concluded that the greater pulmonary effects of the TiO_2 smaller-size particles were related to their larger specific surface area.

Nemmar and coworkers reported on an inhalation study for the risk assessment of carbon particles in human subjects (Nemmar *et al.*, 2002). In this study, they utilized a technique called 'Technegas', which is commonly used in diagnostic nuclear medicine for measuring

the distribution of ventilation (Rizzo-Padoin *et al*., 2001). The Technegas consisted of an aerosol suspension of ^{99m}Tc-labeled ultrafine (<100 nm) carbon particles. The 5 healthy male volunteers participating this study inhaled approximately 100 MBq of Technegas in 3-5 breaths via a mouthpiece. Immediately afterwards, their body images were acquired and blood samples were collected at different time points after the inhalation and measured the radioactivity. Substantial radioactivity in the liver and other areas of the body was seen in the gamma camera images, while radioactivity was also detected in blood. The authors concluded that the inhaled ultrafine ^{99m}Tc-carbon particles, which are quite similar to actual air pollution particles, diffused rapidly into the systemic circulation. This study provided very valuable information about the behaviour of ultrafine particles inhaled by humans.

1.2.3.2.2 Intratracheal instillation assay

Lam *et al*. investigated the toxicity of single-walled carbon nanotubes by intratracheal instillation of mice (Lam *et al*., 2004). In this study, male mice (B6C3F1, 2 months old) were intratracheally instilled with 0.1 or 0.5 mg of carbon nanotubes (1 nm in diameter and several microns long), and killed 7 or 90 days after this single treatment for histopathological study of the lungs. Mouse serum was used as a vehicle control, while carbon black was the negative control and quartz the positive control. This study showed that carbon nanotubes induced dose dependent epithelioid granulomas and, in some cases, interstitial inflammation in animals after 7 days. These lesions persisted and were more pronounced after 90 days. The lungs of carbon black-treated mice were normal, while those treated with high-dose quartz revealed mild inflammation. Altogether, these results demonstrated that carbon nanotubes are much more toxic than carbon black and quartz if they reach the lungs, and are considered to present a serious health hazard following inhalational exposure.

1.2.3.2.3 Direct dermal exposure

Gulson and coworkers (Gulson *et al.*, 2010) conducted a hallmark study involving 17 participants to trace the absorption or penetration of Zn from ZnO NPs in sunscreen applied to healthy human skin under conditions of normal use. In this study, they used an enriched rare stable isotope of Zn (Zn^{68}) and formulated it into sunscreens (in the nano or bulk ZnO form), to measure the levels present in the blood and urine after exposure. The subjects had these sunscreen formulations applied to their backs twice daily for 5 days while doing typical beach activities. Unfortunately the single-label design of this study was unable to determine specifically whether ZnO NPs had penetrated the skin. The important findings from this study was that there was no difference seen between the trace levels of Zn^{68} in bulk or NP formulations in the blood samples of the male participants. However, the NP group had higher levels than bulk group in female participants, although the reason for this is unclear and may be due to some of the female subjects having better hydrated or thinner skin, which may make it easier for the formulations to penetrate through the skin. Although this difference was seen, the amount of sunscreen Zn present in blood samples was $1/1000^{th}$ of usual total blood Zn^{2+} concentrations. What's more, this study also showed that the Zn persisted in the body for some days after the sunscreen was washed off, which could be important for zinc homeostasis and bioaccumulation.

1.2.4 Toxicity assessment of sunscreen NPs

In this project, the NPs of main interest are the metal oxide NPs used in sunscreen formulations, such as ZnO and TiO_2. These NPs are currently used for their broad spectrum UV protection in sunscreens and personal care products.

1.2.4.1 Toxicity assessment of ZnO NPs

Compared to TiO_2, ZnO is theorised to have a lower toxicity potential, as it is a partially water soluble oxide of an essential metal that can be excreted by the body. However, the solubility of ZnO NPs to release Zn^{2+} is one major concern for ZnO toxicity. In addition, in low pH environments such as sweat, stomach fluid, and the lysosomes and endosomes inside cells, the rate of Zn^{2+} release from ZnO NPs would become faster, which would make ZnO more cytotoxic in these environments. It was found by Sasidharan and coworkers that ZnO nanocrystals in the acidic cancer microenvironment are more cytotoxic than in the nearly neutral pH of normal physiological environments, which is mainly due to the faster dissolution of ZnO at acidic pH (Sasidharan *et al*., 2011). In addition, Xia and coworkers reduced the dissolution of ZnO by iron-doping and, in turn, reduced the cytotoxicity of ZnO (Xia *et al*., 2011).

ROS also play an important role in the cytotoxicity of ZnO NPs. Many literature reports have shown enhanced ROS generation in ZnO exposed cells. Xia and coworkers demonstrated that mitochondria superoxide levels were elevated in a mouse immune cell line and human lung epithelial cells exposed to 13 nm ZnO NPs (Xia *et al*., 2008). Also, a study by Applerot and coworkers suggested that the antibacterial effect of ZnO NPs is related to increased ROS-mediated cell injury (Applerot *et al*., 2009). Although, elevated ROS correlates with the cytotoxicity profile of ZnO NPs, this does not necessarily mean that there is also a causative relationship between ROS and the cytotoxicity of ZnO NPs (Shen *et al*., 2013).

One of the very few reports looking into toxicity induced by ZnO NPs after oral dosing of mice has shown that exposure to the extremely high dose of 1 g/kg caused considerable changes in blood coagulation, and biochemical and haematological parameters, as a result of

damage to the liver, spleen, pancreas, kidney, bone and heart (Wang *et al*., 2006; 2008). Changes in immune parameters seen in these animals included an increased neutrophil migration to the stomach, splenic corpuscle enlargement and infiltration of chronic inflammatory cells into the pancreas (Wang *et al*., 2006; 2008). While this data looks at a less likely route of significant exposure to ZnO NPs, it can be theorised that systemic effects will be similar if there is a sufficiently high exposure via the inhalation route, or at sites where the dermal layer is broken.

1.2.4.2 Toxicity assessment of TiO_2 NPs

Unlike ZnO NPs, TiO_2 are insoluble in biological systems. These NPs have previously been considered inert due to their bulk counterpart being used as a negative control in previous particulate *in vitro* studies (Luoto *et al*., 1997; Kilgour *et al*., 2000). *In vitro* studies comparing the cytotoxicity of ZnO and TiO_2 NPs showed much lower cytotoxicity of TiO_2 NPs (11 nm) compared with ZnO NPs (13 nm) in both mouse immune cell line and human lung epithelial cells (Xia *et al*., 2008). In the doses below 10 ± 2 mg/m^3 for airway exposure, TiO_2 NPs are not toxic to mice (Rossi *et al*., 2010). However, TiO_2 NPs (5 nm) at high dose (> 50 mg/kg) are found to cause toxicity following abdominal injection (Liu *et al*., 2009). This study found that nano-anatase TiO_2 in high doses caused serious damage to the liver, kidney, and myocardium of mice and disturbed the homeostasis of blood sugar and lipids in mice.

Also different from ZnO, TiO_2 has different crystalline shapes, with the most common forms being anatase and rutile. The anatase crystalline phase is far more photoactive than the rutile form, and can cause increased oxidation in the presence of light sources such as ultraviolet light (Bickley *et al*., 1991). Therefore, studies were designed to assess if ultrafine TiO_2 particles with similar hydrodynamic diameters, but different crystal phases, had differing

biological effects. The data from these experiments confirmed that anatase was significantly more cytotoxic and pro-inflammatory in the fibroblasts, macrophages and pulmonary systems of rats (Sayes *et al*., 2006; Warheit *et al.*, 2007).

1.3 Human Immune System

The human immune system protects against harmful pathogens, especially those that can be recognized as antigens. Pathogens can be viruses, bacteria, and fungi. Substances can also interact with the immune system, be recognised as antigens and removed from the body and/or cause immune responses – these include toxins, chemicals, and foreign particles (such as NPs) (Cherukuri *et al.*, 2004). Immune system disorders can result in disease and even death. Tissue resident immune cells are a first point of contact where NPs can be actively sequestered by cells. It should also be noted that the immune system has an important role in clearing debris (*i.e.* NPs). Phagocytic immune cells also act as concentrators of NPs (Cherukuri *et al.*, 2004; Unfried *et al*., 2007; Zolnik *et al.*, 2010) – this is important as it is expected that immune cells would therefore be exposed to higher doses of NPs than other cell types. Therefore investigation into the effect of NPs on the function of immune cells is a very important aspect of nanosafety research.

1.3.1 Immune response

The immune response is the mechanism by which the body recognizes and defends itself against potentially harmful antigens. There are two types of immune response: innate and adaptive. The innate immune response, which is also called the nonspecific immune response, is the defense system that is active from birth without prior exposure to specific antigens (Male *et al*., 2013). It provides protection from all antigens in general, though the quality of this protection can vary greatly. The adaptive immune response, which is also called the

specific immune response, is immunity that develops with exposure to specific antigens and offers protection from many pathogens that are able to evade innate immunity (Male *et al*., 2013). The most important part of adaptive immunity is that it has memory, enabling it to respond strongly on a second exposure.

1.3.1.1 Inflammation

Inflammation is a protective process the body uses to remove harmful stimuli and to initiate the healing process. It is one of the first responses of the immune system to infection (Kawai and Akira, 2006). Inflammation can be classified as being either acute or chronic in nature. Acute inflammation is the initial response of the organism to injurious stimuli; it is helpful to the body by removing pathogens, debris and dead tissue to assist the healing process. Conversely, chronic inflammation is harmful as it is persistent inflammation that is unresolved. Inflammation is very important to NP bioactivity, as even without direct toxicity, there can be significant problems if an NP causes inflammation, or worse, if this inflammation becomes chronic. The other possibility of NP exposure is an immunosuppressive effect (Brinker, 2012), if the NPs interfere with immune function, which may increase susceptibility to diseases.

There are two general types of inflammatory mediators, exogenous and endogenous mediators. Exogenous inflammatory mediators are not produced by the immune system, but are produced by external stimuli, such as bacterial products and toxins (Campos *et al*., 2004). Endogenous inflammatory mediators are produced from the immune system itself, such as leukocytes when they reach the site of inflammation. These inflammatory mediators can also be derived from molecules that are normally present in the plasma in an inactive form (Webster and Galley, 2003).

1.3.1.2 Cytokines

Cytokines are small signalling proteins secreted by immune cells. There are two main types of cytokines, according to their different functions. Pro-inflammatory cytokines trigger and up-regulate the inflammatory process, such as Interleukin (IL)-1β, IL-6, IL-8, IL-12, IL17, IL18 and tumour necrosis factor (TNF). Whilst their role in activating the inflammatory cascade is vital, when they are administered systemically to humans, they produce fever, inflammation, tissue destruction, and even death (Dinarello, 2000). In contrast, anti-inflammatory cytokines reduce or halt inflammation and promote healing, and include IL-1 receptor antagonist, IL-4, IL-10, IL-11 and IL-13 (Opal and DePalo, 2000).

Thus ILs and TNF are very important cytokines. The function of the immune system greatly depends on ILs, which were first shown to be secreted by leukocytes, but have since been found to be produced by a wide variety of cell types. TNF is a systemic inflammatory cytokine, and its main function is the regulation of immune cells. Impairment of TNF production has been related to many diseases, including major depression (Dowlati *et al*., 2010), Alzheimer's disease (Swardfager *et al*., 2010) and cancer (Locksley *et al*., 2001).

Cytokines are also associated with oxidative stress, which can cause cytokine induction (Vlahopoulos *et al*., 1999; Florent *et al*., 2007). Cytokines themselves can act in an autocrine or paracrine manner, triggering the release of other cytokines (Carpenter *et al*., 2002; Tian *et al*., 2005), and can also lead to increased oxidative stress, and thus they have an important role in chronic inflammation.

1.3.1.3 Antigen processing

Antigen processing is the mechanism by which immune cells prepare antigens for presentation to T lymphocytes as part of the adaptive immune process. There are two pathways for antigen processing: the endogenous (major histocompatibility complex, class I (MHC I)) and exogenous (MHC II) pathways. The endogenous pathway presents intracellular peptides to MHC class I molecules that are on the cell surface. The exogenous pathway utilizes antigen presenting cells (APCs) to present peptides derived from proteins that the APC has endocytosed via MHC class II molecules, also located on the cell surface (Male *et al*., 2013).

There are two kinds of APCs: professional and non-professional APCs. Professional APCs are specialised cells whose primary role is to internalize antigen, and then display part of that antigen bound to a class II MHC molecule on their cell membrane. T cells then recognize and interact with the antigen-MHC molecule complex. An additional co-stimulatory signal is then produced by the APC, leading to activation of the T cell (Dang *et al*., 1993). There are three main types of professional APCs: dendritic cells (DCs), macrophages and B-cells. In contrast, the non-professional APCs do not normally express MHC II proteins and include: skin fibroblasts, thymic epithelial cells, brain glial cells, pancreatic beta cells and vascular endothelial cells (Nickoloff and Turka, 1994).

1.3.2 Skin immune system

Skin acts as a physical and biological protective barrier for the human body. It protects us from potentially harmful agents like microbes, UV light, and so on. As a physical barrier, the skin also naturally protects from nanoscale objects such as viruses. What's more, the skin is also an important contributor to human immune system responses. In 1986, Bos JD proposed

a distinct “skin immune system” paradigm for the complexity of the immune response-associated cells present in normal human skin (Bos and Kapsenberg, 1986). Approximately half the cell types present in normal human skin have an immune-related function or are local immune cells – these cells include: keratinocytes, immature and mature tissue (myeloid) dendritic cells, monocytes, macrophages, granulocytes, mast cells, T lymphocytes and their subpopulations, and vascular and lymphatic endothelial cells (Bos and Luiten, 2009).

1.3.2.1 Innate and adaptive cells of the skin immune system

Skin immune system cells may also be divided into two groups, *i.e.* innate and adaptive cells, with both groups taking part in immunosurveillance to protect the body from harmful pathogens (Kupper and Fuhlbrigge, 2004). Innate skin immunity is modulated by many biochemical and physical factors, some of which are secreted by the sebaceous and sweat glands, that recruit cellular components to eliminate pathogens and potentially harmful particulates (including NPs). Keratinocytes and macrophages are examples of skin cells involved in innate immunity. The adaptive skin immunity includes cells that are essential in the second line of host defence against specific pathogens, such as mast cells (Bos, 2005). Lymphocytes in the skin are a major part of the adaptive immune response. These lymphocytes in the skin can be stimulated by dermal dendritic cells or epidermal Langerhans cells, to initiate immune responses.

Dermal dendritic cells and Langerhans cells form a bridge between the innate and adaptive immune systems (Banchereau and Steinman, 1998). They can recognize the molecular motifs of microbial agents and thereby become activated, leading to the production of pro-inflammatory cytokines such as TNF-α. During this process, the activation of immature dermal dendritic cells and/or epidermal Langerhans cells can be further enhanced by other

innate immunity factors, such as the pro-inflammatory cytokines TNF-α and IL-1 that are produced by keratinocytes upon contact with pathogens and/or harmful particles (Barker *et al.*, 1991).

1.3.2.2 Differences between skin and systemic immunity

It could be argued that the presence of skin immune cells is the result of a random distribution of tissue-infiltrating T lymphocytes, rather than their specific targeting to the skin. While it has been proposed by some that there is no difference between skin and systemic immunity, there are important differences between these different sites of immunity (Euvrard *et al*., 2003).

One of the primary differences is that the skin is periodically exposed to light and UV radiation, which makes the skin cells more tolerant to these factors than systemic immune cells. For example, keratinocytes are relative insensitive to the DNA-damaging effects of UV exposure and have a high capacity to recover from this form of damage compared to immune cells (Surjana *et al*., 2013).

The skin is also continuously exposed to a variety of antigens from the environment. Although the pulmonary and gastrointestinal tracts also have this characteristic, the skin immune system responds in a distinctive way to these antigens. In pulmonary and gastrointestinal immunology, a major characteristic is the direct submucosal localisation and accumulation of lymphoid tissue, which are thought to play a major role in the production of secretory IgA, independent of systemic immunity. Although secretory IgA has been detected in human cutaneous secretions, the quantity is far lower, and subepidermal extranodular lymphoid tissues are not part of normal human skin. Thus, the skin immune system has

highly distinct characteristics compared to the pulmonary and gastrointestinal immune systems (Bos and Luiten, 2009).

1.3.2.3 Dendritic cells (DCs)

DCs are one of the most important skin immune cell types and are present in skin, lungs and stomach. Their morphology is characterised by the growth of branched projections at certain developmental stages. They have the unique capacity to induce primary immune responses, and they are divided into those homing to the connective tissues (tissue DCs), the lymphoid organs (lymphoid DCs), and epithelia (epithelial DCs: Langerhans cells) (Steinman, 1991).

DCs are among the most important type of APCs involved in immunomodulation, as they respond differently to different kinds of pathogens (Akira *et al*., 2006). If DCs are activated by pathogens, they become more effective in priming the adaptive immune system, whereas in the absence of activation, immature DCs generally induce T-cell tolerance. Therefore, manipulation of DC activation may offer therapeutic potential, such as being an effective way to decrease rejection in transplantation (Xiao *et al*., 2006).

Langerhans cells are members of the DC family, residing in the skin epidermis, respiratory mucosa and epithelia of digestive and urogenital tracts. Like the DCs, Langerhans cells also have the function of antigen presentation and internalizing antigen, and then migrating them to regional lymph nodes, for presentation to naive T cells to initiate the adaptive immune response. It is important to note that Langerhans cells are the main immune cells in the skin epidermis, and constitute the first immunological barrier (Merad *et al.*, 2008). Therefore, investigation of the effect of sunscreen NPs on Langerhans cells is of great significance for the use of topical formulations, such as sunscreens and personal care products.

1.3.3 Effects of Ultraviolet (UV) light on the human immune system

UV light from the sun delivers photons that are energetic enough to open bonds in heterocyclic organic molecules via oxidative chemistry (Waiblinger *et al*., 2000). To an exposed material, this energy can cause serious degradation over time. For example, sunlight causes red rubber items to become brittle in the sun. The same energetic degradation also occurs in biological systems.

UV light is usually defined as radiation with a wavelength between 200 to 400 nm, which includes three parts of the UV spectrum: UVA (320-400 nm), UVB (290-320 nm) and UVC (200-290 nm). Except for industrial activities like arc-welding, UVC is usually not biologically-relevant as it is blocked almost entirely by the atmospheric ozone layer. However, both UVA and UVB can reach the surface of the earth and cause biological effects (van der Mei *et al*., 2007; Andrady *et al*. 2012). Overall, UVB causes more biological damage than UVA, as UVB contributes to approximately 80% of sunlight's harmful effects, while UVA contributes the remaining 20% (Clydesdale *et al*., 2001).

1.3.3.1 UV-induced immunosuppression

There is growing evidence that UV exposure suppresses immune responses to pathogens in both experimental animals and humans (Jeevan and Kripke, 1989; Damian *et al*., 1997; Goettsch *et al*., 1998). As suppression of the immune system is associated with many diseases, the immunosuppressive properties of UV radiation are of significant concern.

As well as localised inhibition of skin immune reactions, UV radiation can also affect the immune system systemically. Local UV-induced immune suppression, where skin is directly UV-irradiated, alters epidermal Langerhans cell function and destroys the DC network. Mice

sensitized via UV skin irradiation fail to generate a contact hypersensitivity response to contact allergens (Toews *et al*., 1980). In studies of UV-induced systemic immune suppression, UV radiation is applied to one site, while an antigen is applied to a distant non-irradiated site. Immune suppression, both locally and systemically, can be induced with relatively low doses of UV. It has been shown that significant immune suppression to *Mycobacterium bovis Bacille Calmette-Guérin* occurs after only 0.35 kJ/m^2 of UVB exposure, which is equivalent to 17.5% of a minimal erythemal dose (MED) of UVB that causes skin reddening (Jeevan and Kripke, 1990). It has been shown that UVA doses equivalent to only 6 minutes of summer sun exposure (as defined in the European Cosmetic Toiletries and Perfumery Association Sun Protection Factor (SPF) Test Method (1994)) can suppress reactivation of memory immunity in humans (Damian *et al*., 1999). Halliday and coworkers have investigated the wavelength dependency for UV-induced immunosuppression using the nickel model of recall immunity in healthy human volunteers. Their study found that UVA contributes to approximately 75% of sunlight-induced immunosuppression (Figure 1.4) (Matthews *et al*. 2010a; Matthews *et al*. 2010b; Halliday *et al*., 2011).

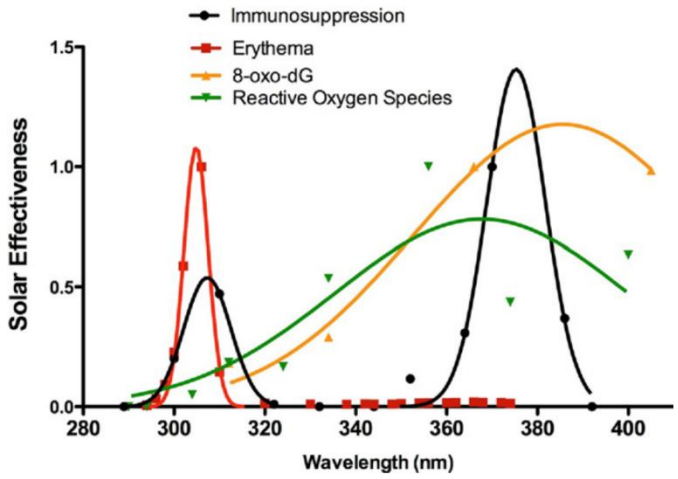

Figure 1.4: Spectrum for UV-induced immunosuppression in humans. [Adapted from (Halliday *et al*., 2011)]

1.3.3.2 Mechanisms of UV-induced immunosuppression

Unlike immunosuppressive drugs that suppress the immune system often non-specifically, UV radiation acts in an antigen-specific way. UV exposure induces the generation of T cells that specifically suppress immune reactions. These cells, initially called T suppressor cells, were recently renamed regulatory T cells (Treg) (Schwarz, 2008).

UV-induced immunosuppression can be examined by suppression of the induction of contact hypersensitivity (CHS) by UV radiation. CHS is considered a measure of T cell function, and most studies indicate that UV radiation leads to its suppression (Tie *et al*., 1995). CHS can be divided into two phases, the first is sensitisation phase and the second is elicitation phase. In sensitisation phase, small haptens react with proteins locally in the skin to create hapten-derivatised proteins, which are taken up by Langerhans cells and presented to specific T cells. In the elicitation phase, T cells are activated, releasing particular cytokines that lead to infiltration of macrophages and neutrophils, and a colour change (e.g. erythema) or swelling (e.g. oedema) (Halliday *et al*., 2012).

When skin is exposed to UV radiation, a multistep process is triggered. The photo receptors in the skin (also called the initiators) convert the physical energy contained within the UV radiation into a biologically recognisable signal. Epidermal DNA and *trans*-urocanic acid (UCA) have both been shown to absorb UV energy to initiate immune suppression (Ullrich, 2005).

Specifically, UV-induced DNA damage has been recognized as the major trigger for most of the biological effects of UV radiation (Kripke *et al*., 1992). UV absorption by cellular DNA results in various types of damage, such as the formation of cyclobutane pyrimidine dimers

(CPDs) and 6,4-photoproducts. DNA repair enzymes bind to the CPDs and revert them to the original pyrimidines (Ley *et al*., 1991).

There are two forms of UCA, *i.e. trans*- and *cis*-UCA; with UV exposure converting *trans*-UCA into the immunosuppressing *cis*-UCA (Norval *et al*., 1995). It has been found that direct injection of *cis*-UCA partially mimics the immunoinhibitory activity of UV radiation (Kondo *et al*., 1995). In addition, *cis*-UCA also inhibits the presentation of tumour antigens by Langerhans cells (Beissert *et al*., 1997).

1.4 Effects of NPs on the human immune system

The NPs that are capable of entering the body are certain to encounter immune cells. Different types of NPs may have different effects on the immune system, as some NPs may stimulate the immune system, while others may suppress it. Thus rigorous investigation of the effects of different types of NPs on the functions of a range of immune cells is a very important aspect of nanosafety research.

1.4.1 Immunostimulatory properties of NPs

The immune system efficiently recognizes foreign substances and mounts a multilevel immune response against them. NPs can also stimulate immunity or trigger an immune response, which has many potential outcomes, some as severe as the induction of allergy or autoimmune diseases (Zolnik *et al.*, 2010). As stated previously, the potential for an inflammatory response is very important to the assessment of NP bioactivity.

1.4.1.1 Inflammatory responses to NPs

During inflammation, immune and non-immune cells may interact with the penetrating NPs to trigger an inflammatory response mediated by cytokines, which will attract more immune cells and begin a process to clear the NPs.

The surface chemistry of NPs is a key factor in their reactivity with the immune system. In general, cationic (positively-charged) NPs are more likely to induce inflammatory reactions than anionic (negatively-charged) and neutral NPs (Kedmi *et al*., 2010). For example, the binding ability of NPs to macrophages is determined by the NP charge displayed to the cell. As macrophages display negatively-charged sialic acid groups on their surface, cationic NPs are more likely to bind and affect macrophages than anionic or neutral particles, potentially inducing inflammation (Dwivedi *et al*., 2009).

NP uptake by immune cells may occur in monocytes, platelets, granulocyte, dendritic cells and, most significantly, in macrophages, which may lead to inflammation (Dobrovolskaia and McNeil, 2007). Different NPs can modulate the inflammatory responses of macrophages in different ways. Lucarelli and coworkers (Lucarelli *et al*., 2004) investigated the effects of SiO_2, TiO_2, ZrO_2 and cobalt NPs on human macrophages *in vitro* by examining their inflammatory responses (via expression of Toll-like receptor (TLR), co-receptors and cytokine production). They found that SiO_2 NPs induced the production of inflammatory cytokines, while Co NPs induced pro-inflammatory effects overall. In contrast, TiO_2 and ZrO_2 NPs did not alter the expression of viral TLR receptors in the study.

1.4.1.2 Effect of NPs on cytokines

As previously mentioned, cytokines are inflammatory signalling proteins secreted by both immune and non-immune cells, and are used extensively in intercellular communication. Cytokine immune signalling in human immune cells has been employed as a biomarker to investigate the immune response (Elsabahy *et al.*, 2010).

Several studies have investigated the effect of NPs on cytokine responses. One *in vitro* study of the potential interference of Co NPs on the production of several cytokines in peripheral blood mononuclear cells (Petrarca *et al*., 2006), found that Co NPs induced TNF-α and IFN-γ release and inhibited IL-10 and IL-2 production in a cytokine pattern similar to that detected in experimental and clinical autoimmunity. Feltis and coworkers (Feltis *et al*., 2012) investigated the cytokine release of THP-1 monocytes exposed to ZnO NPs. In their study, they examined 11 different cytokines of NP-exposed cells by multiplex flow cytometry and ELISA. They found that the cytokine profile of ZnO NP-exposed cells is independent of their cytotoxic response to ZnO NPs. In addition, they also found very strong IL-8 responses, which were dependent on NP size, *i.e*. as particle size decreased, IL-8 expression increased.

1.4.2 Immunosuppressive properties of NPs

Immunosuppression is the potential for an agent to suppress immunity or an immune response. Pharmaceutical down-regulation of the immune response may be beneficial in the treatment of some inflammatory disorders, whereas undesirable immunosuppression could lead to increased susceptibility to infections and cancer (Dobrovolskaia and McNeil, 2007). Some NPs have also exhibited immunosuppressive properties.

It has been found that polymerized lipid NPs prevent eosinophils (a type of granular leukocyte) from binding to targeted selectins, which in turn decreases local inflammation and prevents tissue damage (John *et al*., 2003). Cerium dioxide (CeO_2) NPs have been found to be effective in reducing ROS (Xia *et al*., 2008) and inflammatory mediator production, and have potential use as a novel therapeutic tool for the treatment of inflammation.

In addition, nanodiamonds (NDs) have been reported to help the healing process and therefore could be employed as a treatment in oncology, cardiology, dermatology, and vascular diseases treatment (Schrand *et al*., 2007). However, NDs were also found to increase ROS generation in leukocytes *in vitro* (Puzyr *et al*., 2002). The effects induced by ND particles appear to depend on both its concentration and surface properties (Dwivedi *et al*., 2009).

Many NPs can therefore be engineered to have immunosuppressive properties and may potentially be developed into new therapeutic tools for the treatment of chronic inflammation. However, undesirable immunosuppression from non-therapeutic exposure may occur, and thus immunotoxicity tests are an important part of preclinical NP evaluation (Dobrovolskaia and McNeil, 2007).

1.4.3 Reactive oxygen species (ROS) generation and oxidative stress

ROS are chemically reactive molecules containing oxygen; they include hydrogen peroxide (H_2O_2), superoxide ($O_2^{\cdot-}$) and the hydroxyl radical ($^{\cdot}OH$). The accumulation of ROS increases the oxidative stress to the cell, which leads to adverse biological consequences. Oxidative stress is an imbalance between ROS production and the cell's antioxidant defences (Xia *et al*., 2006). For example, reduced glutathione (GSH) is an antioxidant that protects against ROS

induced cell damage, and when oxidative stress occurs, GSH is converted to oxidised glutathione (GSSG) (Pompella *et al*., 2003). As a result, the GSH/GSSG ratio serves as a measure of the state of oxidative stress (Halliwell and Gutteridge, 2007). Under normal conditions, the level of oxidative stress is very low and thus the GSH/GSSG ratio is high. Conversely, when the GSH/GSSG ratio is low, there is a high level of oxidative stress in the cell.

ROS serves an important role in both photocarcinogenesis and skin aging (Toyokuni, 1998). In addition, ROS can induce DNA damage, such as a single- and/or double-strand DNA breaks, base modifications (e.g. formation of 8-hydroxydeoxyguanosine) and DNA cross-links, all of which, if unrepaired, can lead to carcinogenesis (Martinez *et al*., 2003).

1.4.3.1 Effects of ROS generation from NP exposure

Increased ROS generation by NPs is responsible for oxidative stress in the cell. There is a direct relationship between the ROS generating capability and the pro-inflammatory effects of some NPs (Nel *et al*., 2006). Andre Nel's research group has shown that the hazards of many NPs are best predicted by examining the ROS generation and oxidative injury caused by those NPs (Xia *et al*., 2006).

However, not all NPs will produce ROS. For example, TiO_2 only produces ROS in sunlight (specifically in the anatase form), while other types may produce a lot or none at all, depending on the material. It is important to note that NPs are most often catalysts in the production of ROS, and once *in situ*, may continue to produce ROS indefinitely (Tran and Salmon, 2011). Furthermore, the high surface area properties of NPs can promote the

generation of ROS. Taken together, ROS generation by NPs is clearly an important aspect of their potential toxicity.

There are various methods available which could potentially reduce the production of ROS caused by NPs. These include adding manganese to the TiO_2 NP crystal matrix (Wakefield *et al*., 2004), coating NPs with aluminium-oxide or silicon oxide (Allen *et al*., 2005) or liposomal encapsulation (Bennat and Muller-Goymann, 2000; Lee *et al*., 2007). Other methods include the addition of antioxidant compounds that are sometimes used in sunscreen formulations, including vitamins A, E and C, and b-carotene (Pinnell, 2003).

1.4.3.2 Hierarchical oxidative stress model

A hierarchical oxidative stress model has been developed in Andre Nel's research group to study the oxidative injury made by NPs (Li *et al*. 2002; Xiao *et al*., 2003; Xia *et al*., 2006). At the lowest level of oxidative stress (Tier 1), there are more than 200 protective phase II antioxidants that are regulated by nuclear factor erythroid-2-related factor 2 (Nrf2) (Cho *et al*. 2006; Li and Nel, 2006). These phase II antioxidants include glutathione S-transferase (GST) isoenzymes, superoxide dismutase (SOD), NADPH quinone oxidoreductase 1 (NQO1), heme oxygenase 1 (HO-1), catalase, and glutathione peroxidase (Chan and Kan, 1999; Cho *et al*., 2002; Li and Nel, 2006). Due to the presence of this large and varied pool of cellular antioxidants, there is some considerable benefit from the protective response to Tier 1, and therefore particle-induced ROS generation does not automatically lead to adverse biological events.

If the initial protective responses (Tier 1) are inadequate, a further increase in ROS production can result in pro-inflammatory (Tier 2) and cytotoxic (Tier 3) effects. Pro-

inflammatory effects, caused by an intermediate level of oxidative stress, are mediated by the redox-sensitive MAP kinase and NF-κB cascades that are responsible for the expression of cytokines, chemokines, and adhesion molecules (Chan and Kan, 1999; Li *et al*. 2003; Xiao *et al*., 2003).

If the pro-inflammatory (Tier 2) effects cannot be protected against, then the highest level of oxidative stress (Tier 3), *i.e.* cytotoxic effects, will occur. At this level, perturbation of mitochondrial permeability transition pores and disruption of electron transfer results in cellular apoptosis or necrosis (Hiura *et al*., 2000; Xia *et al*., 2004). This Tier 3 level is also known as toxic oxidative stress.

1.4.3.3 Oxidative stress from NPs

Andre Nel's group also adapted their hierarchical oxidative stress model for NP exposure to investigate the oxidative stress caused by NPs (Xia *et al*. 2006; Xia *et al*. 2008). They assessed different markers for the three tiers of oxidative stress as described above, including Nrf2, HO-1 and NQO1 for Tier 1 oxidative stress responses and found that ZnO NP exposure lead to HO-1 mRNA and protein expression and increased Nrf2 and NQO-1 mRNA expression in RAW264.7 phagocytic cells and BEAS-2B bronchial epithelial cells. Conversely, CeO_2 and TiO_2 NPs did not induce these Tier 1 biomarkers (Xia *et al*., 2008).

For the Tier 2 response, these researchers employed Jun Kinase (JNK), a member of MAP kinase family, as a biomarker and found that ZnO NPs could effectively induce JNK activation in RAW 264.7 and BEAS-2B cells (Xia *et al*. 2006; Xia *et al*. 2008). Finally, for the Tier 3 response, they employed intracellular free calcium measurements and changes in mitochondrial membrane potential as biomarkers and found that ZnO NPs induced a

significant and persistent Ca^{2+} increase, and could lower mitochondrial membrane potential in both cell lines (Xia *et al*., 2008).

As oxidative stress plays such an important role in the metabolism of the cell, such systematic studies of the effect of NPs on cell oxidative stress is of great significance. However, there are factors that still need to be explored. Firstly, NPs were studied in normal cell culture medium containing fetal bovine serum (FBS), which contains high levels of antioxidants that may mask the oxidative effects of NPs. NPs may therefore be introduced to cells that are not affected by FBS-free culture media in order to avoid this effect. Secondly, there is the important situation of NPs that are formulated into sunscreens and their intended use results in co-exposure to UV. The effect of combined exposure to UV light and NPs on oxidative stress in cells is still not well known. Consequently, a significant amount of further work is required to thoroughly investigate this specific aspect of NP effects on cellular oxidative stress.

1.5 Conclusion

Because of the unique properties of nanomaterials, nanotechnology is employed in nearly every aspect of our life. However, we must still be cautious as very little is known about the potential risks of NPs and their novel properties, such as their high surface area leading to enhanced reactivity, while their extremely small size may lead to increased bioavailability – both increasing the potential for adverse biological effects. Unfortunately, the study of nanosafety has lagged far behind the development of new applications of nanomaterials, and we should no longer delay the comprehensive and systematic study of the potential risk posed by widely-used NPs. Tissue resident immune cells are the first point of contact where NPs

can be actively sequestered by cells, and investigations into their effects on the function of immune cells is a very urgent and important aspect of nanosafety research.

It is suggested by many literature reports that ROS generation is related to effects of some NPs, however the relationship between ROS and NPs still needs further investigation. Modulation of the ROS production and cytotoxicity of NPs may help answer the question. Although there are some studies of the effect of NPs on the human immune system, few have examined the potential for altered antigen presentation of immune cells by NP exposure, which warrants further investigation.

1.6 Scope and project outline

Despite the advent of new transparent sunscreens containing NPs of UV-filtering zinc and titanium oxides, the effect of these compounds on innate immunity is poorly understood. This is particularly important as tissue resident immune cells are a first point of contact where NPs can be actively sequestered by cells. In preparing sunscreen formulations, NPs are also being coated with various surfactants – affecting their solubility, bioavailability and dermal penetration, which may also alter their potential inflammatory properties. As there is growing use of such substances in sunscreens, which are crucial to public health in Australia, their safety needs to be established. The aim of this project is to investigate the effect of metal-oxide NPs used in sunscreens on the function of immune cells of the skin. Specific emphasis was placed on the role of zinc ion release, ROS generation, and altered immune functions by exposure of ZnO NPs, and direct comparisons made with TiO_2 NPs.

In this project, the effect of ZnO and TiO_2 NPs on the function of skin immune cells was examined. Firstly, physicochemical properties of NPs are very important to their biological effects and potential toxicity. For this project, different particle sizes, surface coating and shapes of ZnO and TiO_2 NPs were exposed to several human immune cell types that are present in skin, such as monocytes, macrophages and dendritic cells (representing skin Langerhans cells), and their cytotoxicity profiles were assessed. Secondly, the hazards of NPs are best predicted by examining a range of bioactivities, including the ROS generation, oxidative injury and cytokine production caused by NP exposure. These parameters were therefore investigated in the various human immune cell types following NP exposure. In addition, as these metal oxide NPs are commonly formulated in sunscreens, the extent and effects of ROS generation with UVA and NP co-exposure were measured, which is highly relevant to sunscreen usage.

This project will provide important information on the cellular responses of innate immune cells exposed to sunscreen metal-oxide NPs that will help in the safety evaluation of these products, as well as in the safety-by-design approach to developing more effective, less allergenic sunscreen formulations.

Chapter 2. General materials and methods

2.1 Particle characterisation

Particulates require careful and appropriate handling and characterization in order to obtain reproducible experimental results.

ZnO NPs of 30, 80, and 200 nm, with and without a surfactant dispersant (approximately 5% by weight of Orotan 731 DP, a sodium polyacrylate) were supplied by Micronisers Pty. Ltd. (Melbourne, Australia). TiO_2 anatase (25 nm) and rutile (34 nm) NPs were purchased from commercial suppliers. The synthesis of cobalt-doped ZnO (3.5 at% Co) has been previously reported by our research group (Casey *et al.*, 2006).

Particulate suspensions were prepared in milliQ water for primary particle size analysis by transmission electron microscopy (TEM) and dynamic light scattering (DLS). TEM samples for particle size analysis were prepared by pipetting a 4 μL aliquot of the relevant NP suspension in water on a nitrogen glow-discharged, 300-mesh, copper TEM grid, covered with amorphous carbon film. Excess liquid was wicked from the grid and then allowed to air dry. Grids were imaged at a number of different locations to obtain a representative sample of each type of particulate. DLS measurements of primary particle size distribution were performed on a Zetasizer Nano ZS (Malvern) at the Nanometrology section of the National Measurement Institute, Lindfield, New South Wales, Australia. Each sample was prepared by weighing the appropriate amount of NPs and diluting with milliQ water for a final concentration by weight of 200 μg/mL, 24 hr before measurement. Aliquots of 1 mL per sample were loaded into polystyrene cuvettes for analysis. The instrument used a 633 nm He-Ne laser with a scattering angle of 173 °. Each measurement was performed in triplicate at a temperature of 20 ℃.

Size distribution and agglomeration of particle suspensions in RPMI-1640 (Sigma, USA) media and RPMI-1640 media plus fetal bovine serum (FBS, Sigma) were determined quantitatively using a DC1800 disc centrifuge (CPS instruments, USA), with an RPMI-1640 media and sucrose gradient, and confirmed qualitatively by cryo-transmission electron microscopy (cryo-TEM) using a FEI Tecnai G2 (FEI Company, USA).

Disc centrifugation sedimentation (DCS) was undertaken on NPs that had been incubated in cell culture media containing 10% FBS for at least 24 hr prior to analysis. 15 mL of a gradient solution containing 24% w/w sucrose dissolved in RPMI-1640 culture media was loaded into the disc and spun at 24000 RPM for 60 min to equilibrate. An aliquot of 100 μL, at desired concentration of NPs, was directly injected onto the disc for each sample. A standard consisting of polystyrene beads with a diameter of 390 nm was used to calibrate the system before each measurement. Particles are assumed to be spherical and have uniform density for diameter calculations.

Cryo-TEM samples were prepared to examine particle agglomeration in cell culture media by pipetting a 4 μL aliquot of the relevant NP suspension in media onto a nitrogen glow-discharged 300-mesh copper TEM grid covered with lacy formvar-carbon film (ProSciTech, Queensland, Australia). After 30 sec the grids were blotted with filter paper then plunged into liquid ethane cooled with liquid nitrogen. This caused the cell culture media containing NP to form vitreous ice which is effectively transparent to electrons, providing a good model of the agglomeration state of the NP in the *in vitro* culture conditions. The frozen grids were stored in liquid nitrogen until required. They were examined using a Gatan 626 cryoholder (Gatan, California, USA) to keep them below -170 ℃ to prevent the samples from de-vitrifying.

2.2 Particle preparation for *in vitro* studies

Particulates were handled and prepared following a defined protocol to obtain reproducible suspensions for each experiment. All NPs for *in vitro* studies were dispersed into stock solutions prior to being diluted into working solutions. To make the stock solution, 20-40 mg of particulate was weighed out and placed into a 5 mL flat bottom tube, and milliQ water added to achieve a concentration of 20 mg/mL. Then the stock solution was ultra-sonicated (150 W) for 15 mins to disperse and sterilize the solution. After the ultra-sonication, the stock solution was diluted to working solution as follows: the stock solution was vortexed for 30 sec and inverted 10-20 times, and then resuspended by pipetting up and down 3-5 times, before the desired volume of stock solution was added to the media to make 1 mg/mL working solution. Dilutions were made by inverting the working solution 3-5 times, or until no particles were stuck to the bottom of the tube, and pipetting up and down 5 times, before the desired volume of the working solution was added to the media. Considering the NP dissolution and corona formation, NP dilutions were left to stand for 24 hr before dosing into the microplates, as the interaction of NPs and protein in the media are also important to the uptake of the particle. It is known that protein in the media can form a corona, and this corona-NP complex can engage in the uptake process (Dawson *et al*., 2009).

2.3 Cell culture

This project involved the culturing, and incubation with NPs, of five cell types: the human acute monocytic leukemia cell line THP-1, and THP-1 differentiated macrophages; primary human lymphocytes isolated from peripheral blood; human acute myelomonocytic leukemia cell line MUTZ-3, and MUTZ-3 differentiated LCs. All cell cultures and cell culture

exposures were kept in a humidified incubator at 37 ℃ with a 5% CO_2 atmosphere. All cell culture media and solutions for exposures and culturing were kept at 37 ℃ using a water bath, unless otherwise stated. Cell culture and exposure experiments were performed under aseptic conditions in a class 2 biohazard containment hood, and the containers of materials were sterilised by spraying with 70% v/v ethanol in water prior to drying under the sterile airflow within the biohazard hood. Cells were cultured in Cellstar® 75 cm^2 filter-cap polystyrene culture flasks (Greiner Bio-One, Cat. No. 658 175; Greiner, USA) and exposures were carried out in Cellstar® 96-well polystyrene, flat bottomed microplates (Greiner Bio-One, Cat. No. 655 180; Greiner).

2.3.1 THP-1 cell line

The human acute monocytic leukemia cell line (THP-1) (kindly provided by Department of Medicine, University of Melbourne, Melbourne, Australia) was cultured THP-1 culture media (TCM) which consisted of RPMI-1640 media containing 10% FBS (Australian origin, SAFC Biosciences, Sigma-Aldrich Corporation), 100 mg/L gentamycin, 4.5 g/L D-glucose (AnalaR, BDH), 1 mM pyruvate (ReagentPlus®, Sigma-Aldrich), 0.05 mM 2-mercaptoethanol (BioReagent, Sigma-Aldrich) and 2 mM L-glutamine (BioReagent, Sigma-Aldrich) supplementation. Cells were cultured in a humidified incubator at 37 ℃ and 5% CO_2. The cells were cultured to a cell density of between 1 and 2×10^6 cells/mL before being subcultured into fresh media at a dilution factor of 1 in 10, usually once a week, with a doubling time of approximately 26 hr.

In the *in vitro* NP exposure system, cells were centrifuged and resuspended in fresh TCM before seeding into 96-well plates in a volume of 100 µL at 10^5 cells per well. NPs suspended

in TCM were added for a final concentration of 1–100 μg/mL, in a final incubation volume of 200 μL per well.

Macrophages were differentiated from THP-1 monocytes by incubating 8×10^4 cells per well with 20 nM of phorbol-12-myristate-13-acetate (PMA) for 24 hr. Cell photographs were taken via phase contrast light microscopy (Figure 2.1). Macrophage differentiation was confirmed by examining cellular morphology using light microscopy. After which the media was aspirated off and fresh media containing NPs at a concentration of 1–100 μg/mL was added.

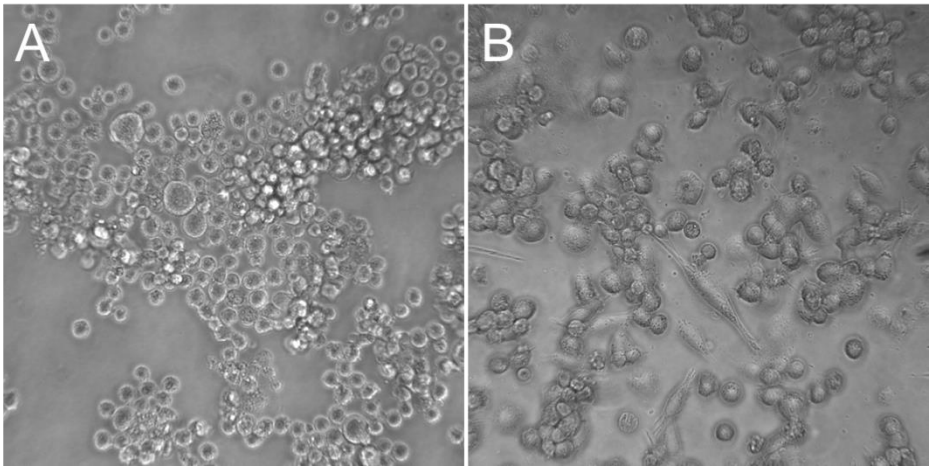

Figure 2.1. Optical microscopic images of THP-1 monocytes (A) and macrophages (B), at 40x objective magnification for both images.

Although PMA has the capability of stopping cell growth, some THP-1 cells still proliferated during the 24 hr period. The lower initial cell concentration was employed to allow for some cell growth during the 24 hr differentiation period – this was needed to obtain the same approximate macrophage cell number per well as was present in the monocyte-containing wells, prior to the addition of particulates and commencement of *in vitro* exposures. This appropriate cell density for seeding wells prior to differentiation by PMA was experimentally

determined as follows. Two different initial THP-1 cell densities (5×10^4 and 8×10^4 cells per well in a volume of 100 µL) were seeded into wells for PMA-induced macrophage differentiation, alongside wells containing unstimulated monocytes, and the cell numbers in each well were determined after 24 hr of incubation by the trypan blue exclusion assay. From Figure 2.2, we can see that macrophages differentiated from THP-1 monocytes at a seeding cell density of 8×10^4 cells per well arrived at the same approximate cell number after 24 hr as the initial cell density of monocytes used for *in vitro* exposures (*i.e.* 10^5 cells per well).

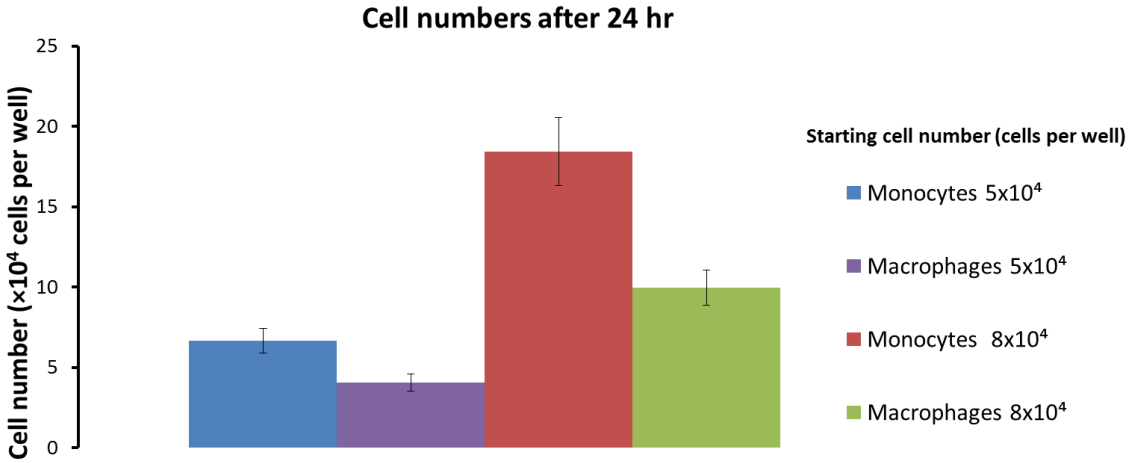

Figure 2.2. Confirmation of cell numbers in THP-1 cell line differentiation protocols. Two seeding cell density (5×10^4 and 8×10^4 cells per well) were used for macrophage differentiation; after 24 hr incubation the cell numbers were determined by trypan blue exclusion assay (mean ± SE of triplicate samples).

The extent of monocyte differentiation into macrophages using this protocol was specifically determined by cell surface marker expression using flow cytometry (FACS Canto II, Becton, Dickinson and Co., Franklin Lakes, NJ, USA), and employing Pacific Blue anti-human CD11b Antibody (BD Bioscience, Cat. No. 558123, USA) as per the manufacturer's instructions. The THP-1 monocytes that were not incubated with PMA exhibited a tailing in its blue fluorescence histogram, and a nominal gating (region "P2") indicated that this

monocyte population was 4% positive for the macrophage specific cell surface marker (Figure 2.3B). After 24 hr incubation with PMA, the same gating region showed that approximately 50% of the cells were positive for the macrophage differentiation marker (Figure 2.3D). The red dots in the 2-D flow cytometry plots of forward vs. side-scatter (Figures 2.3A & 2.3C) represent the undifferentiated monocytes, while the blue dots represent monocytes that have differentiated into macrophages and express the macrophage marker. From the 2-D plots we can also see that after the 24 hr differentiation protocol, the cell has become more granular (*i.e.* increased side-scatter) and slightly larger (*i.e.* increased forward scatter), which was also confirmed by the optical microscopy images (Figure 2.1).

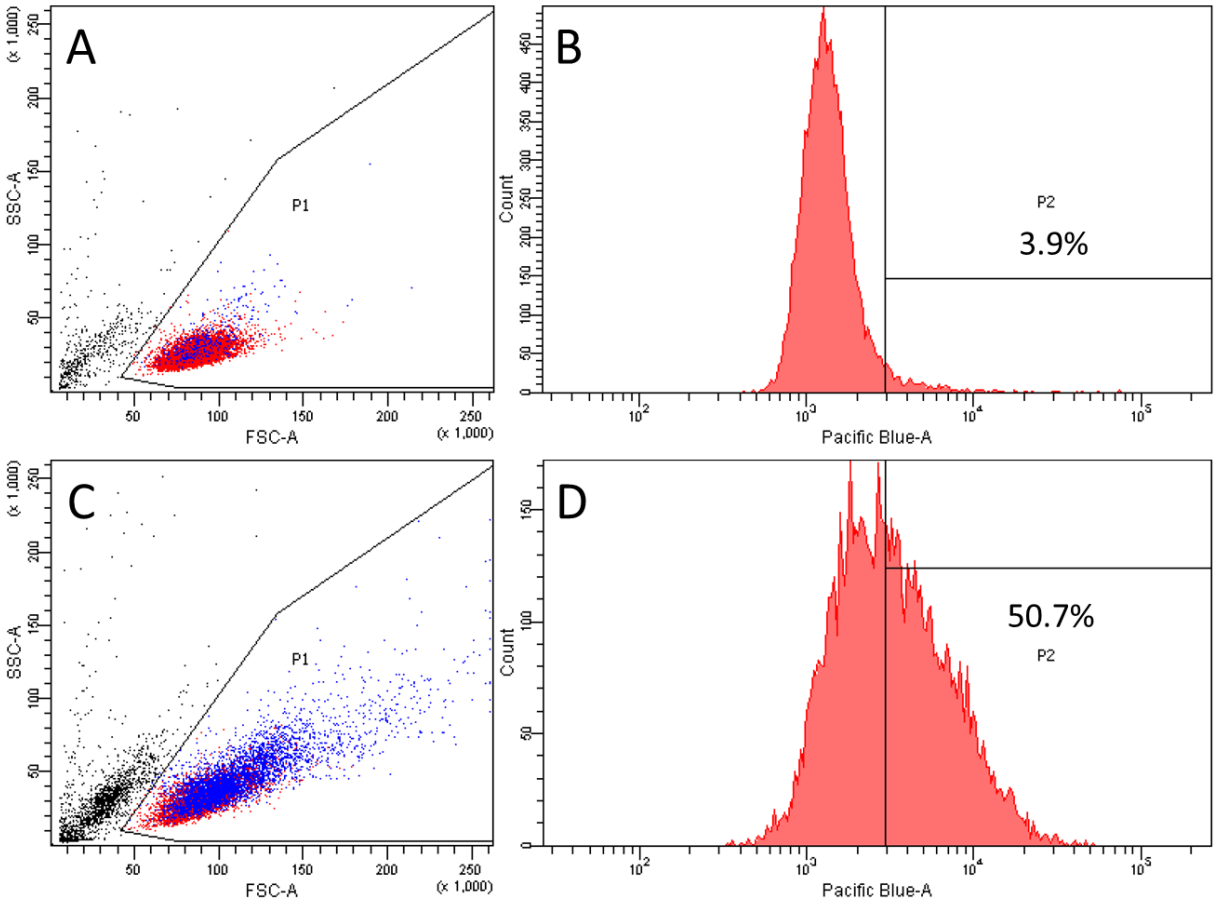

Figure 2.3. Confirmation of the extent of PMA-induced differentiation of THP-1 monocytes to macrophages. A & C are Forward vs Side-scatter plots; B & D are histograms of blue fluorescence intensity (gated on region "P1" in A & C). A & B are THP-1 monocytes without PMA; C & D are THP-1 cells after incubation with 20 mM PMA for 24 hr (Typical plots shown for one of 3 incubations analysed for each condition.).

2.3.2 Primary human lymphocytes

Primary human leukocytes were isolated from 'buffy-coat' material sourced from the Australian Red Cross Blood Service (Melbourne, Australia), which is a by-product of blood donations containing immune cells (under RMIT University Human Research Ethics Committee project number 29/08). BD Vacutainer® CPT glass molecular diagnostic tubes (BD, New Jersey) containing Ficoll™ medium and 0.1 mL of 0.1 M sodium citrate were used to separate leukocytes from any remaining erythrocytes in the buffy-coat. After centrifuging the tubes at 1500 *g* for 15 min at room temperature, the interphase band containing the leukocytes was removed along with the serum and collected in a 50 mL centrifuge tube. This was centrifuged at 300 *g* for 5 min and the supernatant was discarded. The cell pellet was resuspended in 25 mL of warm phosphate buffered saline (PBS) (made from Sigma-Aldrich PBS tablets and milliQ water, sterilised at 121 ℃) and centrifuged again at 300 *g* for 5 min to remove any residual platelets. This wash step was repeated twice. Following this, the leukocytes were resuspended in 25 mL of TCM and counted to determine the concentration. The leukocyte suspension was diluted to a concentration of approximately 5×10^6 cells/mL in warm TCM and 15 mL of this suspension was added to 75 cm^2 culture flasks and incubated at 37 ℃ for 90 min to allow the monocytes to attach. Following the attachment step, the supernatant was transferred to another flask, and returned to the incubator. After overnight incubation, the remaining small portion of monocytes was attached to the flask, and the lymphocytes were collected in the supernatant.

2.3.3 MUTZ-3 cell line

The human acute myelomonocytic leukemia cell line MUTZ-3 (Deutsche Sammlung von Mikroorganismen und Zellkulturen [DSMZ], Braunschweig, Germany) was cultured in MEM-α medium containing ribonucleosides and deoxyribonucleosides (Life Technology, Cat.

No. 12571, USA), 1 g/L glucose (Sigma, USA) and 2 mM L-glutamine (Sigma, USA) supplemented with 20% FBS, 100 mg/L gentamycin (Sigma, USA), and 10% 5637-conditioned medium (Hu *et al.*, 1996; Masterson *et al.*, 2002). Cells were cultured in a humidified incubator at 37 ℃ and 5% CO_2. Cells were centrifuged and resuspended in fresh media before seeding into 96-well plates at 10^5 cells per well. LCs were differentiated from MUTZ-3 monocytes by 9 days of stimulation with 100 ng/ml GM-CSF (Life Technology, Cat. PHC6025), 2.5 ng/ml TNF-α (Life Technology, Cat. PHC3015) and 10 ng/ml TGF-β1 (Life Technology, Cat. PHG9204), and every three days replacement cytokines were added in fresh media (Santegoets *et al.*, 2006). Cell photographs were taken by phase contrast light microscopy (Figure 2.4). After 9 days of stimulation, both stimulated and unstimulated cells were diluted in fresh media before seeding into 96-well plates at 10^5 cells per well. NPs suspended in tissue culture media were added for a final concentration of 10–100 μg/mL, in a final incubation volume of 200 μL per well.

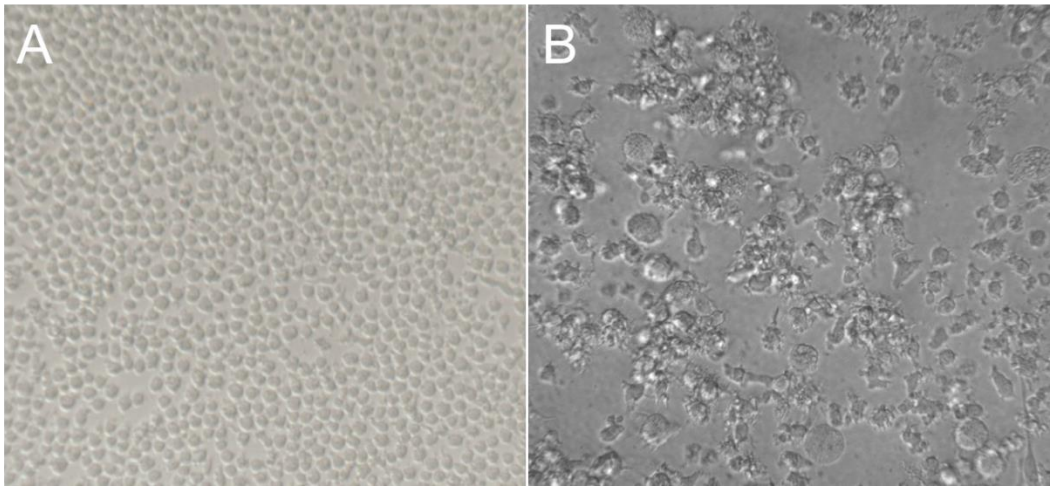

Figure 2.4. Optical microscopic images of MUTZ-3 monocytes (A) and LCs (B), at 40x objective magnification for both two images.

In this study, the extent of differentiation was specifically determined by cell surface marker expression using flow cytometry and the phycoerythrin (PE) labelled anti-human CD207 Langerin antibody (BioLegend, Cat. No. 352204, USA) as per the manufacturer's instructions.

The MUTZ-3 monocytes that were not incubated with cytokines exhibited a tailing in its orange fluorescence histogram, and a nominal gating (region "P2") indicated that this monocyte population was 4% positive for the LC-specific cell surface marker (Figure 2.5B). After 9 days incubation with GM-CSF, TNF-α and TGF-β1, the same gating region showed that approximately 50% of the cells were positive for the LC differentiation marker (Figure 2.5D). The red dots in the 2-D flow cytometry plots of forward vs. side-scatter (Figures 2.5A & 2.5C) represent the undifferentiated monocytes, while the blue dots represent monocytes that have differentiated into LCs and express the LC marker. From the 2-D plots we can also see that after 9 days of differentiation, the cell has become larger and more granular, which was also confirmed by the optical microscopy images (Figure 2.4).

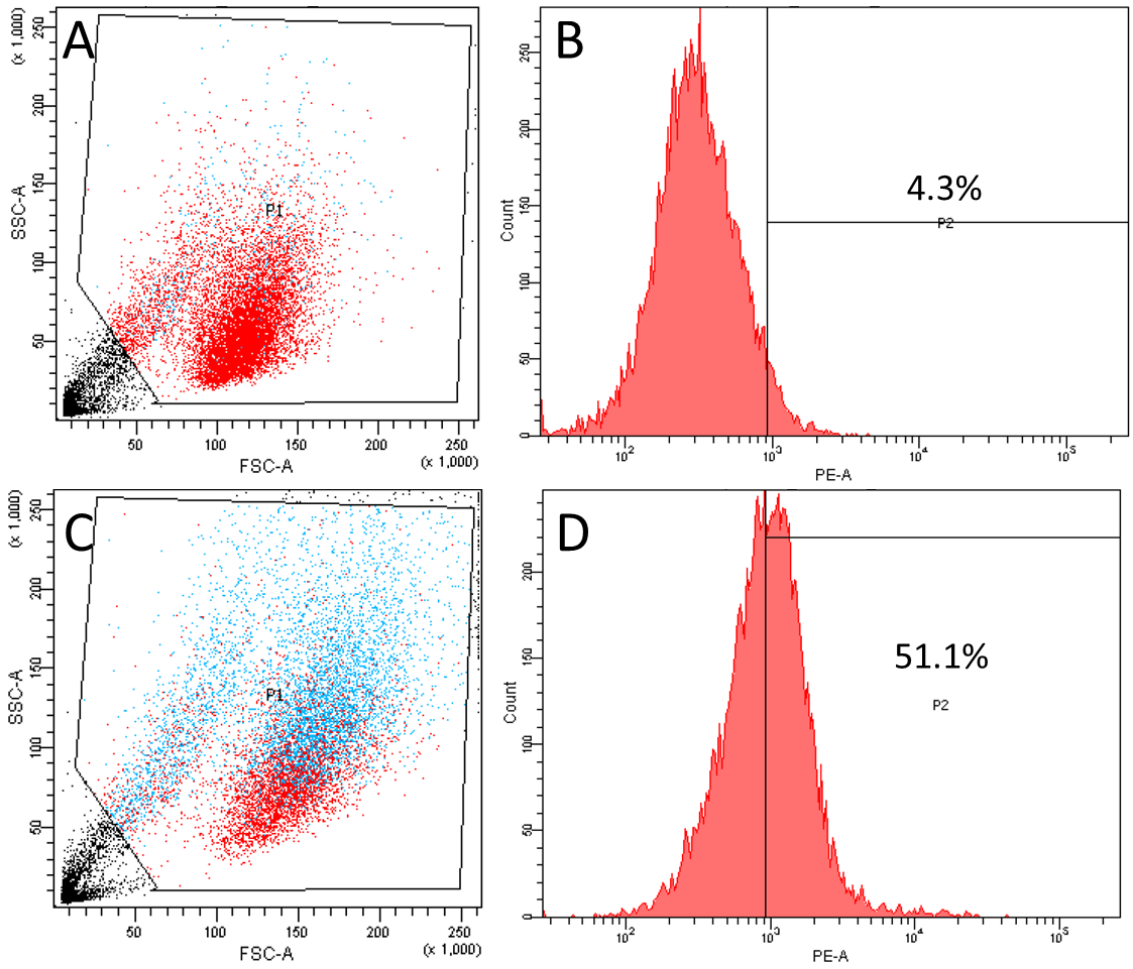

Figure 2.5. Confirmation of the extent of differentiation of the MUTZ-3 monocytes to LCs. A & C are Forward vs Side-scatter plots; B & D are histograms of orange fluorescence intensity (gated on region "P1" in A & C). A & B are MUTZ-3 monocytes without cytokine treatment; C & D are MUTZ-3 cells after stimulation with GM-CSF, TNF-α and TGF-β1 for 9 days (Typical plots shown for one of 3 incubations analysed for each condition.).

2.4 Cytotoxicity assays

The cytotoxicity profile of particulates was examined in this project using three separate measurements of cell viability.

2.4.1 Trypan blue exclusion assay

Trypan blue is a cellular stain that is excluded by the cell membranes of viable cells, and can be used to distinguish between viable and non-viable cells by light microscopy (Strober, 2001). For suspended cells, the samples were simply diluted 1:1 with 0.4% w/v trypan blue solution and then pipetted into an improved Neubauer haemocytometer to visually count the number of live and dead cells. For attached cells, the sample supernatant was removed and collected in a microfuge tube. The sample wells were then washed twice with PBS and these washings were transferred to the same microfuge tube. Following washing, the samples were incubated with 100 µL of TrypLE^{TM} Express (Invitrogen, CA, USA) for 5 min at 37℃, before being dislodged by repeated pipetting and then transferred to the same microfuge tube. Samples were then centrifuged at 200 *g* for 5 min and resuspended in 200 µL of PBS. Samples were then stained and counted as described above.

2.4.2 MTS viability assay

The main assay used to determine cell viability in this project employed a system called CellTiter 96® Aqueous Non-Radioactive Cell Proliferation Assay (Promega), or the MTS assay. The MTS reagent is reduced by viable cells through interaction with dehydrogenase enzymes to produce a soluble formazan dye which absorbs light strongly at 490 nm (Promega, 2009). The amount of light absorbed is directly proportional to the number of viable cells present.

In this project, MTS reagent (40 µL) was added to samples in 96-well plates (final volume 200 µL per well) 4 hr before the desired exposure time-point. After adding MTS reagent, the microplates were incubated for 4 hr in the dark under the cell culture conditions described in section 2.3. After which, the absorbance at a wavelength of 490 nm was recorded using a

plate reader (FlexStation 3 Microplate Reader, Waltham, CA, USA). Wells containing the concentration range of NPs and MTS reagent alone were used to control for any direct optical density effects of NPs, by subtracting these values from the experimental readings. Finally, the absorbance of each sample was divided by the absorbance of the control wells (without NPs) to provide cell viability values as a percentage of control. Each treatment was performed in triplicate per experiment, over three experiments.

2.4.3 Propidium Iodide (PI) fluorescence based assay

PI is a red fluorescent vital dye (Ex 493 nm/Em 630 nm), which can bind to DNA and RNA but is excluded from cells with an intact cell membrane (Darzynkiewicz *et al.*, 1992). Therefore, the number of PI positive cells is directly proportional to the number of nonviable cells present. Flow cytometry was used to perform the PI fluorescence-based cell viability assay as follows. After exposure of the cells to NPs, samples were washed with PBS. Samples were then incubated with PI (Beckman Coulter, California, USA) for 15 min in the dark. After which samples were washed again to remove the extracellular PI and analysed by flow cytometry within 30 min. Each treatment was performed in triplicate per experiment, over three experiments.

2.5 Intracellular ROS generation

The generation of intracellular ROS in the in vitro experiments were measured using fluorescent assays that were compatible with flow cytometry, and with specificity for detecting either intracellular peroxides or mitochondrial superoxide.

2.5.1 Intracellular peroxide generation

Peroxide generation was measured by 2′,7′-Dichlorofluorescin diacetate (DCFDA) (Sigma, St Louis, MO, USA). Cells were centrifuged and then resuspended in fresh media at a concentration of 10^6 cells/mL. Cells were then washed in PBS, which was followed by the addition of 100 µM DCFDA. Cells were then incubated for 30 min in a dark and humidified incubator at 37 ℃ and 5% CO_2 to allow for uptake. Cells were washed again with PBS to remove extracellular DCFDA, after which fresh media was added. Cells were then seeded into black 96-well plates at 10^5 cells per well. NPs suspended in tissue culture media were added for a final concentration of 10–100 µg/mL. After the desired exposure time-points, cells were analyzed using a FlexStation 3 plate reader with excitation and emission wavelengths of 485 and 530 nm, respectively. Each treatment was performed in triplicate per experiment, over three experiments.

2.5.2 Mitochondrial superoxide generation

Mitochondrial superoxide generation was measured by MitoSOX™ Red (Invitrogen, CA, USA), a derivative of dihydroethidium (Ex 510 nm/Em 580 nm). Cells were centrifuged and resuspended in fresh media at a concentration of 10^6 cells/mL. Cells were then washed in Hank's Balanced Salt Solution (HBSS), which was followed by the addition of 2.5 µM MitoSOX™ Red that was then incubated for 30 min in a dark and humidified incubator at 37 ℃ and 5% CO_2 to allow for uptake. Cells were then washed again with HBSS to remove extracellular MitoSOX™ Red, after which fresh media was added. Cells were then seeded into 96-well plates at 10^5 cells per well. ZnO NPs suspended in tissue culture media were then added for a final concentration of 10–100 µg/mL, at a final volume of 200 µL. After the desired exposure time-points, cells were analyzed using flow cytometry. Each treatment was performed in triplicate per experiment, over three experiments.

Chapter 3. Relating cytotoxicity, zinc ions and ROS in ZnO NP-exposed human immune cells

3.1 Introduction

As a result of their high surface-area-to-volume ratio, nanomaterials demonstrate high levels of reactivity when compared to their bulk material counterparts (Roduner, 2006). While this characteristic means that NPs are useful in many industrial and medical applications, the potential for increased exposure to reactive NPs mean that a deeper understanding of the biological properties of NPs at a cellular level is vital (Lee *et al.*, 2007; Zhang *et al.*, 2008a).

Of particular interest to this project are NPs commonly used in commercial sunscreens, *i.e.* ZnO and TiO_2 NPs that combine broad-spectrum UV filtering with transparency to visible light. The public perception of safety concerns regarding nanosunscreens has been promoted by certain community organizations, in contrast to the consensus of scientific research, which now indicates that NPs used in sunscreens do not readily penetrate beyond the skin's stratum corneum (Elder *et al.*, 2009; Sadrieh *et al.*, 2010; Zvyagin *et al.*, 2008). However, there is some evidence that a very small amount of Zn does become bioavailable from the application of sunscreens containing ZnO, irrespective of whether it is in bulk or NP form (Gulson *et al.*, 2010). Moreover, as the epidermis of infants and the elderly is much thinner than adults, NPs from sunscreen may be more likely to penetrate into their stratum corneum. With damaged skin, including that from UV exposure before nano-sunscreen application, NPs may potentially penetrate the outermost dead-cell layer of the epidermis and encounter living tissue (Zhang *et al.*, 2008b). Although many sunscreens are formulated to remain on the skin surface, many dual sunscreen/moisturizer products use excipients that increase skin permeability to deliver active ingredients such as vitamins.

As previously described in chapter 1, if NPs do reach living tissue, they are likely to encounter structural cells of the skin, as well as effector cells of the immune system. The

active scavenging of debris and foreign material by phagocytic immune cells mean that they effectively concentrate NPs and are likely to receive a higher level of exposure than other cell types. Thus a detailed investigation of the effects of ZnO NPs on the function of such immune cells is important in understanding the safe use of these nanomaterials.

Zinc is an essential mineral nutrient involved in over 200 enzymes in the body, and is the second most abundant transition metal, after iron (Wapnir, 1990). It has roles in the structure and function of enzymes, transcription factors, hormonal receptor sites, and biological membranes (Hambidge and Krebs, 2007). Zn also plays a crucial part in signal transduction, gene expression, and regulation of apoptosis (Hambidge and Krebs, 2007; Truong-Tran *et al.*, 2001). Deficiency of Zn affects around 25% of the world's population and can result in food malabsorption syndromes, chronic liver disease, chronic renal disease, sickle cell disease, diabetes, malignancy, and other chronic illnesses (Prasad, 2003). However, a large excess of Zn has been reported to lead to pathologies, such as copper deficiency (Fosmire, 1990), development of prostate cancer (Leitzmann *et al.*, 2003) and immunosuppression (Rink and Gabriel, 2000).

Some studies have reported that Zn^{2+} released from ZnO NPs is at least partially related to their cytotoxic potential (Sasidharan *et al.*, 2011; Xia *et al.*, 2011), as detailed previously in Section 1.2.4. Muller and coworkers also demonstrated that ZnO nanowire-induced cytotoxicity in human monocytes and macrophages resulted from pH triggered, intracellular release of ionic Zn^{2+}, rather than the high-aspect ratio nature of the wires (Muller *et al.*, 2010). Although these studies have shown a relationship between Zn^{2+} and ZnO NP-induced cytotoxicity, whether these parameters can be directly correlated remains unclear and, more importantly, it is uncertain if there is a requirement of contact or uptake of NPs. Thus, the

proportionate contributions to cytotoxicity by extracellular or intracellular dissolution of NPs (with subsequent release of Zn^{2+}) is difficult to ascertain.

The second key determinant to the cytotoxicity of ZnO NPs is increased ROS production that can result in oxidative stress, apoptosis and necrosis. ROS have been implicated in the cytotoxicity of ZnO NPs (Nel *et al.*, 2006) and there is evidence that ZnO NPs can induce elevated levels of ROS in human and mouse immune cells (Hanley *et al.*, 2009; Lin *et al.*, 2009; Xia *et al.*, 2008). Importantly, ZnO itself cannot directly catalyze ROS as zinc ions normally only exists in the +II oxidation state and cannot undergo electron reduction in biological systems. However, ZnO can indirectly raise ROS production by fully occupying oxidative stress defense macromolecules, such as metallothionein, which is then not available to bind other transition metal ions, such as Fe and Cu, that are then free to catalyze Fenton-type reactions (Chevion, 1988; Krezel *et al.*, 2007). Whilst it might be expected that Zn^{2+} cytotoxicity can therefore be directly related to excess ROS production, it is important to consider that organelles like mitochondria also leak electrons, especially after damage, and can be a major source of intracellular superoxide (Musatov and Robinson, 2012). Previous studies have indicated that intracellular ROS generation does appear to be related to the cytotoxicity of ZnO NPs (Xia *et al.*, 2006; 2008), though whether this intracellular ROS is the main cause of cytotoxicity of ZnO NPs, or a result of the damage caused by unbound intracellular Zn^{2+}, remains unclear.

In this section, we have addressed the relationship between ZnO NP-induced cytotoxicity, Zn^{2+} ion release and ROS production. We have also assessed whether the release of Zn ions is primarily intracellular or whether extracellular dissolution of ZnO NPs causes similar cellular outcomes. In addition, we have added antioxidants to the test system, to determine

whether mitigation of the ROS response affects cytotoxicity. Finally, we have investigated the effect of surface chemistry on the toxicity of ZnO NPs. To achieve these research objectives, we have exposed human THP-1 monocytes and macrophages for 24 hr to a broad concentration range of ZnO NPs, or the dialysate generated from ZnO NPs incubated in medium for a prior 24 hr period. We have examined the cytotoxic potential of direct and indirect exposure of cells to these ZnO NPs at high to extreme concentrations, and concurrently measured available intracellular Zn^{2+} and ROS levels. In addition, we have added vitamins C and E with ZnO NPs into the test system and again measured cytotoxicity and ROS levels. Finally, we have modified the surface of ZnO NPs with 3-aminopropyltriethoxysilane (APTES) and polyethylene glycol (PEG) and examined its effect on the cytotoxicity profile of ZnO NPs.

3.2 Materials and methods

3.2.1 Particle characterization.

ZnO NPs of 30, 80, and 200 nm, with and without a surfactant dispersant were employed as test NPs in this study. TiO_2 anatase and rutile NPs are used as insoluble control NPs. The methods for particle characterization for these NPs are described in section 2.1.

3.2.2 Micro X-ray fluorescence microscopy (μXFM).

THP-1 cells were removed from culture media and immediately fixed for 2 hr in 2.5% w/v glutaraldehyde in 0.1M sodium dimethylarsinite (cacodylate) in 2 mM $CaCl_2$, pH adjusted with HCl to 7.3–7.4. Cells were subsequently washed in 2 mM $CaCl_2$ and 0.1 M sodium dimethylarsinite in distilled water for 10 min. Postfixation was carried out for 20 min in 1:1 osmium tetroxide 2% w/v stock in 0.2 M sodium dimethylarsinite with 4 mM $CaCl_2$,

resulting in a final concentration of 1% w/v osmium tetroxide in 0.1 M sodium dimethylarsinite with 2 mM $CaCl_2$. The cells were then washed in 0.1 M sodium dimethylarsinite in 2 mM $CaCl_2$ and then in distilled water for 10 min to remove excess osmium tetroxide.

The elemental distribution was mapped using a Fresnel zone-plate scanning x-ray fluorescence microprobe at the Australian Synchrotron XFM beamline (0). With this instrument probe size, the resolution and elemental sensitivity can be traded off against one-another, and in this case the resolution was around 350 nm (x) by 250 nm (y). An incident beam of 10 keV X-rays was used to induce K-shell ionization of elements with atomic numbers below 30 ($Z \leqslant$ Zn). The specimen was oriented normal to the incoming X-ray beam and scanned using an integration of 2.5 sec per scan point. A single element silicon-drift diode detector (Vortex, SII NanoTechnology, CA, USA) was used to detect the X-ray fluorescence spectrum at each pixel. Elemental maps were generated from the three dimensional data sets (x, y, energy) using the MAPS software suite (v1.6.5) (Vogt, 2003).

3.2.3 Cell culture and cytotoxicity assays.

THP-1 monocytes and THP-1-derived macrophages were employed in this study. The detailed THP-1 differentiation protocol and cell culture procedures are described in section 2.3. NP working suspensions were mixed thoroughly by vortexing and inversion of tubes, before 100 µL of each NP working suspension was pipetted into the appropriate wells of a 96-well plate already containing 100 µL of TCM and the relevant number of THP-1 monocytes or macrophages. Plates were then incubated at 37 ℃ and 5% CO_2 for the desired period of time before being analysed for a range of endpoints, including the MTS cytotoxicity assay (as described in section 2.4).

3.2.4 Intracellular zinc ion measurement.

Intracellular zinc ions were measured by zinquin ethyl ester (Biotium, CA, USA), a UV-excitable fluorescent zinc indicator (Ex 364 nm/Em 385 nm). Cells were seeded in 96-well plates and incubated with ZnO NPs for 24 hr, as described above for the cell culture procedure. After 24 hr of co-culture with NPs, cells were washed with PBS to remove extracellular zinc. Cells were then incubated with 25 μM zinquin ethyl ester for 30 min in a dark and humidified incubator at 37°C and 5% CO_2 to allow for cellular uptake. Once the zinquin ethyl ester is internalized, its ethyl ester group is cleaved by cytosolic esterases which impede its efflux across the plasma membrane. After 30 min, the cells were washed again with PBS to remove extracellular zinquin ethyl ester. Finally, fresh media was added and cells were analyzed using flow cytometry (FACS Canto II, Becton, Dickinson and Co., Franklin Lakes, NJ, USA). Each treatment was performed in triplicate per experiment, over three experiments.

3.2.5 Total cell-associated zinc measurement.

Solutions from the cell culture experiments were characterized for zinc concentration per cell via Inductively Coupled Plasma (ICP) Time of Flight (TOF) Mass Spectrometry (MS). Prior to extraction, cells were washed 3 times in cell culture media to remove extracellular NPs. Each well was then washed twice (2 x 200 μL) with double distilled (DD) concentrated nitric acid, in order to extract all material present. Each solution was then diluted with ~3 vol% DD nitric acid in ultra-pure (milliQ) water (15 mL). For drift correction, the internal standard Sc, was added to each solution (at 59 ppb, diluted from a commercial stock solution). Each sample solution was then filtered via a 0.45 μm nylon syringe filter to prevent blockage of the ICP-MS nebuliser. Solutions were then measured with an GBC Optimass 9500 ICP-TOF-MS instrument. A commercial stock solution of Zn was used for calibration standards (~5, 10, 30,

60, and 120 ppb). All standards were ionic-strength adjusted, so as to contain the same high concentration of nitric acid present in the samples.

3.2.6 NP solubility.

The solubility of ZnO NPs in medium with 10% v/v FBS was determined by dialysis. A dialysis tube (benzoylated cellulose to reduce pore size, 12 kDa size cutoff, 9 mm flat width, Sigma Aldrich D-2272), filled with medium/FBS (5 mL) was inserted into cell culture media (RPMI-1640, 20 mL) at 37°C containing ZnO NPs. After dialysis for 24 hr, dialysates were added to the cell culture system, and the cytotoxicity following a 24 hr exposure period was measured as a loss of cell viability by the MTS assay. Each treatment was performed in triplicate per experiment, over three experiments.

3.2.7 Intracellular ROS generation.

Both intracellular peroxide and mitochondrial superoxide generation of NP-exposed cells were measured in this study. In this section, intracellular ROS was measured after the 24 hr exposure time-point, as described in section 2.5.

3.2.8 Mitigation of superoxide generation.

In this study, the lipophilic antioxidant vitamin E (α-tocopherol) or the hydrophilic antioxidant vitamin C (L-ascorbic acid) were co-exposed with ZnO 30 nm NPs to THP-1 monocytes to determine whether they could mitigate superoxide generation in this system. For each antioxidant, two different concentrations (0.1 and 10 μg/mL) were examined in this study. The effect of antioxidants was investigated by measurement of superoxide generation (section 3.2.7) and cytotoxicity (section 3.2.3).

3.2.9 Surface modification of ZnO NPs.

Surface-modified ZnO NPs were synthesized according to the literature, with minor alterations to the procedure (Grasset *et al.*, 2003). A typical procedure for the synthesis of 3-aminopropyltriethoxysilane (APTES) modified ZnO 30 NPs (denoted as "APTES@ZnO" NPs) is given as follows. Briefly, 2 g ZnO 30 NPs were dispersed into 200 mL anhydrous toluene under nitrogen gas flow in a 250 mL round bottom flask. After 1 hr of stirring magnetically, 1 mL APTES was added under nitrogen protection. The mixture was refluxed under a nitrogen gas flow for a further 15 hr. Finally, after cooling down to room temperature, the reactant was centrifuged (2,500 *g*) and washed 3 times using fresh toluene and anhydrous ethanol to remove the excess APTES, then dried in a vacuum oven overnight to remove the solvent.

PEGylated ZnO NPs (denoted as "PEG@ZnO" NPs) were synthesized by a similar procedure, whereby PEGylated silane was used instead of APTES. Specifically, PEGylated silane was synthesized following a procedure from the literature, with some alterations (He *et al.*, 2010). Firstly, 0.8 mL (4 mmol) of tetraethyleneglycol monomethyl ester was dissolved into 10 mL dry pyridine with vigorous stirring under nitrogen gas flow at 70 ℃. After stirring for 1 hr, 1 mL (4 mmol) of 3-(triethoxysilyl) propyl isocyanate (TESPIC) was added dropwise into the mixture. The reaction was kept for 24 hr at 70 ℃ under the protection of a nitrogen atmosphere. After that, the solvent was evaporated under vacuum to afford the product as a light yellow liquid.

3.2.10 Biological effect of surface-modified ZnO NPs on THP-1 cell lines.

To test the biological effect of surface-modified ZnO NPs, we employed THP-1 cell lines as candidate cells. In this study, we investigated the biological effects of surface-modified ZnO

NPs by examining the cytotoxicity, intracellular zinc ions and uptake of these NPs on THP-1 monocytes and macrophages. The cytotoxicity of surface modified ZnO NPs was measured by MTS assay, which is described in section 2.4.2. Intracellular zinc ions were measured by zinquin ethyl ester, detail of the assay method is described in section 3.2.4. The uptake of ZnO NPs was investigated by measuring the total cell-associated zinc using ICP-MS, detail of the assay method is described in section 3.2.5.

3.2.11 Statistics.

Data were presented as mean ± standard error of mean (SEM) and was analysed using two-way ANOVA and Bonferroni post hoc test (Prism 5.0, GraphPad Software, La Jolla, CA, USA), with a p value < 0.05 considered significant.

3.3 Results

3.3.1 Particle characterisation.

Zinc oxide NPs with a diameter of 30, 80 and 200 nm, in both untreated and surfactant-dispersed forms (designated as "ZnO" or "sZnO", respectively), as well as TiO_2, as anatase and rutile NPs, were mainly employed in this study. The primary particle size in water was assessed using dynamic light scattering (DLS, Table 3.1). Primary particle size was also measured via DLS in cell culture media, but interference from suspended protein particulates confounded the results. To measure the agglomerate size, the disc centrifugation technique was used instead. The surface areas for primary particles and agglomerates were also calculated assuming a spherical agglomerate distribution. Values for these data are summarized in Table 3.1. All particles were also imaged in both water by TEM and cell

culture media (+10% serum) by cryo-TEM, and sample images have been collated in Figures 3.1 and 3.2.

Table 3.1 Particle characterization* (Shen *et al.*, 2013).

Particle	Disc Centrifuge Agglomerate Size (mean [peak half-width])	Agglomerate Surface Area (m^2/g)	Primary Particle Size (nm)	Primary Particle Surface Area (m^2/g)
TiO_2 Anatase	111 nm [55 – 209 nm]	13.62	DLS: 25 ± 3	60
TiO_2 Rutile	229 nm [101 – 380 nm]	6.50	DLS: 34 ± 3	44
ZnO 30	1.33 µm [0.68 – 1.98 µm]	0.80	DLS: 36 ± 6 (TEM: 25 ± 7)	30
ZnO 80	1.32 µm [0.65 – 1.32 µm]	0.81	DLS: 83 ± 8	13
ZnO 200	1.29 µm [0.88 – 1.69 µm]	0.83	DLS: 200-500	3
sZnO 30	75 nm [50 – 100 nm]	14.27	**	**
sZnO 80	90 nm [50 – 130 nm]	11.89	**	**
sZnO 200	460 nm [240 – 670 nm]	2.33	**	**

*Disc centrifuge analysis was used to measure agglomerate size of ZnO and TiO_2 NPs (mean [peak half-width]) after 24 hr exposure to cell culture media with 10% serum. Primary particle size was also determined by DLS for each particle in a dispersed solution in water (mean ± SEM, n=2). Surface areas were calculated assuming nominally spherical particles and particle agglomerates. Acknowledgement of Victoria Coleman and the National Measurement Institute (NMI) for assistance with disc centrifugation assay. ** Primary particle size for surfactant-dispersed NP is the same as for pristine material.

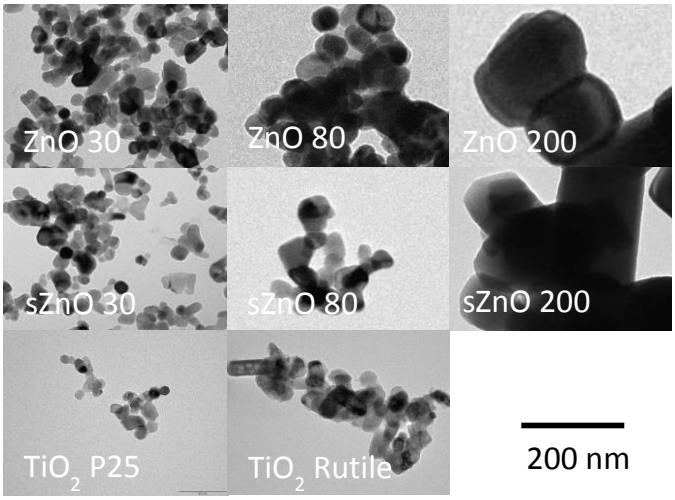

Figure 3.1 TEM images of the ZnO and TiO_2 NPs used in this study (scale bar applies to all images). NPs were dispersed in distilled water prior to imaging (provided by Lynne Waddington and Andrew Hastings) (Shen *et al.*, 2013).

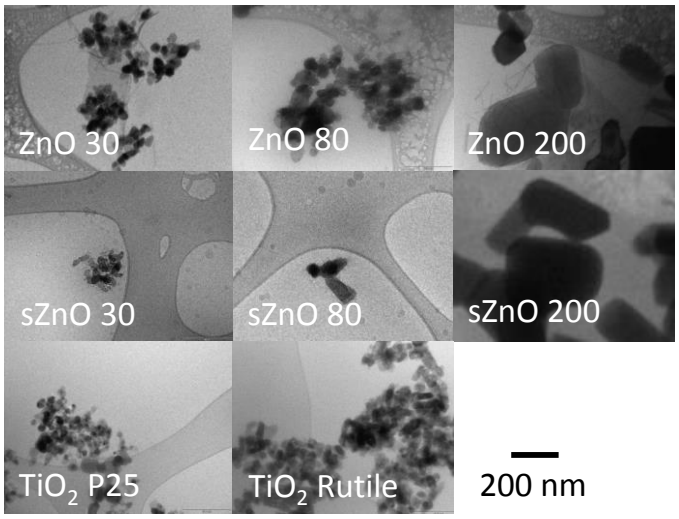

Figure 3.2 Cryo-TEM images of the ZnO and TiO_2 NPs used in this study (scale bar applies to all images). NPs were incubated in cell culture media with 10% serum for 24 hr prior to imaging (provided by Lynne Waddington and Andrew Hastings) (Shen *et al.*, 2013).

3.3.2 Micro X-ray fluorescence microscopy (μXFM).

As endogenous cellular zinc can be present throughout the cell, we used a modified ZnO 30 nm NP that had been lattice doped with cobalt (~3.5 atom %), which is X-ray fluorescent and is naturally of very low abundance in cells. This modification did not alter the cytotoxicity

profile of the ZnO NPs to THP-1 cells (Figure 3.3). Importantly this process did not require the addition of an optically fluorescent tag (*i.e.* external modification of the NPs that may influence cell uptake), and thus allowed us to directly image the uptake of these, only slightly modified, ZnO NPs by μXFM. The μXFM elemental map of ZnO-exposed, THP-1 differentiated macrophages (Figure 3.4) showed low levels of dispersed zinc throughout the cells (a co-located phosphorus map is shown to indicate the extent of the cell cytoplasm and nucleus). These data also showed aggregates of co-localized zinc and cobalt, indicating that the NPs had remained intact during intracellular uptake. Whilst only a small number of cells were examined, NP distributions were consistent with agglomeration in a small number of large vesicles in the cytoplasm. NPs were not observed to be co-located with the nucleus. While these images alone do not confirm internalization of the NPs, we have since undertaken other studies using a combination of sequential focused ion beam ablation, μXFM, and scanning EM that clearly indicate cytoplasmic uptake of the NPs (James *et al.,* 2013).

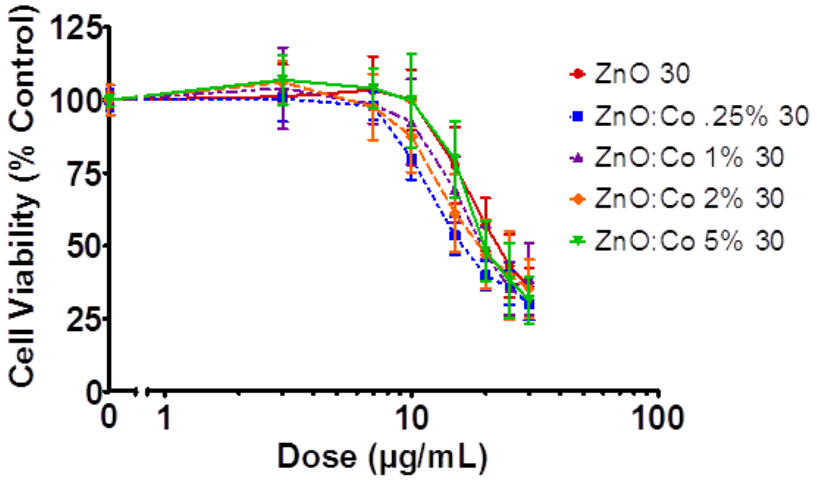

Figure 3.3 Cell viability of macrophages 24 hr post ZnO 30 and Co-doped ZnO 30 treatment. Data represents mean ± SEM of 3 experiments in quadruplicate. Nominal Co doping % values are shown in the key (5% nominal is ~3.5 atom % actual). There was no statistical difference between any of the curves as determined by two-way ANOVA with Bonferroni post hoc test ($P>0.05$) (provided by Sean O'Keefe) (Shen *et al.,* 2013).

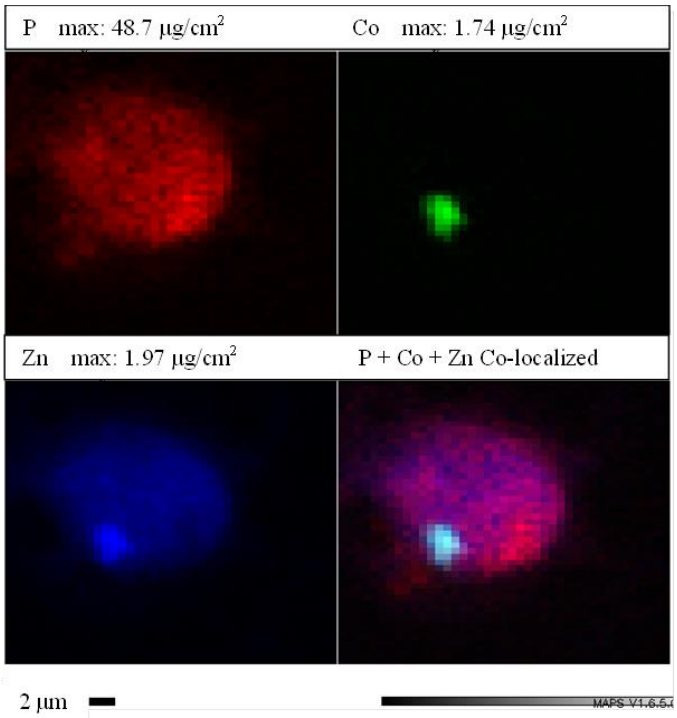

Figure 3.4 µXFM synchrotron elemental maps of ZnO NPs (doped with 3.5 atom % Co) in exposed THP-1 macrophages, illustrating large agglomerates of NPs associated with the cells after 24 h. Phosphorus (red) highlights the cytoplasm and nucleus, and zinc (blue) is present throughout the cell, although co-localization with cobalt (green) clearly indicates the NPs, which were typically associated with a small number of vesicles and not found in the nucleus. The co-localized image is displayed on the bottom right (in association with Bryce Feltis and Simon James) (Shen *et al.*, 2013).

3.3.3 Cytotoxicity profiles.

THP-1 immune cells (monocytes and macrophages) were exposed to ZnO concentrations of 1, 10, 25, 50, 75 and 100 µg/mL and cytotoxicity investigated after 24 hr of exposure using the MTS dye assay for cell viability. Figure 3.5 shows that the viability of ZnO-exposed cells decreased in a dose-dependent manner at >20 µg/mL for both monocytes and macrophages. In addition, ZnO NPs displayed similar cytotoxicity to $ZnCl_2$. The viability data also showed that the cytotoxicity of ZnO NPs was size-dependent, with cytotoxicity increasing as NP size

decreased. To examine the effects of dispersion on cytotoxicity, each of the pristine NPs were formulated as surfactant-dispersed preparations (approximately 5% surfactant by weight). Surfactant alone did not alter cell viability up to a concentration of 100 µg/mL (data not shown). We observed decreased viability in THP-1 immune cells when they were exposed to surfactant-dispersed ZnO NPs compared with the equivalent-sized pristine ZnO NPs. These results were consistent with our previous findings, which demonstrated both NP size and dispersion dependent cytotoxic effects in this cell type (Feltis *et al.*, 2012).

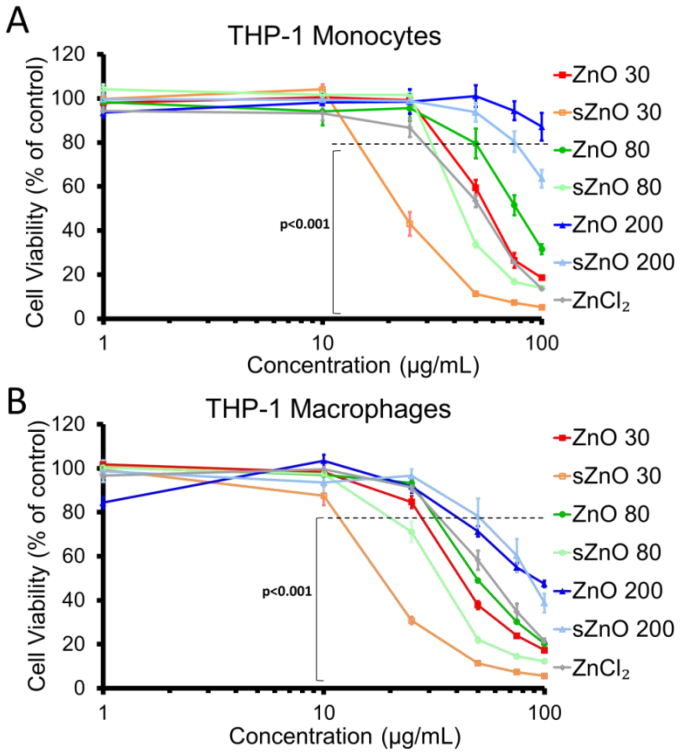

Figure 3.5 Cell viability of human THP-1 monocytes (A) and macrophages (B) after 24 hr exposure to pristine or surfactant dispersed (s) ZnO NPs or $ZnCl_2$ (zinc ion control) (mean ± SEM, n=3 experiments), showing that particle size and dispersion influence cytotoxicity. All concentrations at or below the horizontal line were highly significantly different from untreated control cells ($p < 0.001$) (Shen *et al.*, 2013).

As the solubility of ZnO NPs was a significant confounding issue in this study, we also employed TiO_2 NPs as an insoluble control. We observed little to no change in the viability

(~10% reduction at the highest concentration) of THP-1 immune cells exposed to TiO_2 NPs for 24 hr (Table 3.2), which was very low compared to the cytotoxicity observed with ZnO NP exposures.

Table 3.2 Cell viability and relative generation of mitochondrial superoxide of human THP-1 cells after 24 hr exposure to TiO_2 NPs (insoluble NP control) (Shen *et al.*, 2013).

Monocytes	**Dose (μg/mL)**	**Viability (% of control) (Mean ± SEM; n=3)**	**Mitochondrial superoxide level (% of control) (Mean ± SEM; n=3)**
TiO_2 Anatase	10	100 ± 3	91 ± 21
	50	96 ± 2	94 ± 2
	100	92 ± 2	99 ± 2
TiO_2 Rutile	10	103 ± 2	93 ± 2
	50	99 ± 2	95 ± 2
	100	91 ± 3	98 ± 3
Macrophages	**Dose (μg/mL)**	**Viability (% of control) (Mean ± SEM; n=3)**	**Mitochondrial superoxide level (% of control) (Mean ± SEM; n=3)**
TiO_2 Anatase	10	99 ± 1	136 ± 4*
	50	94 ± 1	127 ± 4
	100	90 ± 2	128 ± 12
TiO_2 Rutile	10	101 ± 2	141 ± 8**
	50	97 ± 1	124 ± 9
	100	89 ± 3	129 ± 16

Asterisks denote concentrations significantly different from untreated control cells (* $p < 0.05$, ** $p<0.01$).

3.3.4 Intracellular zinc ions.

Intracellular dissolution of zinc ions from ZnO NPs was investigated using zinquin ethyl ester, a specific fluorescent zinc indicator (Coyle *et al.*, 1994). In this experiment, THP-1 immune

cells were exposed to ZnO NPs at concentrations of 10, 50, and 100 µg/mL and intracellular zinc ion levels were measured after 24 hr of exposure by flow cytometry. The available intracellular zinc levels in monocytes increased with increasing ZnO NP concentrations (Figure 3.6). Direct binding of zinquin to the ZnO NPs was also assessed by flow cytometery, with no fluorescent signal being observed (Figure 3.7). Therefore, it appears that zinquin is able to distinguish between zinc in NP form and other forms of more readily available zinc.

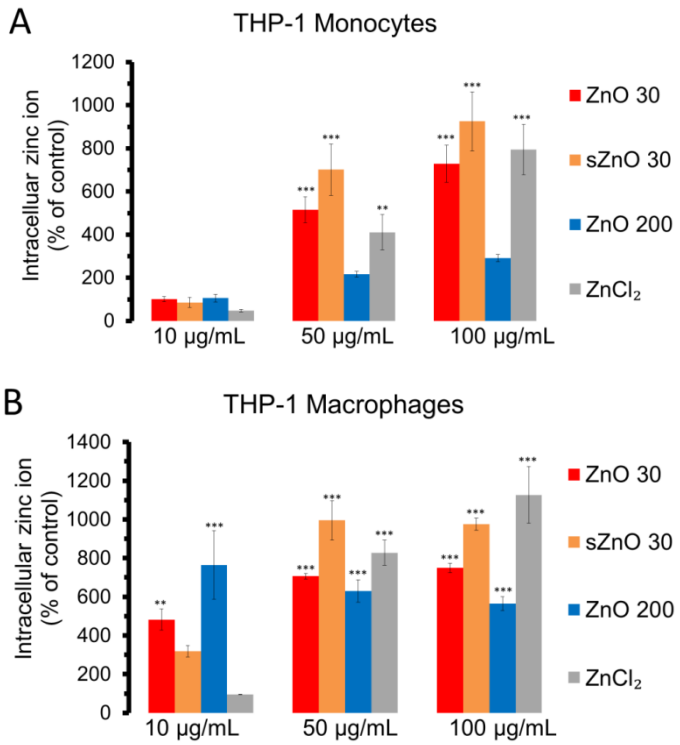

Figure 3.6 Intracellular zinc ion levels in THP-1 monocytes (A) and macrophages (B) after 24 hr exposure to ZnO NPs and $ZnCl_2$ (zinc ion control), relative to the endogenous available zinc in untreated (control) cells (mean ± SEM, n=3 experiments). Available intracellular zinc was greater with increasing NP concentration and smaller particle size. Asterisks denote concentrations that were significantly different from untreated control cells (** $p < 0.01$, *** $p<0.001$) (Shen *et al.*, 2013).

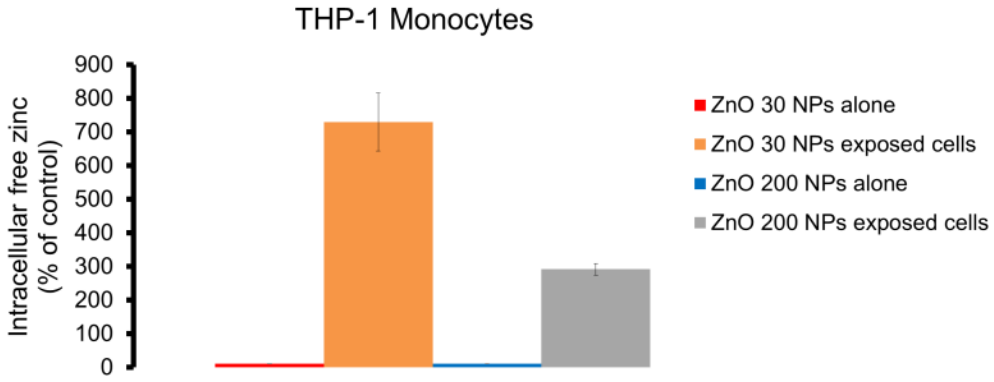

Figure 3.7 Zinquin fluorescence induced by ZnO NPs (100 μg/mL) alone or with exposed THP-1 monocytes, compared to the endogenous available zinc in untreated (control) cells (mean ± SEM, n=3 experiments) (Shen *et al.*, 2013).

A strong correlation ($R^2 = 0.945$, $p<0.0001$) between viability and intracellular zinc levels was observed across all ZnO NP formulations and concentrations for ZnO NP exposed monocytes (Figure 3.8A). A similar correlation was also observed in macrophages ($R^2 = 0.554$, $p = 0.0055$), though it was slightly weaker, presumably as a result of the complexity that these highly phagocytic cells add to the system (Figure 3.9A).

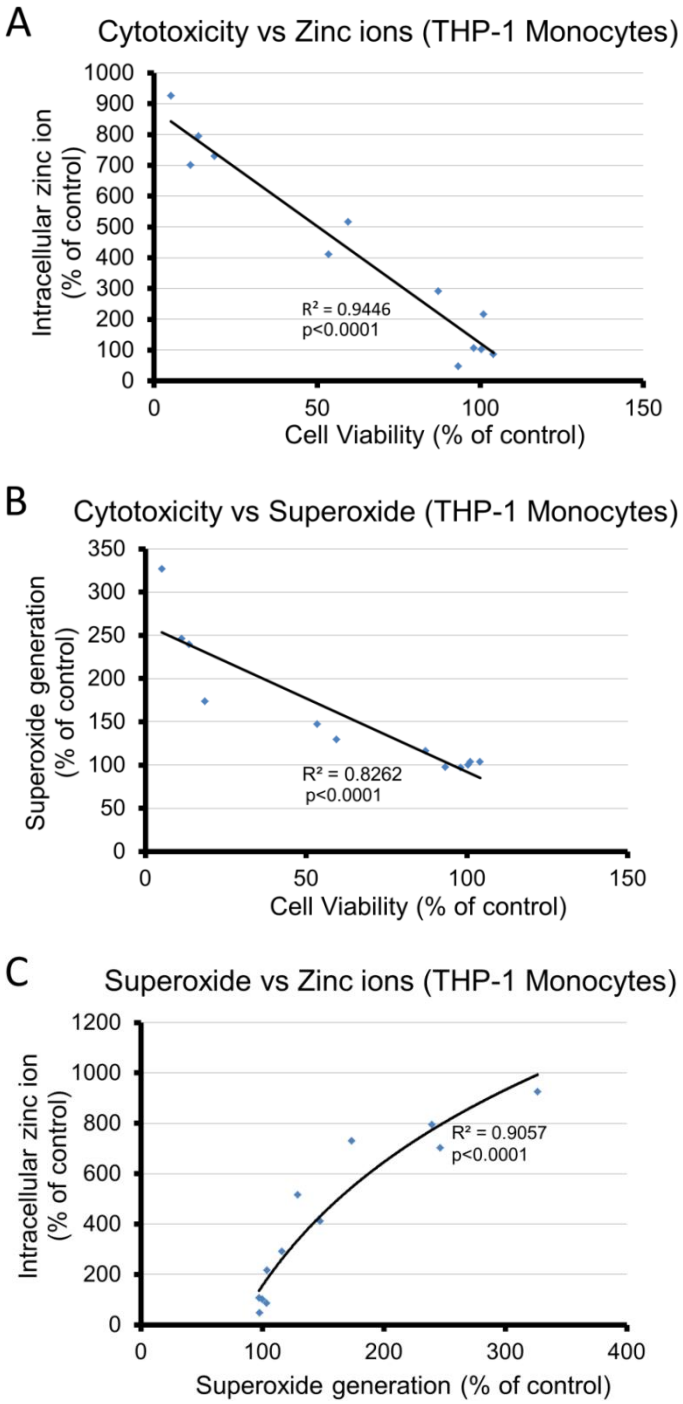

Figure 3.8 Intercorrelation of cell viability, intracellular zinc and superoxide levels in ZnO NPs (and $ZnCl_2$ as the zinc ion control) treated THP-1 monocytes. Strong relationships were observed between all of these factors, regardless of specific NP size or dispersion (Shen *et al.*, 2013).

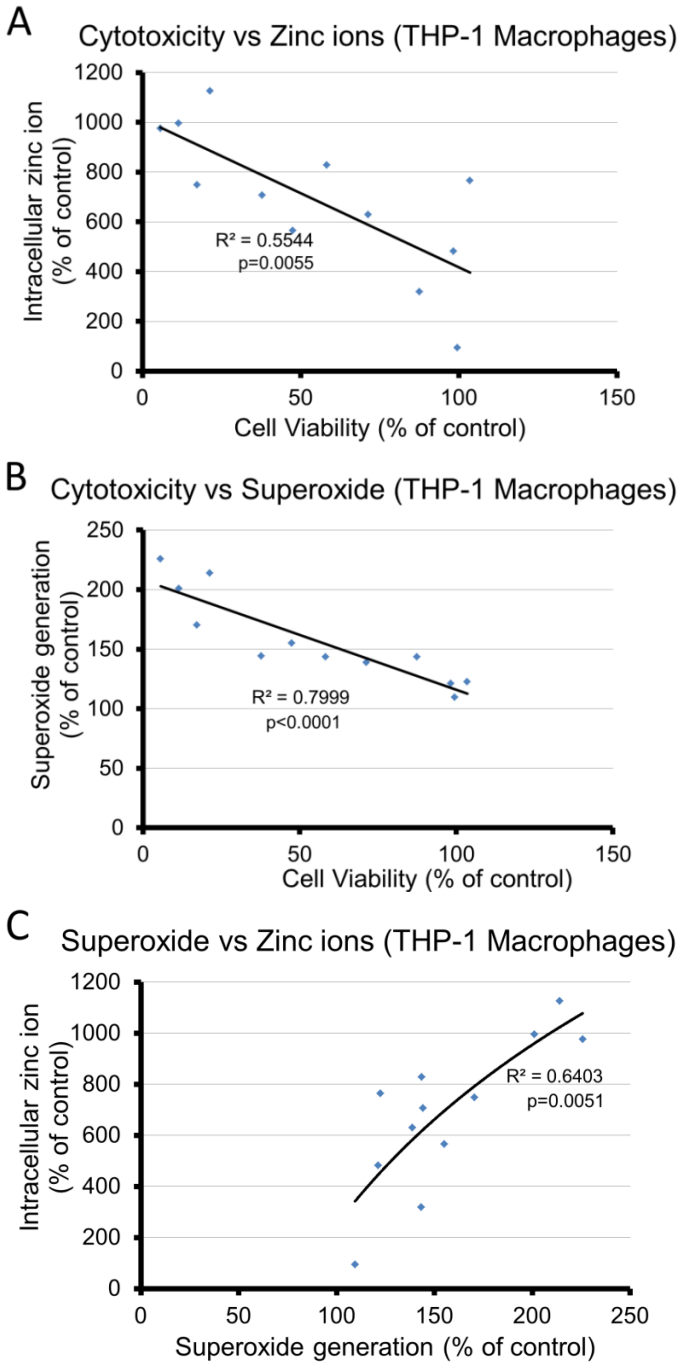

Figure 3.9 Intercorrelation of cell viability, intracellular zinc and superoxide levels in ZnO NPs (and $ZnCl_2$ as the zinc ion control) treated THP-1 macrophages (Shen *et al.*, 2013).

3.3.5 Total cell-associated zinc.

The total cell-associated zinc was assessed by ICP-MS, which showed very high zinc levels (Table 3.3), particularly at the highest ZnO NP concentration (100 μg/mL). This large excess of zinc suggests that most of the cell-associated ZnO NPs were most likely undissolved. The

total cell-associated zinc levels from sZnO NP- and $ZnCl_2$-exposed cells were near control levels, suggesting that the uptake of these more highly dispersed materials was substantially less.

Table 3.3 ICP-MS analysis of total cell-associated Zn levels* (Shen *et al.*, 2013).

Particle and Concentration	Mass of zinc (pg/cell) in Macrophages	Estimated no. of nanoparticles/cell in Macrophages	Mass of zinc (pg/cell) in Monocytes	Estimated no. of nanoparticles/cell in Monocytes
ZnO 30; 100 µg/mL	99.4 ± 2.8	1,244,575	22.9 ± 3.3	285,249
ZnO 30; 50 µg/mL	24.6 ± 2.5	300,548	5.1 ± 0.6	61,247
ZnO 30; 10 µg/mL	1.3 ± 0.1	6,614	0.3 ± 0.0	236
sZnO 30; 100 µg/mL	1.8 ± 0.1	13,145	1.9 ± 0.0	21,478
sZnO 30; 50 µg/mL	2.1 ± 0.1	16,229	0.5 ± 0.1	3,083
sZnO 30; 10 µg/mL	0.6 ± 0.0	0	0.2 ± 0.0	0
ZnO 200; 100 µg/mL	74.6 ± 0.3	3,145	56.6 ± 2.8	2,398
ZnO 200; 50 µg/mL	28.4 ± 0.3	1177	19.6 ± 0.7	825
ZnO 200; 10 µg/mL	1.7 ± 0.1	38	0.5 ± 0.0	11
$ZnCl_2$; 100 µg/mL	1.0 ± 0.0	-	0.4 ± 0.0	-
$ZnCl_2$; 50 µg/mL	0.8 ± 0.0	-	0.4 ± 0.0	-
$ZnCl_2$; 10 µg/mL	0.2 ± 0.0	-	0.3 ± 0.0	-
Control	0.8 ± 0.0	-	0.2 ± 0.0	-

*Inductively-coupled plasma mass spectroscopy (ICP-MS) was used to measure total cell-associated Zn in NP-exposed cells after 24 hr. Cell populations per well were 100,000 and 175,000 for macrophages and monocytes, respectively. NP numbers were calculated assuming nominally spherical particles with a density of 5.606 g/cm^3, after the subtraction of control concentrations of zinc. Data are expressed as mean ± standard error of duplicate wells. Acknowledgement of Bryce Feltis and Vidura Jayaratne for assistance with ICP-MS.

3.3.6 NP solubility.

Whilst the data above has shown that available intracellular zinc levels were highly related to the cytotoxicity of ZnO NPs, it was still unclear whether this Zn^{2+} mediated cytotoxicity was induced by intracellular or extracellular dissolution of NPs. To address this question, we exposed human THP-1 monocytes for 24 hr to the dialysate generated from the ZnO NPs with the highest surface area to volume ratio (ZnO 30 nm at 0.05–5 mg/mL) incubated in medium during a prior 24 hr period. Whilst we had seen that direct exposure to ZnO NPs induced cytotoxicity at high concentrations (Figure 3.5), the NP-free dialysates were not found to be cytotoxic, even when dialysates from extremely high initial ZnO NP concentrations (5 mg/mL) were tested (Figure 3.10). These data were consistent with our previous findings of a zinc precipitate that forms in biological media (Turney *et al.*, 2012). The Zn ion concentration of the dialystate was also measured in this study. By the dialysis method, the dialystate had a Zn ion level of 2.8 µg/mL for ZnO 30 NPs at 100 µg/mL after 24 hr incubation in cell culture media.

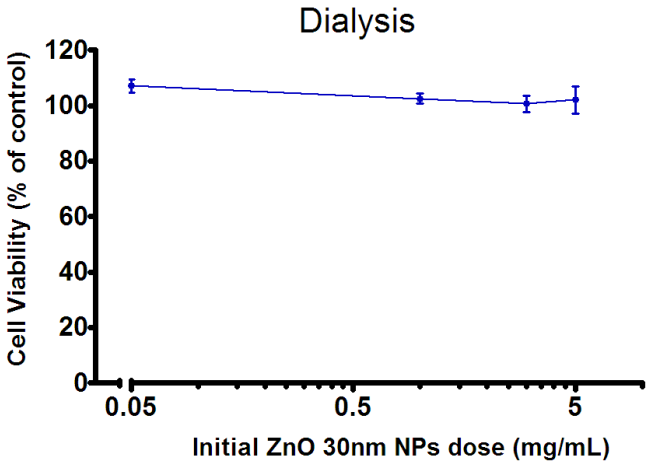

Figure 3.10 Cell viability of human THP-1 monocytes after 24 hr exposure to NP-free dialysates from initial ZnO NP concentrations (mean ± SEM, n=3 experiments) (Shen *et al.*, 2013).

3.3.7 Intracellular ROS generation.

The less specific ROS fluorophore that primarily detects peroxides (2',7'-dichlorofluorescin diacetate, DCFDA) did not show an elevation in ROS when the immune cells were exposed to ZnO NPs after 24 hr (Figure 3.11).

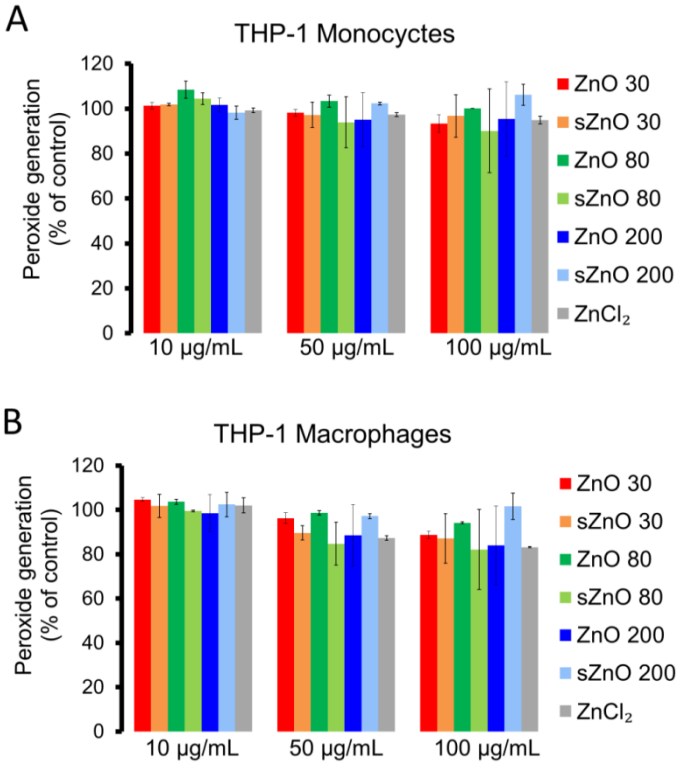

Figure 3.11 Generation of intracellular reactive oxygen (primarily peroxides by DCF) in THP-1 monocytes (A) and macrophages (B) treated with ZnO NPs or $ZnCl_2$ (zinc ion control) (mean ± SEM, n=2 experiments) (Shen *et al.*, 2013).

Mitochondrial superoxide generation was measured using the MitoSOX^{TM} Red reagent via flow cytometry. These experiments showed that with increasing concentrations of pristine ZnO NPs, mitochondrial superoxide levels were also marginally increased in both THP-1 monocytes and macrophages (Figure 3.12). Surfactant-dispersed ZnO NP exposed cells generated more mitochondrial superoxide (likely due to higher available surface area) than with pristine NPs at equivalent doses, while the Zn ion control ($ZnCl_2$) induced similar

superoxide levels to ZnO NPs. These data exhibited a strong inverse correlation between cell viability and the generation of superoxide in both monocytes (R^2 = 0.826, $p<0.0001$) and macrophages (R^2 = 0.800, $p<0.0001$, Figures 3.8B & Figure 3.9B). In addition, a strong correlation was also observed between intracellular superoxide and zinc ion levels in monocytes (R^2 = 0.906, $p<0.0001$), with a slightly weaker correlation in macrophages (R^2 = 0.640, $p=0.0051$) (Figures 3.8C & Figure 3.9C). Mitochondrial superoxide generation in THP-1 cells exposed to TiO_2 NPs was slightly, though not significantly, less than untreated cells in monocytes and 27-36% higher in exposed macrophages, though this is still lower than any of the ZnO NP exposed cells (Table 3.2).

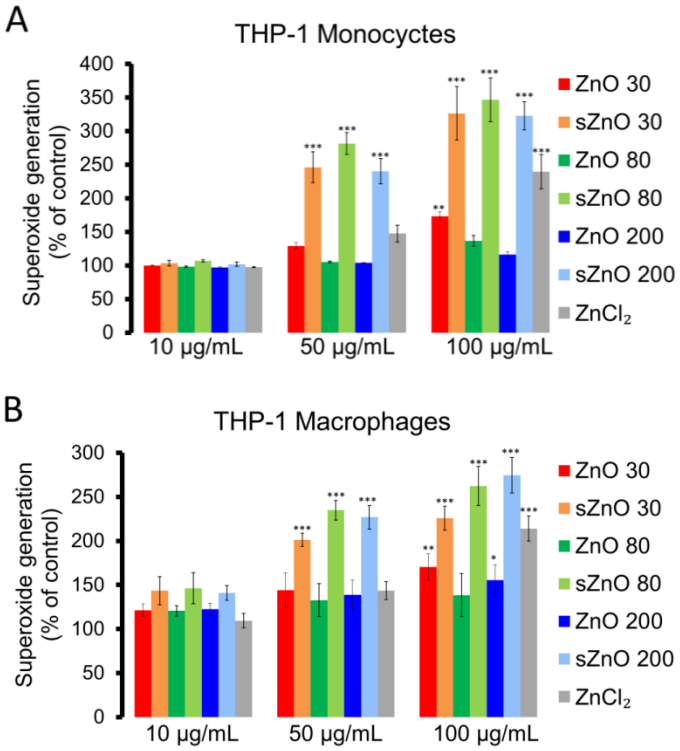

Figure 3.12 Generation of mitochondrial superoxide by THP-1 monocytes (A) and macrophages (B) after 24 hr exposure to ZnO NPs and $ZnCl_2$ (zinc ion control) (mean ± SEM, n=3 experiments). Similarly to intracellular zinc, superoxide was greater with increasing NP concentration and smaller particle size. Asterisks denote concentrations that were significantly different from untreated control cells (* $p<0.05$, ** $p < 0.01$, *** $p<0.001$) (Shen *et al.*, 2013).

3.3.8 Mitigation of superoxide generation.

Although intracellular superoxide generation was highly correlated to the cytotoxicity of ZnO NPs, it remained difficult to determine whether the observed increased intracellular superoxide was the cause of cytotoxicity, or just a consequence of mitochondrial membrane leakage, leading to cell death. As a preliminary exploration, the lipophilic antioxidant vitamin E (α-tocopherol) or the hydrophilic antioxidant vitamin C (L-ascorbic acid) were co-exposed with ZnO 30 nm NPs to cells, which showed a small decrease in cell viability within the tested concentration range (Figure 3.13A). In these co-exposure experiments, intracellular superoxide generation was slightly inhibited by both antioxidants (Figure 3.13B), but cell viability was not improved. Thus, while there was a strong correlation between cytotoxicity and reactive oxygen generation, increases in intracellular superoxide levels were not the sole cause of ZnO NP-induced cytotoxicity in this test system.

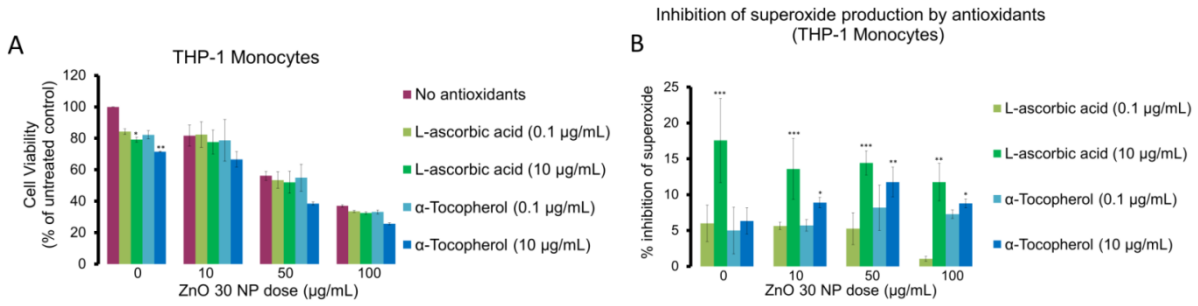

Figure 3.13 Cell viability (n=2 experiments) (A) and inhibition of mitochondrial superoxide (n=3 experiments) (B) in human THP-1 monocytes after 24 hr exposure to ZnO 30 nm NPs and antioxidants (mean ± SEM). Antioxidants did not significantly improve viability, though they did cause a small reduction in superoxide levels. Asterisks denote concentrations that were significantly different from the "no antioxidant" control cells (* $p<0.05$, ** $p < 0.01$, *** $p<0.001$) (Shen *et al.*, 2013).

3.3.9 Surface modification of ZnO NPs.

The surface modification of ZnO NPs was achieved within our joint RMIT-Monash research group by using a grafting method through the silanization reaction between organo-siloxane and the hydroxyl groups on ZnO NP surfaces. Prior to biological testing, modified NPs were comprehensively characterized by Mingdeng Luo (Monash University). Fourier transform infrared (FTIR) spectra confirmed the successful silanizaton reactions between ZnO and the coating agents (data not shown). The capping agents were adsorbed onto the ZnO surface through Zn–O–Si bonds. Compared with the bare ZnO NPs, the modified ZnO NPs exhibited characteristic peaks of the corresponding ligands. Scanning electron microscopy (SEM) was applied to characterize the primary particle size and the morphology of different grafted ZnO NPs (Figure 3.14). Analysis of SEM images revealed monodispersed hexagonal ZnO NPs with a diameter of around 40 nm. Powder X-ray diffraction (XRD) spectra confirmed that the ZnO NPs had a hexagonal wurtzite type crystal structure, both before and after surface modification (Figure 3.15). Surface charges of the different ZnO NPs were characterized by the measurement of zeta potential in water with different pH values (Figure 3.16). Pristine ZnO NPs had an isoelectric point (IEP) at about 9.1, while the IEPs of PEGylated ZnO and amino-modified ZnO NPs were 8.2 and >10, respectively. Furthermore, all the NPs were positively-charged at physiological pH (7.4). The weight loss of modified ZnO NPs was measured by thermal gravimetric analysis (TGA). Taken together, these data indicate that surface modification of ZnO NPs was successfully achieved and conferred the NPs with different surface properties.

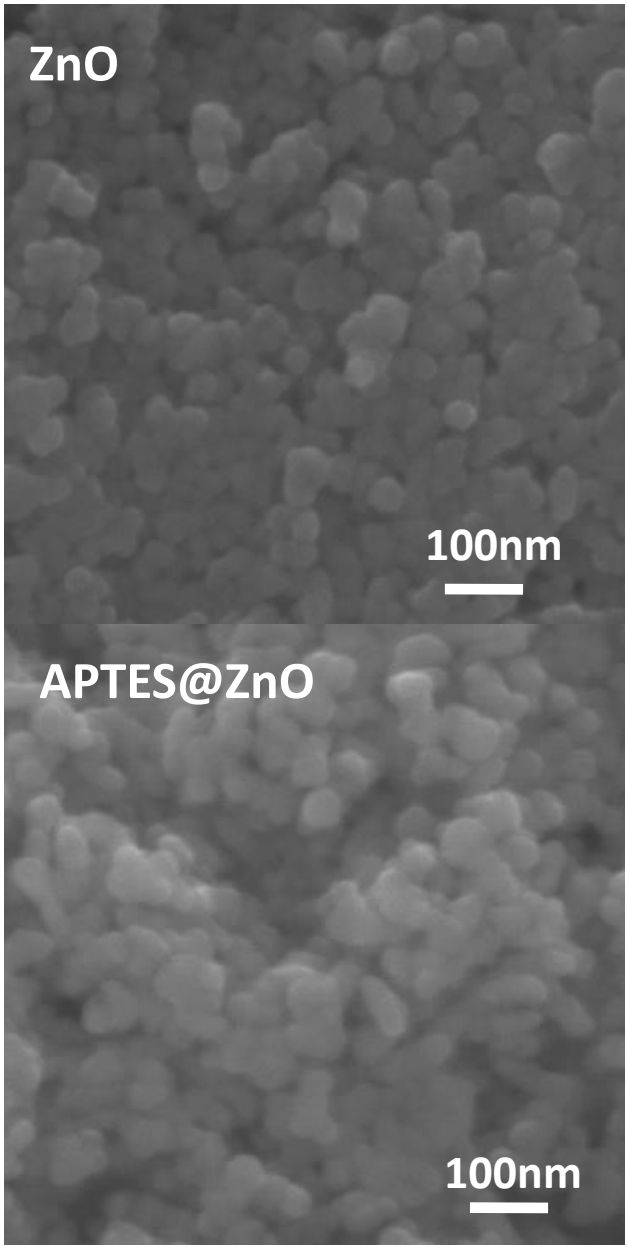

Figure 3.14 SEM images of ZnO and APTES@ZnO NPs (provided by Mingdeng Luo).

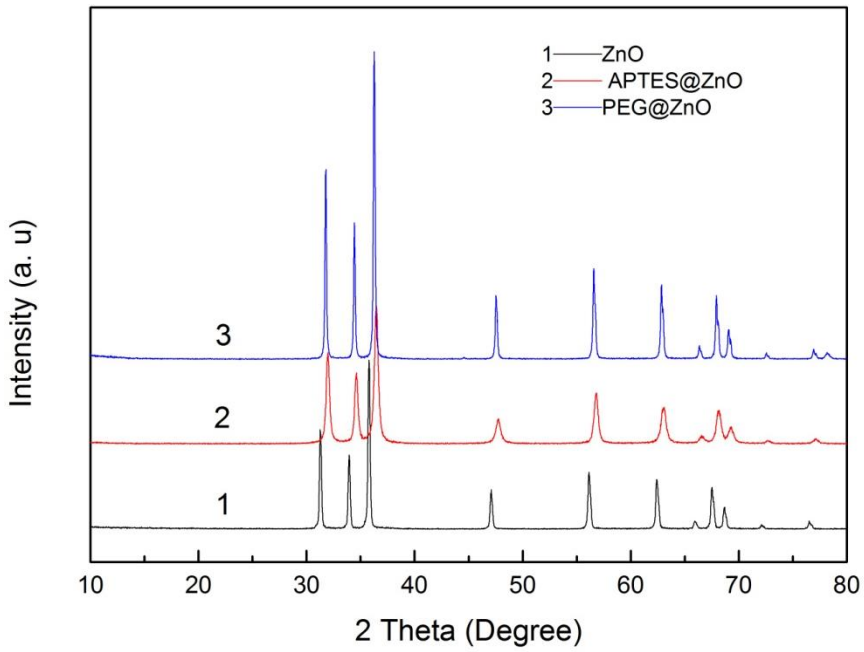

Figure 3.15 XRD patterns of bare and modified ZnO NPs (provided by Mingdeng Luo).

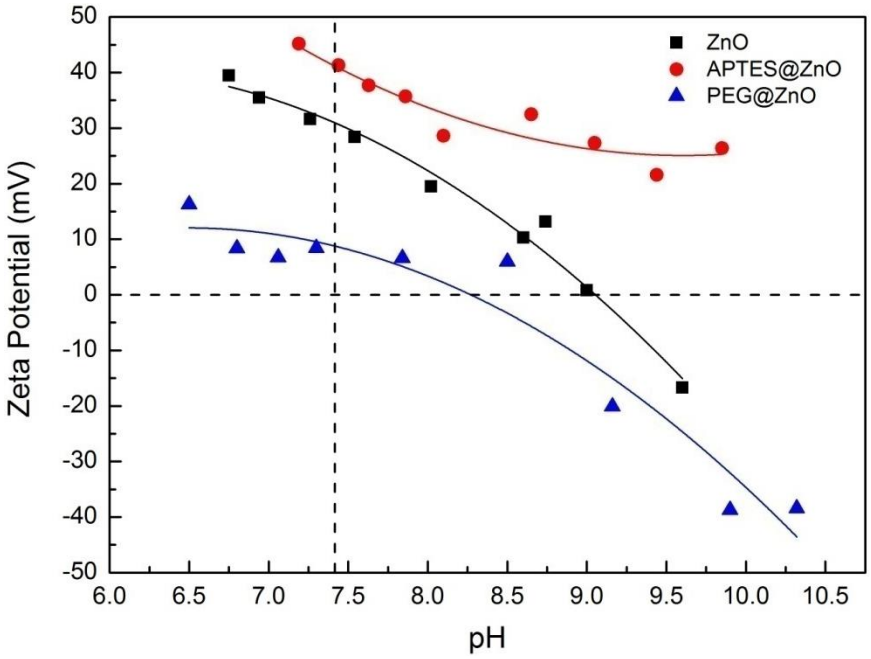

Figure 3.16 Zeta potential of pristine and surface modified ZnO NPs in water with different pH values (provided by Mingdeng Luo).

3.2.10 Biological effect of surface modified ZnO NPs on THP-1 cell lines.

The biological effects of surface modified ZnO NPs on human THP-1 monocytes and macrophages were compared with pristine ZnO NPs, by examining the cytotoxicity, intracellular zinc ions and uptake of these NPs.

The cytotoxicity of the pristine and surface modified ZnO NPs was measured by the MTS assay. In this study, THP-1 monocytes and macrophages were exposed to ZnO NPs at concentrations of 10, 50, and 100 μg/mL. As shown in Figure 3.17, all of the ZnO NPs showed a dose-dependent cytotoxicity. In the case of monocytes, the amino-modified ZnO NPs (ZnO 30 APTES) showed similar cytotoxicity as pristine NPs, while the cytotoxicity of PEGylated ZnO NPs was significantly less than that of pristine NPs. At high dose (50 and 100 μg/mL) the cell viability of PEGylated ZnO NPs treated monocytes was almost twice that following treatment with pristine NPs. In the case of macrophages, all ZnO NPs were not cytotoxic at the lowest dose (10 μg/mL). At 50 μg/mL, ZnO 30 APTES had slightly less cytotoxicity compared with pristine NPs, while PEGylated ZnO NPs showed markedly reduced cytotoxicity. At the highest dose (100 μg/mL), all NP-exposed macrophages showed very low cell viability. This is mainly due to the phagocytic properties of macrophages, which make it more sensitive than monocytes.

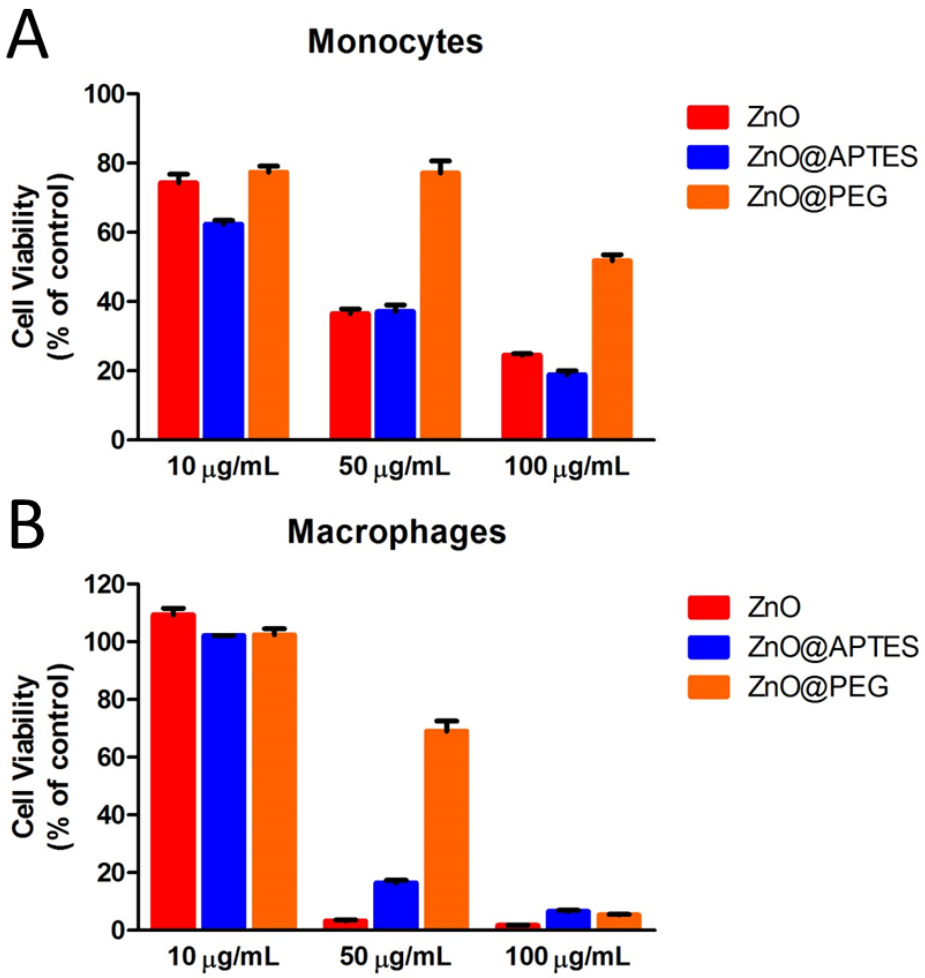

Figure 3.17 Cell viability of human THP-1 monocytes (A) and macrophages (B) after 24 hr exposure to pristine or surface modified ZnO NPs (mean ± SEM, n=3 experiments).

The intracellular zinc ion levels of cells exposed to pristine and surface modified ZnO NPs was measured by zinquin ethyl ester. The available intracellular zinc ions in both monocytes and macrophages increased gradually with increasing doses of ZnO NPs (Figure 3.18). More interestingly, at doses of 10 and 50 μg/mL cells exposed to PEGylated ZnO NPs showed the lowest levels of intracellular Zn ions compared to cells exposed to either pristine NPs or APTES modified ZnO NPs. At the highest concentration of 100 μg/mL, all ZnO NP types caused very high levels of intracellular Zn ions.

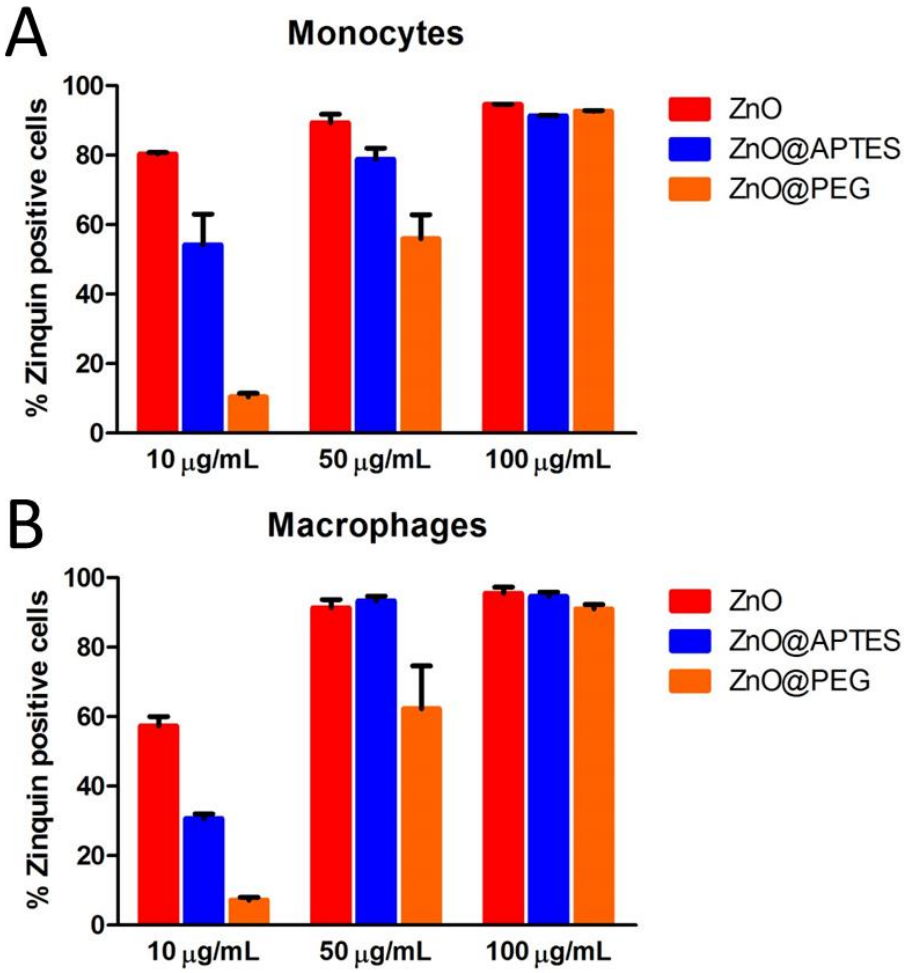

Figure 3.18 Intracellular zinc ion levels in THP-1 monocytes (A) and macrophages (B) after 24 hr exposure to pristine or surface modified ZnO NPs (mean ± SEM, n=3 experiments).

The uptake of ZnO NPs was investigated by measuring the total cell-associated zinc using ICP-MS (Table 3.4). We can see that a high level of zinc was present in all NP-exposed cells at the NP concentration investigated (50 μg/mL). The total cell-associated zinc in macrophages was about twice as much as that in monocytes. What is more, the total Zn from cells exposed to PEGylated ZnO NPs was much less compared to pristine and APTES-coated ZnO NPs, suggesting that the uptake of PEGylated ZnO NPs was significantly reduced by the PEG coating.

Table 3.4 Total cell-associated Zn concentrations determined by ICP-MS (with assistance by Mingdeng Luo).

Material and concentration	**Mass of zinc in monocytes (pg/cell[a])**	**Mass of zinc in macrophages (pg/cell[a])**
Untreated cells	n.d.[b]	n.d.[b]
ZnO; 50 μg/mL	15.87 ±0.42	25.33 ±2.84
ZnO@APTES; 50 μg/mL	15.42 ±2.59	29.93 ±3.53
ZnO@PEG; 50 μg/mL	0.98 ±0.11	1.77 ±0.08

[a] Cell populations per well were 100,000 both for monocytes and macrophages.

[b] The concentration of zinc in untreated cells was below the instrument detection limit.

3.4 Discussion

The currently understood paradigm for ZnO NP cytotoxicity is that in mammalian immune cells, ZnO NPs undergo endocytosis into the cells, dissolve into bioavailable zinc and increase oxidative stress, which then causes cytotoxicity (Figure 3.19). This study has identified that the relationship between these factors can be quantified, and a strong intercorrelation exists between intracellular zinc, oxidative stress (generated specifically from mitochondria) and cytotoxicity. In addition, extracellular dissolution of ZnO NPs in cell culture media has been shown not to be sufficient to cause cytotoxicity, indicating a lack of soluble bioavailable zinc within the cell culture environment. Finally, intracellular ROS, whilst strongly related to cytotoxicity, can also be modulated by antioxidant treatment without altering the cell viability – suggesting the standing premise that "ROS induces cytotoxicity" may be an oversimplification of a more complex series of events.

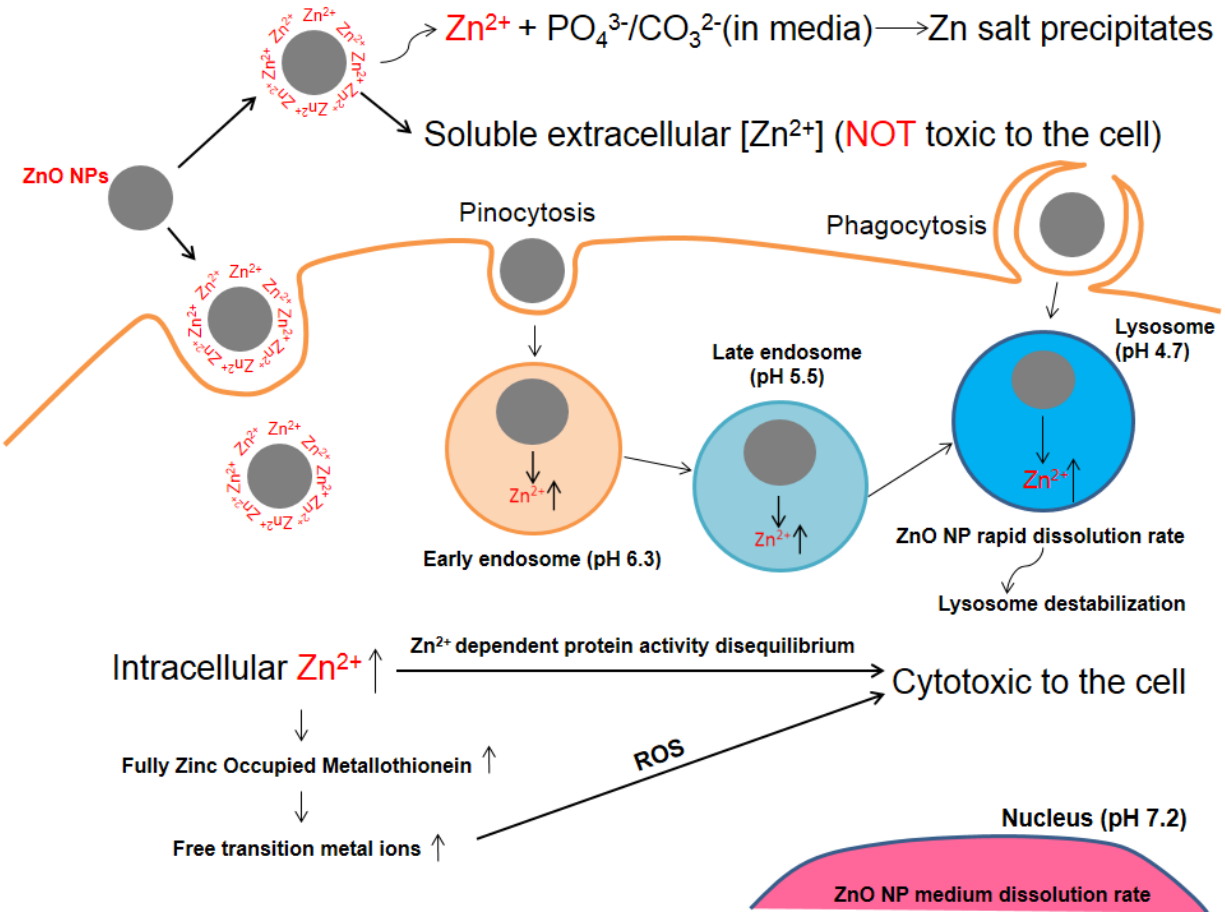

Figure 3.19 Scheme describing the mechanism of the cytotoxicity of ZnO NPs (Shen *et al.*, 2013).

This study has employed high concentrations of ZnO NPs, and although similar concentration ranges are typically used in *in vitro* studies (Muller *et al.*, 2010; Xia *et al.*, 2008), it is always important to note that these are not likely to be encountered in most *in vivo* exposure scenarios. However, such high concentrations are required to provide sufficient contrast for dose-response effects suitable for mechanistic studies, in order to elucidate the structure-activity relationships, which in this case are likely to still apply at lower *in vivo* doses.

The dual label μXFM technique, using a combination of the Co and Zn X-ray fluorescent signals, allowed for direct visualization of intact NPs without needing to modify surface chemistry with fluorescent labels or other tags. As zinc is an essential element for cellular

processes, background zinc will affect the observations, particularly in the nucleus. Therefore, we employed cobalt-doped (3.5 atom %) 30 nm zinc oxide NPs that were tested and showed no altered biological activity. Cobalt is also almost absent from the cytosol and therefore represents a cleaner signal for NP localization. Although this method alone did not specifically identify their intracellular location, it has been combined with other techniques, such as tomography or ion-beam ablation, to explore the intracellular localization of the particles (James *et al.,* 2013). The most notable finding from this work was that NPs were not observed in the nucleus. Alternate imaging techniques like scanning a cell via TEM could potentially provide similar findings, although the synchrotron technique may also allow for quantitation of larger numbers of cells.

Whilst the present study showed strong correlations between cytotoxicity and zinc ion levels, it was also necessary to control for the possibility that particle size effects were not the result of dissolution of the material. Although titania is a very different material to ZnO, the TiO_2 NPs were formulated at very similar sizes to the smallest ZnO NP used in this study, and are also of very low solubility and bioactivity. Thus, had there been intracellular NP effects that were based solely on NP size and not the chemical reactivity of the material, the presence of TiO_2 NPs of similar size would act as a control. Additionally, TiO_2 NPs are also widely formulated in sunscreens and there is always some interest in comparing these two nanomaterials. We have also previously observed TiO_2 NP uptake by immune cells via μXFM (data not shown), but the cytotoxicity of TiO_2 NPs was much less than ZnO NPs. At the highest test concentration (100 μg/mL), the majority of cells exposed to ZnO 30 nm were killed after a 24 hr exposure (viability = 20%), whereas the TiO_2 NPs at the same concentration had very little effect (viability = 90%, Table 3.2). Whilst there are expected to be some differences in uptake, the majority of the differences in cytotoxicity are likely due to

the large solubility differences between TiO_2 and ZnO NPs, the former of which are much more stable in the mildly acidic pH conditions present in the intracellular endosome (Kocbek *et al.*, 2010).

NP solubility in general can be quite variable and dependent on the source material, ZnO NPs in particular are quite unstable at both high and low pH (Zhou *et al.*, 2006). As dissolution of ZnO NPs and the subsequent release of Zn in some reactive form play such an important role in the cytotoxicity of ZnO NPs, we might have expected the extracellular dissolution to be more important than what was observed in this study. This lack of effect from soluble, extracellular zinc can be explained by some recent work, where our research group has shown that soluble zinc, when exposed to cell culture media and serum, rapidly forms a poorly soluble, amorphous zinc-carbonate-phosphate nanosized precipitate (Turney *et al.*, 2012). It may be that this precipitation effectively protects the cells from being exposed to cytotoxic concentrations of extracellular soluble zinc, as demonstrated in our dialysis experiment where this precipitate was presumably too large to pass through the dialysis membrane. This also raises the possibility of secondary nanomaterials formed from dissolving zinc containing materials under such circumstances. In the lower pH conditions present in some intracellular microenvironments, the dissolution of ZnO NPs will be much faster, resulting in a higher concentration of bioavailable zinc. It has not yet been established whether these zinc precipitates can form under cytosolic conditions. Cellular organelles such as the early endosome (pH 6.3), late endosome (pH 5.5) and lysosome (pH is 4.7) (Casey *et al.*, 2010) are at progressively lower pH levels, and it may be that the specific uptake pathway the NPs ultimately take greatly influences their intracellular stability. Indeed, some groups have suggested that the surface structure of the NP might be critical in selecting these pathways (Lundqvist *et al.*, 2008).

Measurement of total cell-associated zinc by ICP-MS yielded significantly different results to quantifying available intracellular zinc with a specific zinc ion fluorophore. As the ICP-MS measurement assesses total zinc from intracellular NP agglomerates, and also from agglomerates partially phagocytosed or attached to the outside of the cell, the measured zinc levels were very high (Table 3.3). From these data, free zinc levels (measured by zinquin, Figure 3.6) were similar between the ZnO 30 and sZnO 30 samples, yet total zinc levels (measured by ICP-MS) was vastly higher in the ZnO 30 sample, despite the sZnO 30 samples being only slightly more cytotoxic than the ZnO 30 NPs. This suggests only a small portion of the large agglomerates present in the ZnO 30 samples (Table 3.1) were actually dissolved intracellularly. In contrast, total zinc levels of dispersed ZnO and $ZnCl_2$ exposed cells were very low, suggesting that the total amount of these materials associated with the cells was much less, and the intracellular dissolution was more complete, with very little "unavailable" (agglomerated) zinc being detected. These data also showed the expected differences in uptake efficiency between the THP-1 monocytes and the more phagocytic macrophages, with the latter containing approximately twice as much total zinc.

We have shown that the cytotoxicity of ZnO NPs is highly related with the intracellular zinc ion release. As long as the ZnO NPs enter the cell, it is difficult to prevent them from dissolving due to the intrinsic properties of both NPs and intracellular fluid, which means that reducing the cytotoxicity of NPs by controlling their dissolution inside cells is difficult. Nevertheless, efforts have been made to reduce the dissolution of ZnO NPs by iron doping, which further reduced the cytotoxicity of ZnO NPs (Xia *et al.*, 2011). Although the iron in the doped ZnO NPs slowed the dissolution rate, it did not alter the uptake fate of such NPs. Therefore this approach is not an ideal methodology for the safe design of engineered

nanomaterials (Nel *et al.*, 2006). However, if we could decrease the uptake of NPs, it would reduce the cytotoxicity much more effectively. As NPs are taken up by the cell with a protein corona (Dawson *et al.*, 2009), if the formation of the protein corona is inhibited or reduced, it would be possible to reduce the overall cellular uptake of NPs. It was recently reported that the PEGylation of NPs is very effective in inhibiting the nonspecific binding of NPs to blood proteins and macrophages (Karakoti *et al.*, 2011). In this study, we also showed that modification of the surface of ZnO 30 NPs with a PEG, but not APTES, coating successfully reduced the uptake of ZnO NPs, which resulted in reduced cytotoxicity of ZnO NPs. In addition, ZnO@APTES can bind a greater quantity of protein, which is attributed to its highly positively-charged aminated surface. It may be that the decreased protein binding of PEGylated ZnO NPs inhibits the formation of its protein corona, which then decreases the uptake of such NPs into cells.

ROS is also considered to be a very important factor for the cytotoxicity of ZnO NPs and numerous studies have reported that intracellular ROS generation has at least some role in cell death induced by ZnO NPs (Song *et al.*, 2010; Xia *et al.*, 2006). As mitochondria are a major intracellular source of ROS, MitoSOX^{TM} Red was employed to measure the mitochondrial superoxide levels in our *in vitro* cell system. In this study, DCFDA were also employed to detect the intracellular peroxide, however no elevation in peroxide was observed when these cells were exposed to ZnO NPs (Figure 3.13). The strong relationship between cytotoxicity of ZnO NPs and intracellular superoxide in the current *in vitro* cell system shows a mechanistic link, but does not necessarily imply causality. There are two primary possible orientations for the “cause and effect” relationship between ROS and cytotoxicity, neither of which are mutually exclusive: The first is that the increased intracellular superoxide results in damage to organelles, which eventually fail and cause cytotoxicity. Conversely, the increased

intracellular superoxide arises from mitochondrial membrane damage, leading to electron leakage and subsequent ROS. In this scenario the failure of the mitochondria would be instigated by displacement of vital co-factors with zinc ions. However, we also cannot discount the possibility that both of these processes occur simultaneously within the cells.

The introduction of the two antioxidants vitamin E (α-tocopherol), vitamin C (L-ascorbic acid) into our *in vitro* co-exposure cell system was an attempt to ascertain the proportionate contribution of ROS to cytotoxicity. These two antioxidants were chosen for their different properties: α-tocopherol is a lipophilic antioxidant, which can quench lipid radicals; and L-ascorbic acid is water soluble, which mostly quenches the free radicals in aqueous phases. The results (Figure 3.12B) indicated that both antioxidants slightly suppress ROS, but do not affect cytotoxicity, which at the very least suggests that some of the observed intracellular superoxide levels were not responsible for ZnO NP-induced cytotoxicity in this test system. It is proposed that zinc displacement of redox-active metal ions (the primary source of ROS generation by zinc) also causes dysfunction in systems that are dependent on these other metals as co-factors. It has also been observed in other studies that ZnO NPs can cause lysosome destabilization in exposed THP-1 macrophages (Cho *et al.*, 2011), or that reactive forms of intracellular Zn^{2+} from the dissolution of ZnO NPs can cause Zn^{2+} dependent protein activity disequilibrium (Cho *et al.*, 2012) both of which could reduce cell viability. It may have been possible to suppress ROS further by using higher concentrations of antioxidants, but the concentrations we employed already showed a small decrease in cell viability, and higher doses would have confounded the interpretation of cytotoxicity data due to the direct effect of the antioxidants on the cells. Furthermore, poor penetration of the antioxidants into the cells is unlikely to explain the slight effect of these treatments, as vitamin E partitions into the cell membrane compartment and vitamin C is readily taken up by immune cells.

In this section, we have demonstrated that the intracellular dissolution of ZnO NPs, with subsequent release of bioavailable Zn, is the main determinant of cytotoxicity for ZnO NPs. Moreover, these factors both correlate strongly with each other and with intracellular reactive oxygen generation, providing strong evidence that both of these determinants are required for ZnO NP cytotoxicity in human immune cells.

Chapter 4. Comparison of UVA-induced ROS and sunscreen NP-generated ROS in human immune cells

4.1 Introduction

UV-induced ROS have been implicated in photocarcinogenesis and skin ageing (Scharffetter-Kochanek *et al.*, 1997). This is because UV-induced ROS can induce DNA damage that, if unrepaired, can lead to carcinogenesis (Ichihashi *et al.*, 2003). Such DNA damage includes single- and/or double-strand DNA breaks, base modifications (e.g. formation of 8-hydroxydeoxyguanosine (8-OHdG) and other oxidative products) and DNA cross-links (Ichihashi *et al.*, 2003). Sunscreens contain UV attenuators, such as organic chemical and/or physical UV filters, which can prevent all forms of damage from UV irradiation. However, it has been reported that organic sunscreen UV filters can actually enhance UV-induced ROS once they penetrate the epidermis (Hanson, *et al.*, 2006).

In recent years, the effective broad-spectrum UV attenuation properties of ZnO and TiO_2 NPs have made them attractive as active components in sunscreens and other personal care products. While organic sunscreens generally absorb UV light more effectively in the UVB range, only a few are able to absorb UVA. The broadest UVA attenuation is achieved with avobenzone, but this compound tends to break down on exposure to UV light and also has potential to be photo-allergenic (Paris, *et al.*, 2009). In contrast, ZnO possesses stable broad-spectrum UV filtering capabilities and is an attractive alternative to the less photo-stable avobenzone. Compared to chemical sunscreens, physical sunscreens do not break down under UV light and are therefore potentially longer-acting. In addition, the transparent properties of NP sunscreens make these products more aesthetically pleasing than the opaque formulations containing bulk particle-sized inorganic UV-filters.

As the use of NP compounds in sunscreens increases, so has public concern about their safety. One of the primary concerns raised about NPs is their potential to generate ROS, particularly when exposed to UV light (FoE, 2013). It is important to note that similar NPs are also well-known photocatalysts used in industry, which can produce a variety of ROS for an extended period under certain conditions (Barker, *et al.*, 2008). Furthermore, the high surface area properties of NPs can also increase the rate of generation of ROS. As previously discussed in section 1.4.3.3, elevated levels of mitochondrial superoxide following in vitro exposure to ZnO NPs has been confirmed in both mouse immune cell lines and human lung epithelial cells (Xia et al., 2006; Xia et al., 2008). In Braydich-Stolle's study (Braydich-Stolle et al., 2009), cytotoxicity profiling of TiO2 NPs in a mouse keratinocyte cell line showed that rutile TiO2 NPs initiated apoptosis through formation of ROS. Although there are numerous studies investigating ROS production by ZnO and TiO_2 NPs (Braydich-Stolle *et al.*, 2009; Hanley *et al.*, 2009; Lin *et al.*, 2009; Nel, *et al.*, 2006; Xia *et al.*, 2006; Xia *et al.*, 2008), there is currently a paucity of studies that investigate cellular ROS generation in the presence of both sunscreen NPs and UV irradiation. As these materials are used in sunscreens, UV co-exposure is certain, and thus it is vital to investigate ROS generation in cells co-exposed to both NPs and UV, rather than solely investigate ROS generation from NP exposure alone.

It is important to consider the most appropriate form of UV irradiation for potential interactions with NP exposure in the biological test system. As described in section 1.3.3, UVC is usually not biologically relevant, except for exposure from industrial processes, such as arc welding and microbial photosterilization. The higher energy of UVB causes more overall direct cellular damage than UVA, but the shorter UVB wavelengths only penetrate into the epidermis. However, UVA can penetrate through to the dermis and interact with cells

of the immune system and is the major contributor to sunlight's immunosuppressive effects (Halliday, *et al.*, 2011).

There is strong evidence (detailed in section 1.2.3.2) that there is negligible dermal penetration of intact metal oxide NPs past the outermost dead cell layer of the strata corneum (Gulson *et al.*, 2010). However, any intact particles that do penetrate the skin are most likely to be scavenged by phagocytic immune cells present in the dermis and peripheral vasculature, such as macrophages and their monocytic precursors. Consequently, it was stated in chapter 3 that there is a potential for these cell types to be exposed to a higher intracellular concentration of sunscreen NPs with concurrent UVA exposure. Therefore, in this study we have co-exposed human THP-1 monocyte-like cells to both UVA and metal oxide NPs, and assessed ROS generation – specifically intracellular peroxide and mitochondrial superoxide levels. We examined ROS generation in monocytes rather than macrophages because although both cell types phagocytose NPs, the lower basal ROS activity in monocytes (Feltis *et al.*, 2012; Shen *et al.*, 2013) facilitated the direct comparison of the individual effects of UVA and NP exposure on ROS generation with the effects of UVA and NP co-exposure. We also assessed the time course of intracellular ROS generation under these exposure conditions in order to evaluate the relative contribution and impact of UVA-induced ROS compared with sunscreen NP-generated ROS.

4.2. Materials and methods

4.2.1 Materials.

ZnO NPs with primary particle diameters of 30 and 200 nm, with and without surfactant dispersant (Orotan 731 DP) were used in this study. Anatase TiO_2 (25 nm) and rutile TiO_2

(34 nm) NPs were kindly provided by CSIRO, Clayton, Australia. Full physical characterization methods and results for these materials are described in sections 2.1 and 3.3.1.

4.2.2 Cell culture, UV irradiation and cytotoxicity assays.

THP-1 monocytes were used in this study. The particle preparation for addition to the test system is described in section 2.2, while the THP-1 cell culture and *in vitro* NP exposure methods are described in section 2.3.1. Immediately following the addition of NPs, the cells were exposed to UVA radiation (6.7 J/cm^2) using a solar simulator (Vilber Lourmat, Marne-la-Vallee, France). Control groups included wells containing cells without NPs, and with either UVA irradiation or no UV (sham) radiation exposure – the sham irradiation group controlled for potential effects of time spent outside of the incubator during the irradiation procedure. Following UVA irradiation, the cells were returned to the incubator. After 20 hr, MTS reagent was added to each well and incubated for 4 hr before being measured at 490 nm on a plate reader as described in section 2.4.2. Wells containing the concentration range of NPs and MTS reagent alone was used to control for any direct optical density effects of NPs by subtracting these values from the experimental readings. All treatments were performed in triplicate for each of three experiments.

4.2.3 Intracellular ROS generation.

In this study, ROS generation over a 22 hr time-course was measured in the forms of intracellular peroxide and mitochondrial superoxide by DCFDA and MitoSOX^{TM} Red, respectively.

For the DCFDA assay, fluorophore-preloaded cells were seeded into black 96-well plates at 10^5 cells per well, and then co-exposed with NPs and UVA, as described in sections 2.5.1 and 4.2.2, respectively. The specific fluorescence was measured after incubation time points of 1, 4, 8 and 22 hr. All treatments were performed in triplicate for each of three experiments.

For the MitoSOX^{TM} Red assay, fluorophore-preloaded cells were seeded into standard 96-well plates at 10^5 cells per well, and then co-exposed with NPs and UVA, as described in sections 2.5.2 and 4.2.2, respectively. After incubation time points of 1, 4, 8 and 22 hr, cells were fixed (in -20℃ ethanol) and analyzed using flow cytometry. All treatments were performed in triplicate for each of two experiments.

4.2.4 Statistics.

Data were presented as mean ± standard error of mean (SEM) and was analysed using two-way ANOVA and Bonferroni post hoc test (Prism 5.0, GraphPad Software, La Jolla, CA, USA), with a p value < 0.05 considered significant.

4.3 Results

4.3.1 Cytotoxicity of sunscreen NPs

The viability of THP-1 monocytes 24 hr after exposure to UVA dose was unchanged and was 103.5 ± 1.7%, compared to the viability in untreated cells of 100.0 ± 2.2% (n=3 experiments). When these cells were co-exposed to both UVA and sunscreen NPs (Figure 4.1), the cell viability after 24 hr was not significantly altered from exposure to NPs alone (Figure 3.5A), which indicates that the UVA dose used in this study is not directly cytotoxic.

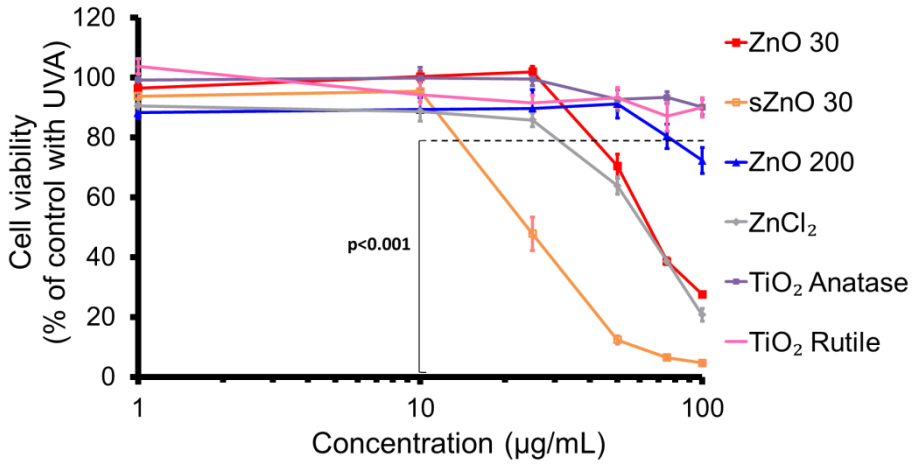

Figure 4.1 Cell viability of human THP-1 monocytes after 24 hr exposure to sunscreen NPs, following initial co-exposure to 6.7 J/cm^2 UVA (mean ± SEM, n=3 experiments). All concentrations at or below the horizontal line were highly significantly different from control cells receiving UVA irradiation alone ($p < 0.001$).

4.3.2. Peroxide generation.

We observed that UVA exposure induced high levels of intracellular peroxide, *i.e.* at 1 hr the peroxide levels were 7-fold higher than that of sham-irradiated control (Figure 4.2). Comparing peroxide generation at each time point to that of the sham control at 1 hr, we observed that UVA-induced peroxide generation steadily increased (although this did not reach statistical significance; p=0.18) over the 22 hr time period to reach 8.5-fold (Figure 4.2A). We also saw that a comparison of the peroxide generation at each time point with its respective sham control at that same time point, exhibited an apparent decrease in the relative UVA-induced peroxide generation over time (Figure 4.2B).

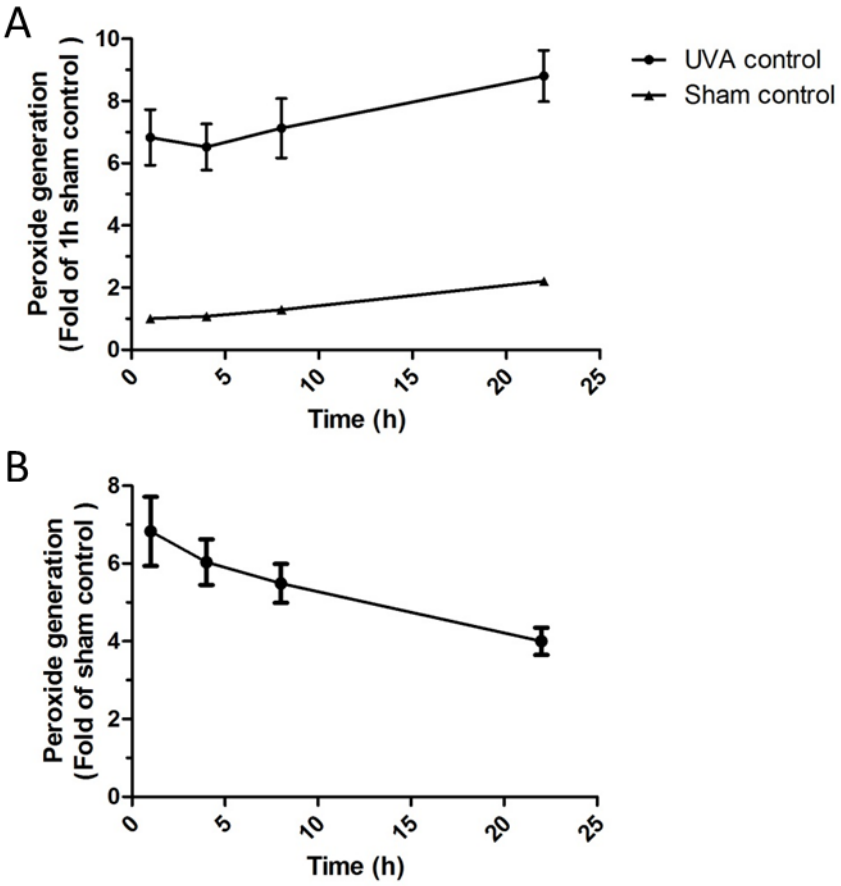

Figure 4.2 Generation of intracellular peroxide by THP-1 monocytes over the 22 hr time course after initial exposure to 6.7 J/cm^2 UVA; represented as a ratio of the sham control at 1 hr (A), and as a ratio of the respective sham control for each time point (B) (mean ± SEM, n=3 experiments in triplicate).

In this study, we also employed hydrogen peroxide (H_2O_2) at 1 mM as a positive control. This concentration of H_2O_2 was chosen to generate the same level of peroxide ROS in THP-1 monocytes as the experimental UVA dose (6.7 J/cm^2) (Figure 4.3). The kinetic profile of peroxide generation over 22 hr for 1 mM H_2O_2 and 1.67 MED UVA was also very similar. In Figure 4.3A, the time course of the peroxide generation in H_2O_2-treated cells increased from 7-fold at 1 hr to 8.5-fold at 22 hr compared to the 1 hr sham control. When comparing the peroxide generation at each time point to its respective sham control at that same time point, we also observed a similar decrease trend in relative UVA-induced peroxide generation over time (Figure 4.3B).

In order to compare UV-induced peroxide production to sunscreen NP-generated peroxide, cells were exposed to NPs both with and without UVA co-exposure. Overall, the co-exposure of cells to ZnO NPs and UVA showed a dose-dependent decrease in intracellular peroxide generation (Figure 4.4). At low and intermediate doses of the pristine ZnO 30 nm ("ZnO 30") or ZnO 200 nm ("ZnO 200") particulates that did not directly alter cell viability (*i.e.* 10 and 50 μg/mL) (Figure 4.1), the intracellular peroxide levels were not significantly altered by co-exposure with UVA. At the highest dose (100 μg/mL) these particulates decreased intracellular peroxide levels, but also reduced cell viability.

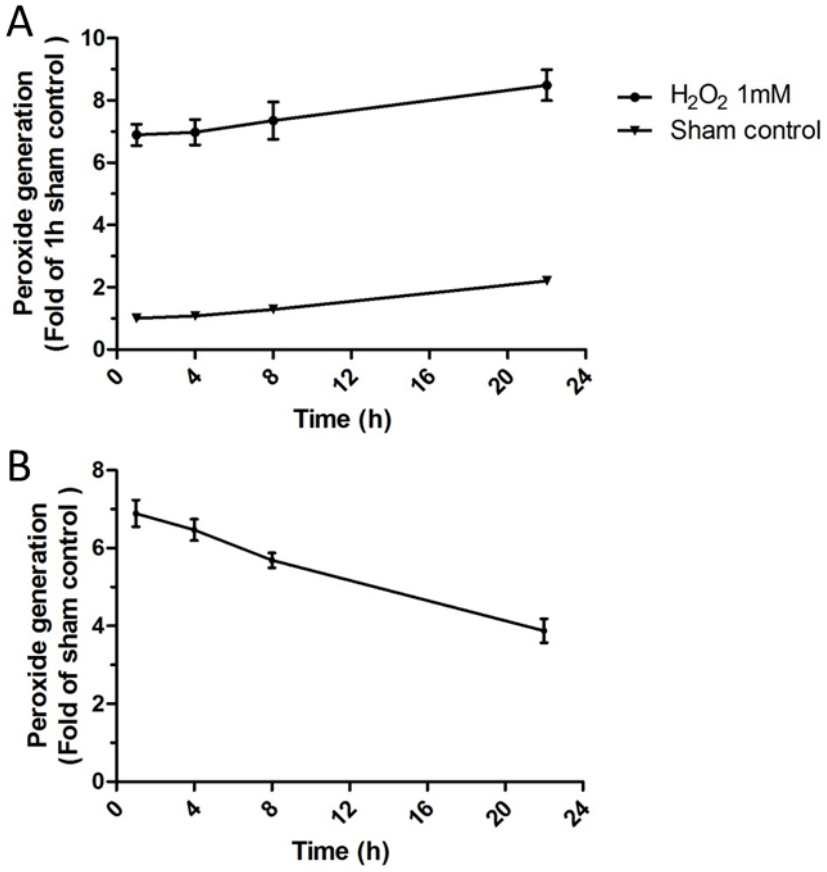

Figure 4.3 Generation of intracellular peroxide by THP-1 monocytes over the 22 hr time course after exposure to 1 mM H_2O_2; represented as a ratio of the sham control at 1 hr (A), and as a ratio of the respective sham control for each time point (B) (mean ± SEM, n=3 experiments in triplicate).

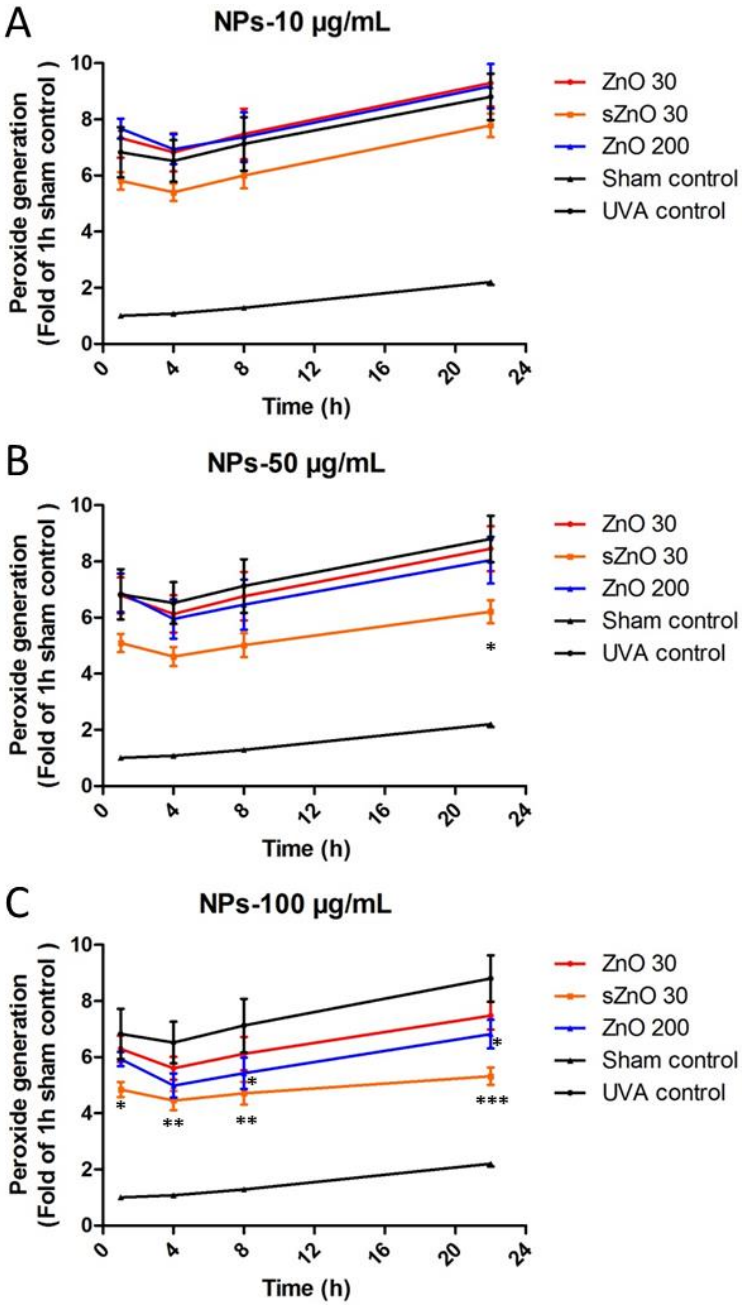

Figure 4.4 Generation of intracellular peroxide by THP-1 monocytes over the 22 hr time course after exposure to ZnO 30 NPs or ZnO 200 bulk particles at 10 µg/mL (A), 50 µg/mL (B), and 100 µg/mL (C), following initial co-exposure to 6.7 J/cm^2 UVA; represented as a ratio of the sham control at 1 hr (mean ± SEM, n=3 experiments in triplicate). Time points marked with stars were significantly different from control cells receiving UVA irradiation alone (* $p < 0.05$, ** $p < 0.01$, *** $p < 0.001$).

The surfactant-dispersed ZnO 30nm ("sZnO 30") was seen to be the most effective particulate, by significantly reducing the peroxide generation in UVA co-exposed monocytes at the intermediate dose (50 μg/mL) (Figure 4.4). At the highest dose, the sZnO NPs further decreased peroxide levels, but also markedly reduced cell viability. Therefore, as the lowest dose of sZnO 30 NPs did not alter cell viability, this slight peroxide reduction appeared to be mainly attributable to attenuation of UV by the particles, even in their dispersed state.

In order to verify this, we measured the UV-vis spectra of the three particulates, which confirmed a much higher absorbance for sZnO 30 than for ZnO 30 in the UVA spectral wavelengths (Figure 4.5). We also found no significant differences in UVA absorbance for ZnO 200 and ZnO 30, which would explain why their peroxide generation profile was very similar (Figure 4.4). As expected, this UVA attenuation also increased with dose, which may account for the observed decreases in peroxide generation in THP-1 monocytes with increasing NP dose. Re-plotting Figure 4.4 as a ratio of the respective UVA control for each time point (as opposed to the 1 hr UVA control) resulted in different profiles in which peroxide generation did not increase over time (Figure 4.6).

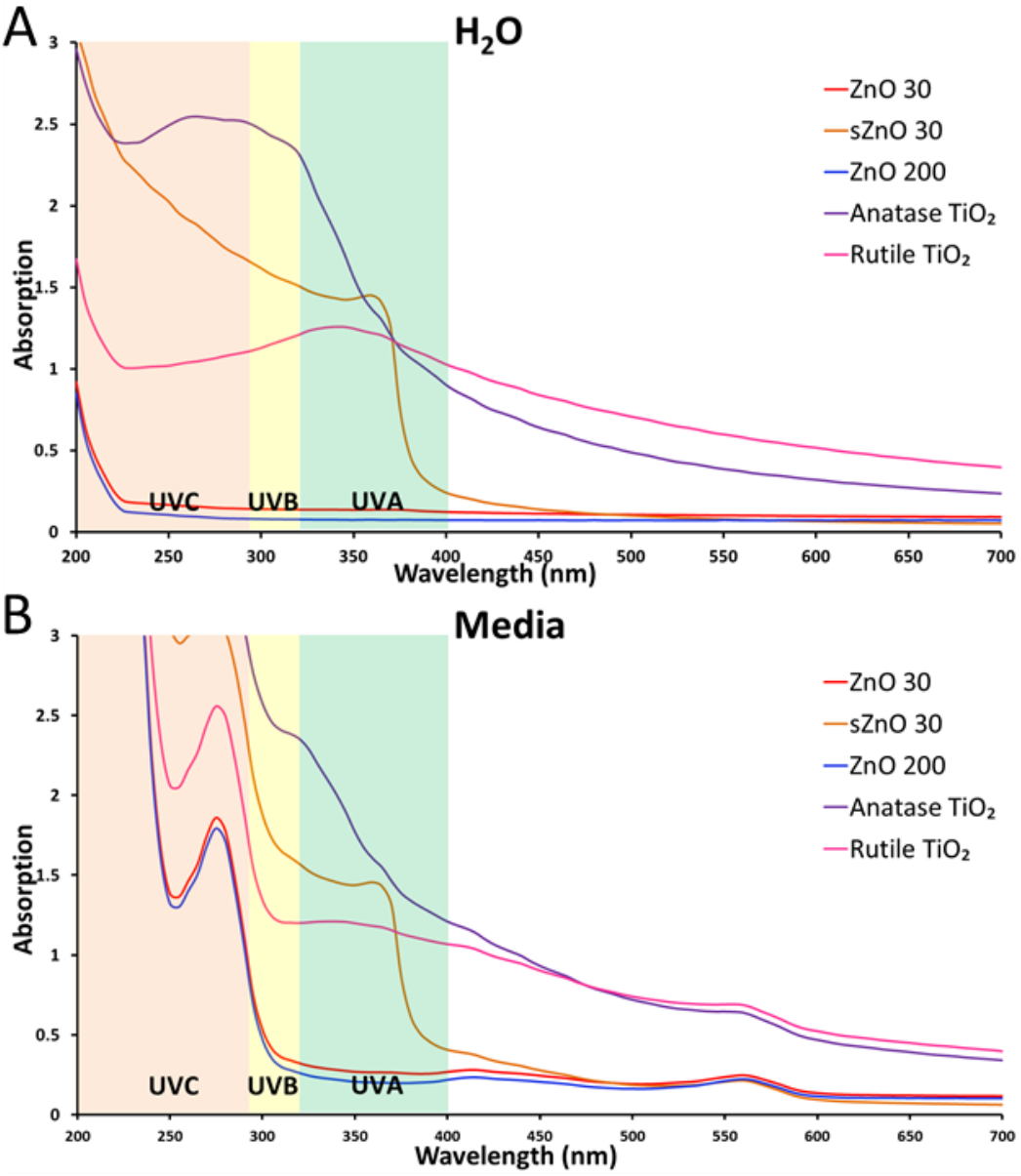

Figure 4.5 UV-Vis spectra of ZnO and TiO_2 NPs (100 µg/mL) in water (A) and RPMI-1640 phenol red media with 10% FBS (B).

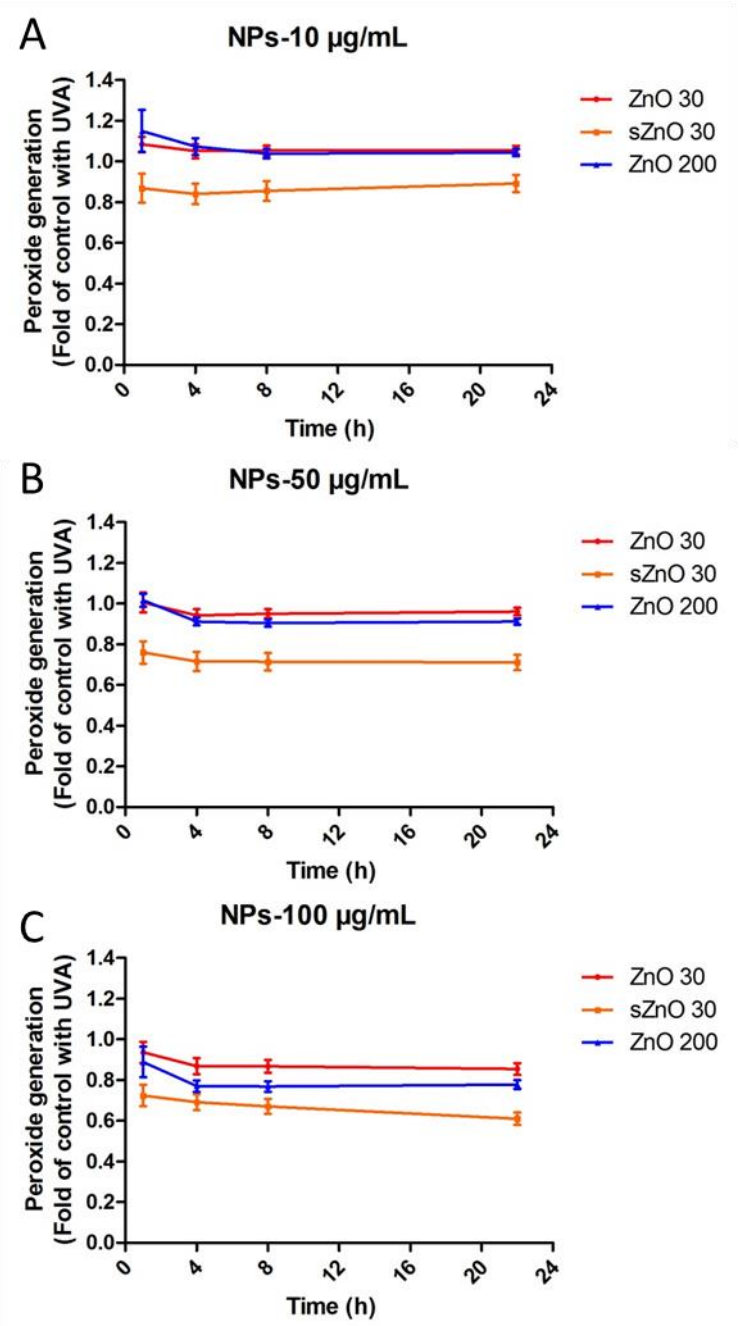

Figure 4.6 Generation of intracellular peroxide by THP-1 monocytes over 22 hr of exposure to ZnO 30 NPs or ZnO 200 bulk particles at 10 µg/mL (A), 50 µg/mL (B), and 100 µg/mL (C), following initial co-exposure to 6.7 J/cm^2 UVA; represented as a ratio of the respective UVA-exposed control for each time point (mean ± SEM, n=3 experiments in triplicate).

Titania NPs, unlike ZnO, did not cause cytotoxicity in UVA-exposed cells at concentrations less than 1 mg/mL (Figure 4.7). The observed peroxide production profile in the TiO_2-UVA co-exposure system was different between the crystalline forms, with anatase TiO_2 NPs behaving substantially different from both rutile and ZnO NPs (Figure 4.8). For anatase TiO_2 NPs, the peroxide levels increased with increasing concentration (Figure 4.8). In contrast, rutile TiO_2 behaved similarly to ZnO, with peroxide levels decreasing with increasing concentrations. Consequently at the highest dose of 100 μg/mL TiO_2, the peroxide generated by cells exposed to anatase in the presence of UVA was twice that seen with rutile and UVA co-exposure (Figure 4.9). It should be noted that the increased generation of ROS by co-exposure to anatase TiO_2 and UVA irradiation was still insufficient to reduce cell viability, until extremely high concentrations were used (1 mg/mL) (Figure 4.7). In this study, we also measured peroxide generation without UV. In the absence of UV (Figure 4.10), we observed that ZnO and TiO_2 alone generated much less peroxide than with UVA exposure alone (Figure 4.2).

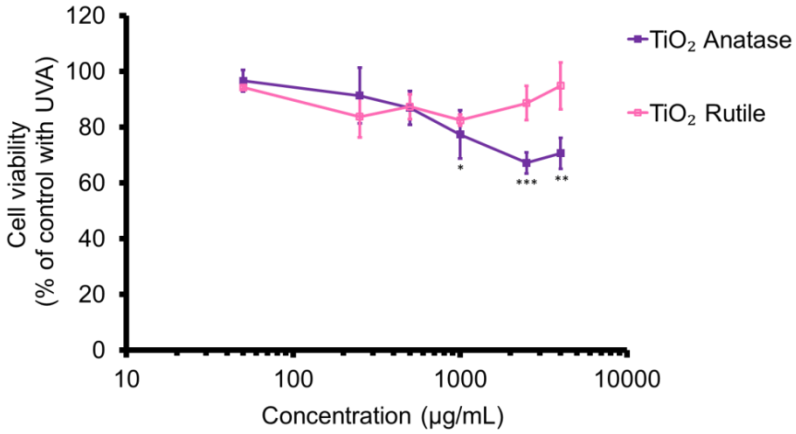

Figure 4.7 Cell viability of human THP-1 monocytes after 24 hr exposure to TiO_2 anatase or rutile NPs, following initial co-exposure to 6.7 J/cm^2 UVA (mean ± SEM, n=3 experiments in triplicate). Asterisks denote significant difference from control cells receiving UVA irradiation alone (* $p < 0.05$, ** $p < 0.01$, *** $p < 0.001$).

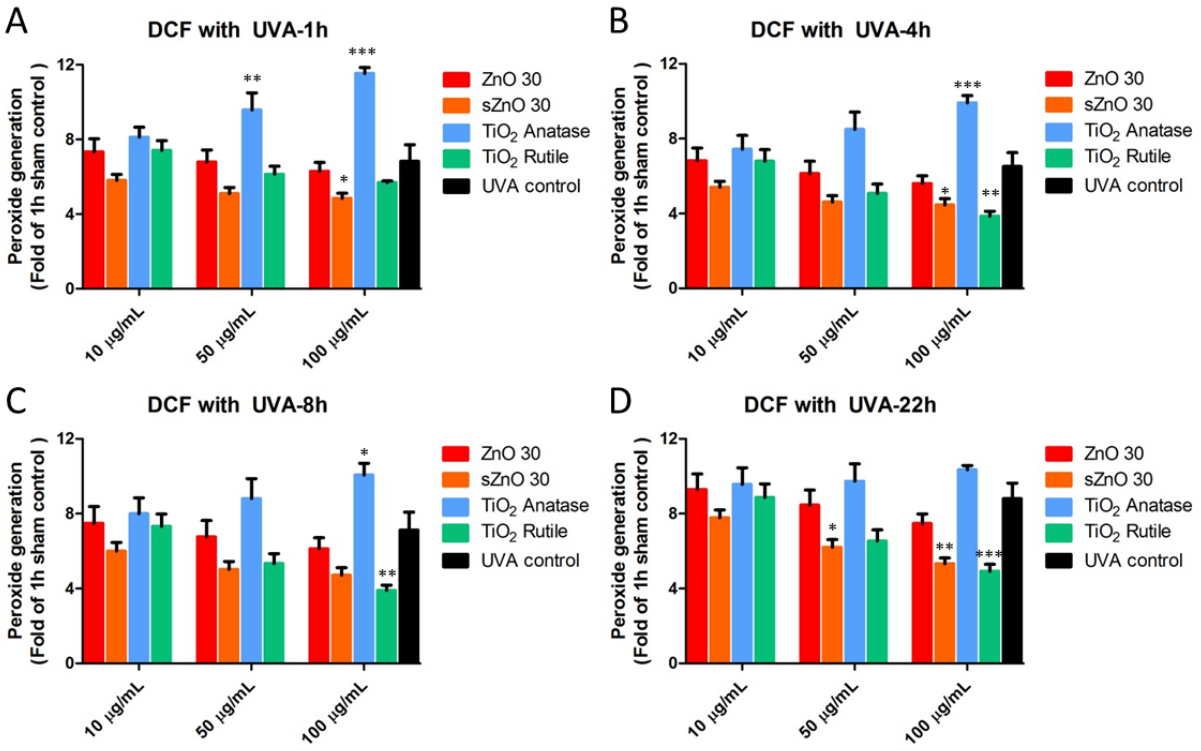

Figure 4.8 Generation of intracellular peroxide by THP-1 monocytes after 1 hr (A), 4 hr (B), 8 hr (C) and 22 hr (D) exposure to ZnO or TiO_2 NPs, following initial co-exposure to 6.7 J/cm^2 UVA; represented as a ratio of the sham control at 1 hr (mean ± SEM, n=3 experiments in triplicate). Asterisks denote significant difference from control cells receiving UVA irradiation alone (* $p < 0.05$, ** $p < 0.01$, *** $p < 0.001$).

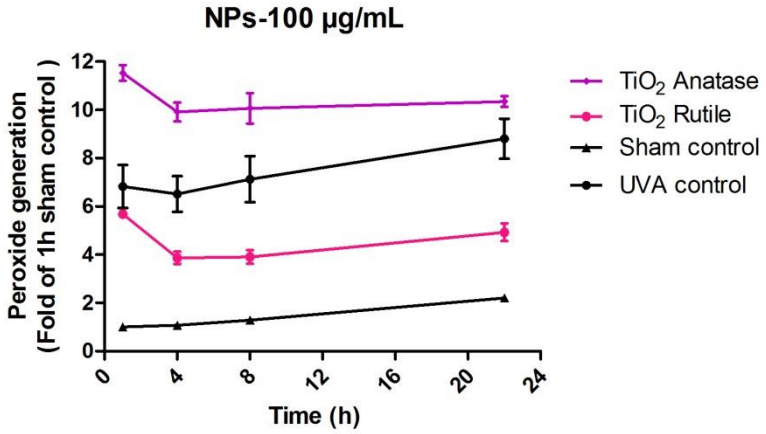

Figure 4.9 Generation of intracellular peroxide by THP-1 monocytes over 22 hr exposure to 100 µg/mL TiO_2, following initial co-exposure to 6.7 J/cm^2 UVA; represented as a ratio of the sham control at 1 hr (mean ± SEM, n=3 experiments in triplicate).

4.3.3 Superoxide generation

UVA-irradiated cells also produced high levels of mitochondrial superoxide when compared to negative controls (Figure 4.11). However, these increased levels of superoxide were not as high as peroxide levels produced under UVA, as superoxide levels were 3.3 fold higher at the 1 hr time point compared to the 7-fold higher peroxide generation.

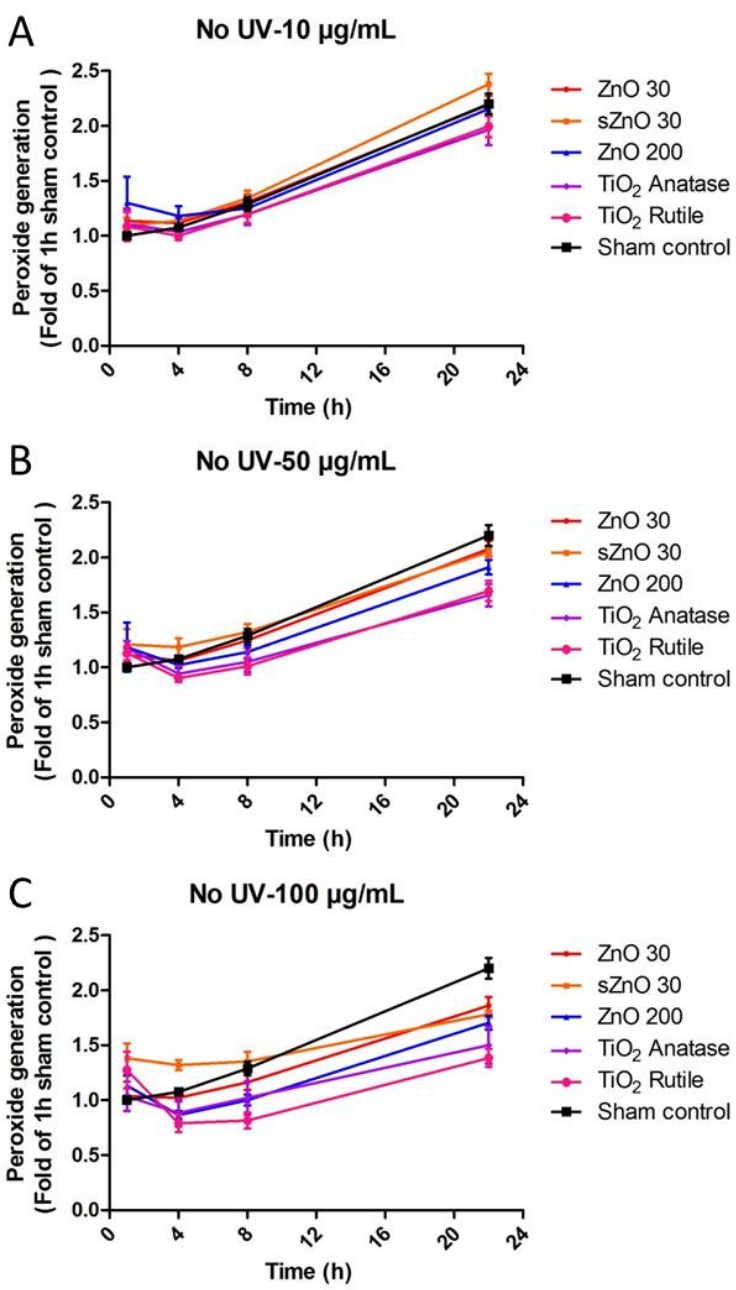

Figure 4.10 Generation of intracellular peroxide by THP-1 monocytes over 22 hr of exposure to ZnO or TiO_2 NPs at 10 µg/mL (A), 50 µg/mL (B), and 100 µg/mL (C); represented as a ratio of the sham control at 1 hr (mean ± SEM, n=3 experiments in triplicate).

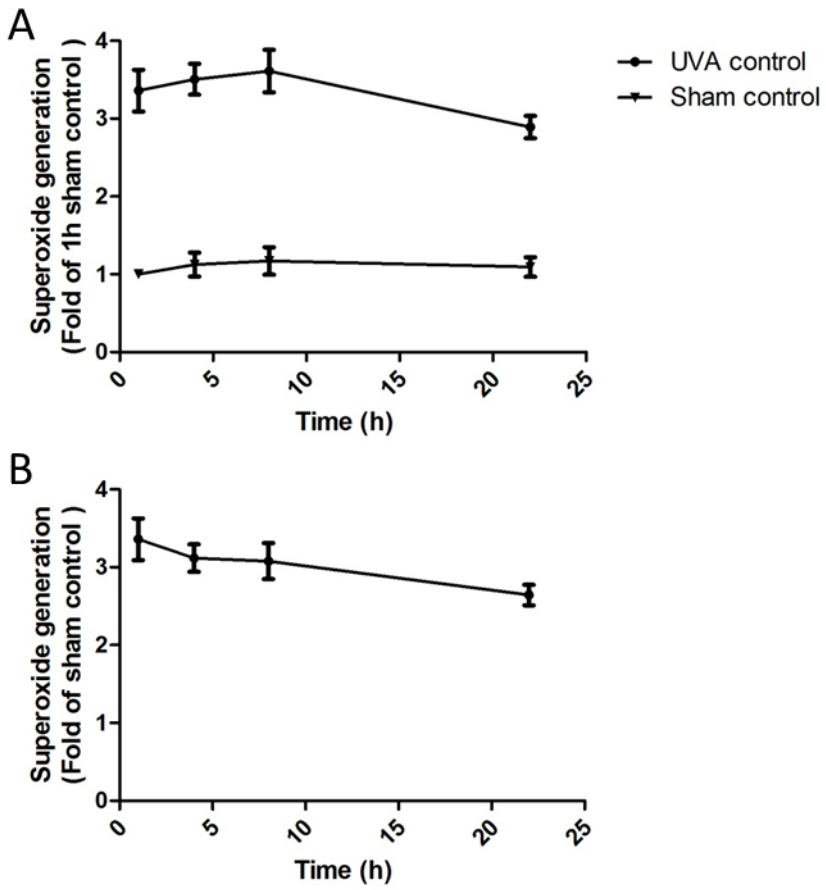

Figure 4.11 Generation of mitochondrial superoxide by THP-1 monocytes over the 22 hr time course, following initial exposure to 6.7 J/cm^2 UVA; represented as a ratio of the sham control at 1 hr (A), and as a ratio of the respective sham control for each time point (B) (mean ± SEM, n=2 experiments in triplicate).

In order to investigate the effect of UVA and NP co-exposure, we compared the mitochondrial superoxide generation after exposure to NPs at either equivalent cytotoxicities (EC50) for ZnO, or at 100 μg/mL for TiO_2 NPs, with and without UVA irradiation. At equivalent cytotoxicity dose the oxidative stress on the cell will also be equivalent, unlike using the same mass based concentration, it therefore becomes possible to comparatively measure the sources of the oxidative stress. At the 1 hr time point, with the exception of anatase TiO_2, the other NPs did not alter superoxide generation (Figure 4.12).

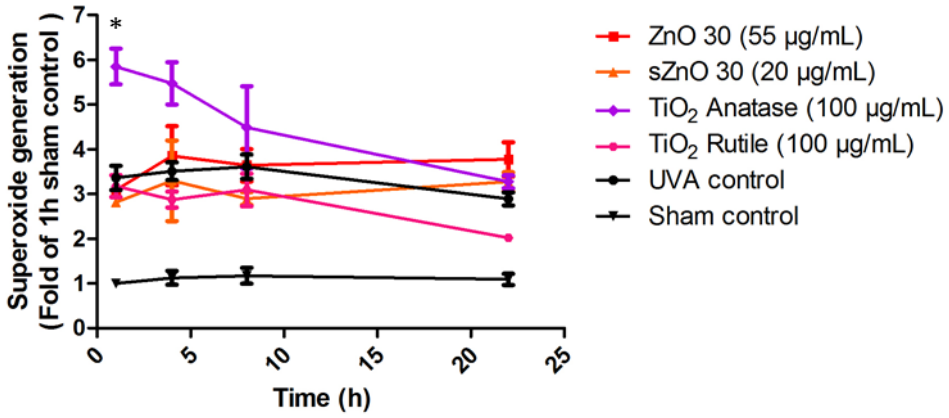

Figure 4.12 Generation of mitochondrial superoxide by THP-1 monocytes over 22 hr exposure to ZnO or TiO_2 NPs, following initial co-exposure to 6.7 J/cm^2 UVA; represented as a ratio of the sham control at 1 hr (mean ± SEM, n=2 experiments in triplicate). Time points marked with stars were significantly different from control cells receiving UVA irradiation alone (* $p < 0.05$).

The kinetics for mitochondrial superoxide generation in cells with UVA and particulate co-exposure was also different to that for peroxide generation (Figure 4.12). In TiO_2-exposed cells, superoxide levels continued to gradually decrease over time after the initial rapid decline for anatase-exposed cells, whereas both ZnO 30 and sZnO 30 marginally increased mitochondrial superoxide levels over the same period.

4.4 Discussion

In this study, we compared the ROS generation by UVA and sunscreen NPs in human immune cells. The UVA component of sunlight's UV spectrum is 95%, with the remaining 5% being the UVB component that causes erythema of the skin. The UVA dose used in this study was the UVA component of sunlight corresponding to 1.67-fold of the Minimal Erythemal Dose (MED) (6.7 J/cm^2) (Kuchel, *et al.*, 2002), which is equivalent to the UVA component of

approximately 30 minutes of noonday summer sun in Sydney, Australia, at 33.86 ºS latitude. This UVA dose was not directly cytotoxic to the cells in this *in vitro* test system.

In measuring intracellular peroxide generation, we employed the ROS fluorophore DCFDA, which is sensitive to all forms of peroxide, including hydrogen peroxide (Halliwell, *et al.*, 2004). In our study, we have seen that UVA-induced peroxide generation steadily increased if we compared peroxide generation at each time point to that of the sham control at 1 hr. This fixed-time point control comparator was necessary, as we also observed that when comparing the peroxide generation at each time point to its respective sham control at that same time point, there was an apparent decrease in relative UVA-induced peroxide generation over time (Figure 4.2B). This experimental artefact was due to changes in the test to control ratios that were a product of both treatment and control peroxide levels increasing over time, most likely as a function of normal cellular metabolism (Poljsak *et al.*, 2005). This is illustrated by the observation that the peroxide generated by the sham control increased by an amount very similar to the UVA-treated control (Figure 4.2A). Thus, when expressed as a ratio of its respective sham control, the 24 hr value is approximately half that of the value obtained from the 1 hr time point (Figure 4.2B), which may be a significant confounder in the interpretation of time course measurements using DCFDA, or indeed any measurement of this fluorophore at a single time point. In our study, we also observed a similar kinetic profile of peroxide generation over 22 hr for both 1 mM H_2O_2 and 1.67 MED UVA. Again, the increase in cellular peroxide is likely to be from normal cellular metabolism and shows that these DCFDA artefacts are consistent across different experimental systems for this cell type.

As it is a critical component for determining the relative risk of NPs when used in sunscreen formulations, we have investigated ROS generation by these NPs in human THP-1 monocyte

immune cells following UVA co-exposure. The concentrations of ZnO NPs required in this system to generate detectable levels of ROS were close to the concentrations required to induce cytotoxicity (see Figure 4.1). Regarding peroxides, co-exposure of cells to ZnO NPs and UVA resulted in a dose-dependent decrease in peroxide generation. As the three ZnO particulates displayed different cytotoxicity profiles, the respective contributions of reduced viable cell number versus UVA attenuation towards the decreased peroxide generation varied between these particulates. The re-plotting of Figure 4.4 relative to respective UVA controls for each time point (Figure 4.6) showed that peroxide generation did not increase over time, presumably for similar reasons discussed previously for the UVA and H_2O_2 positive control data.

In our study, two forms of TiO_2 were also examined, one of primarily anatase crystalline structure and the other being primarily rutile, with similar particle sizes but different shapes. We showed that intracellular peroxide levels generated by anatase TiO_2 NPs were much higher than for rutile TiO_2 NPs (Figure 4.9). As the anatase phase of TiO_2 is known to be more photocatalytic than rutile (Barker, *et al.*, 2008), this result was not unexpected. Unlike most sources of rutile TiO_2, the rutile material used in this study was shown to be pure by XRD. Given that the rutile material is known to be far less photocatalytic than anatase, the small amount of anatase present in typical rutile sources is presumably insufficient to induce biologically relevant levels of peroxide. This critical threshold for anatase levels, above which ROS production is no longer reduced, is obviously very important in determining the most desirable form of TiO_2 NPs for use in sunscreens.

Overall, the peroxide levels generated by UVA alone in this study was 6-7 fold higher than that produced by all of the particulates alone. Furthermore, co-exposure to UVA and ZnO or

rutile TiO_2 NPs results in less peroxide generation than from UVA alone. Taken together, we can conclude that the levels of peroxide induced by ZnO and rutile TiO_2 NPs, when concentrated into immune cells, are not a significant concern. High anatase TiO_2 containing materials are an exception, as peroxide generation was enhanced in UVA and anatase NP co-exposure compared to UVA alone. Even in this case, recent skin penetration studies suggest that intact sunscreen NPs do not penetrate beyond the stratum corneum of healthy skin (Elder, *et al.*, 2009; Sadrieh *et al.*, 2010; Zvyagin *et al.*, 2008), meaning that the exposure of viable cells to NPs is likely to be negligible, especially as the effect of peroxides formed at or near the skin surface will be diffusion limited.

In this study, we also investigated the mitochondrial superoxide generation. The fold increases in superoxide levels under UVA over the 24 hr time course were only half of those seen for peroxide generation. This suggests that cytoplasmic peroxide is more inducible by UVA than mitochondrial superoxide. Furthermore, mitochondrial superoxide levels did not change significantly over time, in contrast to the steady increase observed in intracellular peroxide levels. This suggests that normal cellular metabolism generates superoxide quite slowly, or that superoxide accumulation is tightly controlled in the mitochondria by protective antioxidant pathways (Miriyala, *et al.*, 2011).

Comparing the mitochondrial superoxide generation after co-exposure to NPs and UVA, we observed higher superoxide generation with anatase TiO_2, in contrast to the other NPs that exhibited a very similar level of mitochondrial superoxide production to UVA alone (Figure 4.12). This again reinforces that anatase TiO_2 generates ROS (both cytoplasmic peroxide and mitochondrial superoxide) under UVA, and is therefore not an ideal UV component for use in sunscreen formulations.

Interestingly, different kinetics for mitochondrial superoxide generation were seen between the particulate materials, following NP and UVA co-exposure. In TiO_2-exposed cells, the superoxide levels gradually decreased over time, whereas both ZnO NPs marginally increased mitochondrial superoxide levels. A possible explanation for these differences is that while cellular metabolism efficiently reduces mitochondrial superoxide (as illustrated by the decreased TiO_2 signal), ZnO itself appears to induce further mitochondrial superoxide. In our previous studies, we have shown a strong relationship between intracellular zinc ion levels (elevated by dissolution of endocytosed ZnO NPs) and mitochondrial superoxide generation (Shen *et al.*, 2013). Therefore these cells must cope with combined superoxide generation from two sources (UVA and zinc ion-mediated), leading to a net positive increase over the 22 hr period. This marginal increase in ZnO NP-induced superoxide production strongly correlates with "soluble" or readily bioavailable zinc from the NPs and appears to be a more significant influence on the mitochondrial superoxide system over this time than UVA exposure.

Clearly, the least reactive test material in this system was rutile TiO_2, where exposed cells produced less cytoplasmic peroxide and mitochondrial superoxide, and showed no significant loss in viability. Unfortunately, TiO_2 NPs of either crystalline structure do not effectively attenuate UVA near 400 nm and thus, unlike ZnO, rutile TiO_2 is not an adequate substitute for chemical UVA filters such as avobenzone (Yang, *et al.*, 2010). Whilst ZnO NPs appear to be more bioactive than rutile, they have several preferred characteristics for use in sunscreens. These include: the larger ZnO particle size further reduces skin penetration potential (Gulson *et al.*, 2010; Zvyagin *et al.*, 2008); its solubility in sweat and the acidic conditions within endosomes reduce its potential for persistence on skin and in the body (compared to the very

insoluble TiO_2); that zinc as an essential metal ion with tightly-regulated mammalian homeostatic mechanisms (while TiO_2 is not biologically essential); and the reactivity of ZnO in the environment (Lombi *et al.*, 2012), reducing its potential for environmental biopersistence and ecotoxicity.

In this section, we investigated intracellular peroxide and mitochondrial superoxide generation of sunscreen NP-exposed THP-1 monocytes in the presence and absence of UVA. We demonstrated that, with the exception of anatase TiO_2, ROS generation in these human immune cells from sunscreen NP and UVA co-exposure is less than or equal to cellular ROS produced by UVA alone. In conclusion, for sunscreen formulations, photocatalytic ROS generation induced by ZnO NPs and TiO_2 NPs of low anatase content appear to be of very low toxicological concern.

Chapter 5 ZnO NPs can simultaneously cause pro-inflammatory and anti-inflammatory effects in antigen presenting cells

5.1 Introduction

ZnO NPs are extensively used in our lives, especially on our skin. As ZnO has a high capacity for attenuating UV radiation, and also a transparent appearance in the nano-size form, the most common use of ZnO NPs on the skin is in the formulation of sunscreens. Besides these nanosunscreens, ZnO particulates are also used topically to treat skin conditions, such as in baby powder and barrier creams to treat diaper rashes (Zak *et al.*, 2011). Nano ZnO is also regarded as being an antibacterial agent for humans and animals, which is an added benefit for its use in personal care products (Stoimenov *et al.*, 2002). This has been demonstrated by Perelshtein *et al.*, who successfully deposited 0.75 wt% of ZnO NPs (30 nm) onto the surface of bandage fabrics with excellent bactericidal efficacy (Perelshtein *et al.*, 2009).

There is much evidence (detailed in section 1.2.3.2) showing that almost all of topically-applied ZnO NPs remain on the skin surface and do not penetrate beyond the stratum corneum of healthy skin (Elder, *et al.*, 2009; Zvyagin, *et al.*, 2008). However, if the skin is damaged, such as with sun burned skin or wounds, applying a ZnO NP-containing product on the skin may result in some penetration through the skin, with an unknown potential for harm. In these scenarios, ZnO NPs may penetrate into the stratum corneum and meet immune cells, which may treat NPs as foreign invaders and trigger immune responses.

Besides the major function of being a natural barrier, the skin is also an important contributor to the immune system and its function. Almost half of the cell types in the skin are immune related, including keratinocytes, immature and mature dendritic cells (DCs), monocytes, macrophages, granulocytes, mast cells, T lymphocytes and their subpopulations, and vascular

and lymphatic endothelial cells (Bos *et al.*, 2009). Of these, DCs are one of the most important skin immune cell types (detailed in section 1.3.2.3), and are professional antigen presenting cells (APCs) with the ability to internalize antigen, and then migrate to initiate specific immunity.

Langerhans cells (LCs) are DCs that are usually found in the epidermal layer of the skin, and form a cellular network that surveys the epidermis for foreign invaders (Merad *et al.*, 2008). Their location at the barrier surface provides these LCs with early access to skin pathogens and foreign chemicals, including NPs. If the skin is attacked by pathogens, LCs can transport their antigens to lymph nodes where they are presented to naïve T cells and initiate specific immune responses. Thus, as most of the ZnO NPs used for personal care products are applied on the skin surface, those ZnO NPs that actually penetrate the skin to reach viable cells would encounter LCs as the first immune cell type. If sufficient ZnO NPs penetrate the skin, they may potentially change the antigen presentation functions of these cells, so it is very important to investigate the effect of ZnO NPs on human LCs.

Major histocompatibility complex (MHC) class I and II are important cell surface markers for APCs, and are responsible for the activation of T cells and initiation of immune responses. Changes in MHC expression can reflect potential changes in the antigen presentation functions of these cells. Kitamura *et al.* have shown that stimulation of DCs with the Toll-like receptor 4 agonist lipopolysaccharide (LPS) suppressed the expression of zinc transporters, which in turn decreased the intracellular free zinc levels in DCs while increasing their surface expression of MHC II (Kitamura *et al.*, 2006).

As it is difficult to isolate primary LCs directly from skin, LCs are usually generated from peripheral blood mononuclear cells (CD14+ monocytes) or from blood- or bone marrow-derived CD34+ hematopoietic progenitor cells (Romani *et al.*, 1994; Strobl *et al.*, 1996). However, generating LCs from primary cells often faces obstacles, such as donor variability and scarcity of LC precursors. To obtain an unlimited and readily available source of LCs, in the present study we differentiated the CD34+ acute myelomonocytic leukemia cell line MUTZ-3 into LCs using *in vitro* stimulation with cytokines (Masterson, *et al.*, 2002; Santegoets, *et al.*, 2006).

As NPs may have the potential to cause allergic responses or immune suppression, it is important to assess the antigen presentation capacity of immune cells affected by NPs. In this study, we investigated the antigen processing and presentation of ZnO NP-exposed monocytes and LCs, as well as the response of adaptive elements of immunity caused by these changes. The cytokine profiles of ZnO NP-exposed monocytes and LCs were also examined in this study. We have shown that ZnO NPs cause simultaneous pro-inflammatory and anti-inflammatory effects in antigen presenting cells.

5.2 Materials and methods

5.2.1 Materials

ZnO NPs with primary particle diameters of 30 and 200 nm, with and without surfactant dispersant were used in this study. Full physical characterization methods and results for these materials are described in section 2.1 and 3.3.1.

5.2.2 Cell culture and *in vitro* test system.

MUTZ-3 monocytes and LCs were used in this study. MUTZ-3 LCs are differentiated from MUTZ-3 monocytes by stimulation with cytokines for 9 days, and the details of the cell culture and differentiation methods are described in section 2.3.3. The particle preparation for addition to the test system and the cytotoxicity assay are described in sections 2.2 and 2.4, respectively.

5.2.3 MHC I and II expression

MHC I and II expression were measured on MUTZ-3 monocytes and MUTZ-3 derived LCs incubated with NPs for 24 hr, using specific MHC I and II antibodies (HLA-ABC and HLA-DR from BD Pharmingen, San Diego, CA, USA). Cells were seeded in 96-well plates and incubated with ZnO NPs for 24 hr as described above for the cell culture procedure. After 24 hr of co-culture with NPs, cells were washed with PBS, and then incubated with MHC I and II antibodies for 30 min in a dark and humidified incubator at 37 ℃ and 5% CO_2. The cells were then washed again with PBS to remove unattached antibodies. Finally, fresh media was added and cells were analyzed using flow cytometry. Each treatment was performed in triplicate for each of two experiments.

5.2.4 Lymphocyte Proliferation Assay

The human acute monocytic leukemia cell line (THP-1) was cultured following the protocol as previously described in section 2.3.1. Macrophages were differentiated from THP-1 monocytes by incubating 8×10^4 cells per well with 20 nM phorbol-12-myristate-13-acetate (PMA) for 24 hr. After which, the media was aspirated off and fresh media containing NPs at a concentration of 10 and 50 μg/mL was added. 24 hr later, NP-exposed THP-1 macrophages were washed 3 times in cell culture media to remove extracellular NPs. Then these pre-

exposed macrophages are examined for their ability to stimulate proliferation of blood lymphocytes. The isolation procedure for blood lymphocytes is described in section 2.3.2. Blood lymphocytes were incubated with THP-1 macrophages using cell number ratio of 100:1. After 7 days of incubation, cell proliferation was examined by the MTS assay according to section 2.4.2. Each treatment was performed in triplicate.

5.2.5 Cytokine profiling

After exposure of cells with NPs for 20 hr, 100 μL of cell supernatant was removed and frozen at -80 ℃ for cytokine analysis. Human IFN-γ, IL-1β, IL-2, IL-4, IL-5, IL-6, IL-9, IL-10, IL-12 p70, IL-13, IL-17A, IL-22 and TNF-α were measured on thawed cell supernatants via flow cytometry using a Human Th1/Th2/Th9/Th17/Th22 13plex FlowCytomix Multiplex kit (eBioscience, San Diego, CA, USA). In this kit multi-beads are designed with two different sizes and spectral coating with antibodies specifically to different cytokines. To set up the assay for the flow cytometer, two sets of beads are gated based on their size. Each set of beads consists of several bead populations internally dyed with different intensities of a fluorescent dye. In this kit the two different bead sizes make it possible to distinguish up to 20 bead sets in one fluorescence channel. Although 13 cytokines were simultaneously analysed in the samples for this project, a maximum of 20 different bead sets distinguished by internal dye intensity and bead size allow the simultaneous quantification of 20 analytes in a single small volume sample. In this study, enzyme linked immunosorbant assay (ELISA) was also used to specifically measure IL-8 on thawed cell supernatants. Each treatment was performed in triplicate for each of two to three experiments.

5.3 Results

5.3.1 Cytotoxicity profiling

In this study, we initially investigated the cytotoxicity of ZnO NPs on human LCs. Pristine and surfactant-coated ZnO NPs with a diameter of 30 nm were examined as the test NPs. ZnO particulate with a diameter of 200 nm was employed as the bulk material control. As zinc ions are an important factor in the cytotoxicity of ZnO, we also employed $ZnCl_2$ as the zinc ion control.

The LCs were successfully differentiated from MUTZ-3 monocytes after 9 days of *in vitro* stimulation with GM-CSF, TNF-α and TGF-β1 (see section 2.3.3). In this study, both MUTZ-3 monocytes and LCs were exposed with NPs for direct comparison. After 24 hr of exposure to ZnO NPs, we can see that MUTZ-3 LCs are >2-fold more sensitive to ZnO NPs than MUTZ-3 monocytes (Figure 5.1). That is, MUTZ-3 LCs exhibited an EC50 of ~50 μg/mL, while the EC50 for MUTZ-3 monocytes was >100 μg/mL. In addition, surfactant-dispersed ZnO 30 was more cytotoxic to both cell types than the pristine ZnO NPs, but had a similar cytotoxicity profile to $ZnCl_2$.

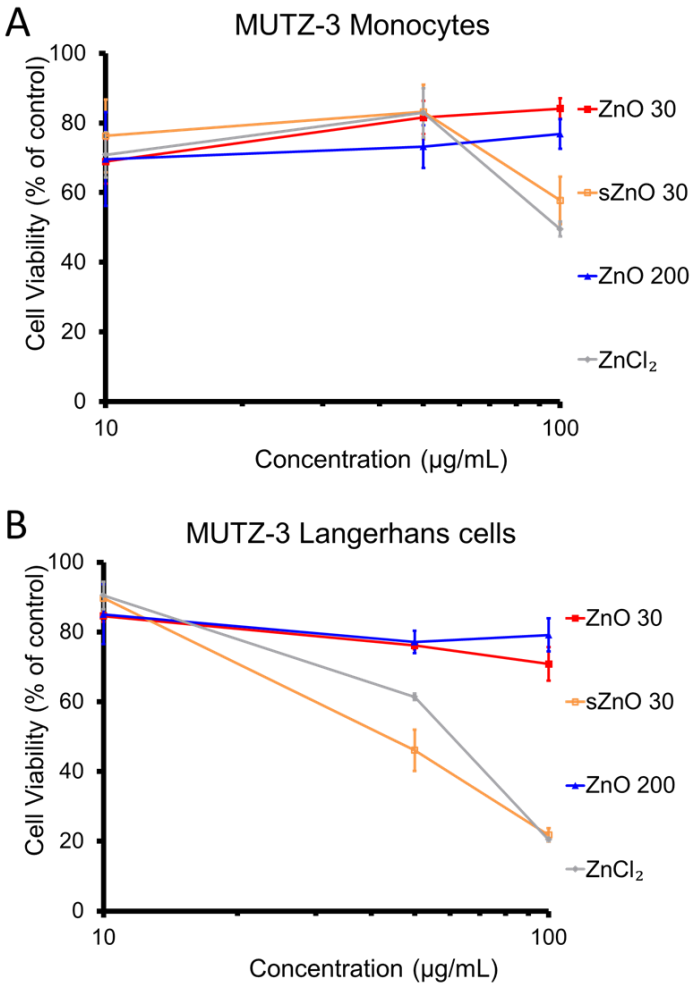

Figure 5.1 Cell viability of human MUTZ-3 monocytes (A) and Langerhans cells (B) after 24 hr exposure to pristine or surfactant-dispersed (s) ZnO NPs, or $ZnCl_2$ (zinc ion control) (mean ± SEM, n=3 experiments).

5.3.2 MHC I and II expression

In this study, we employed specific monoclonal antibodies for MHC I and II to investigate the antigen processing and presentation of immune cells after exposure of ZnO NPs. After 24 hr exposure to ZnO particulates or $ZnCl_2$, the MHC I expression in both MUTZ-3 monocytes and LCs was suppressed in a dose-dependent manner (Figure 5.2). We also observed a similar dose-dependent reduction in the MHC II expression profile (Figure 5.3), as was seen with MHC I.

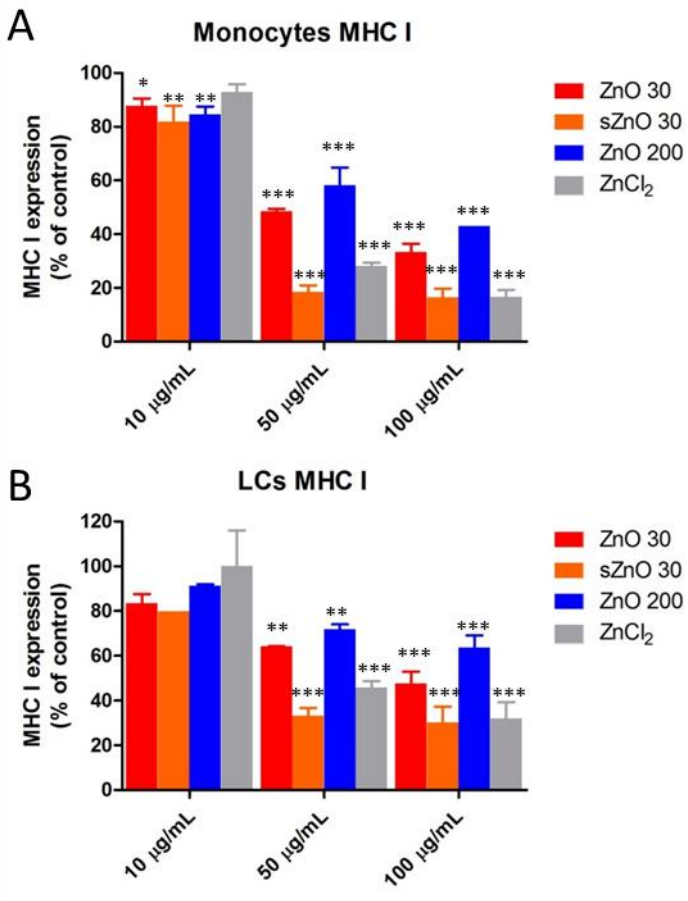

Figure 5.2 MHC I expression of human MUTZ-3 monocytes (A) and Langerhans cells (B) after 24 hr exposure to pristine or surfactant-dispersed (s) ZnO NPs or $ZnCl_2$ (zinc ion control) (mean ± SEM, n=2 experiments). Concentrations marked with stars were significantly different from untreated control cells (* $p<0.05$, ** $p < 0.01$, *** $p<0.001$).

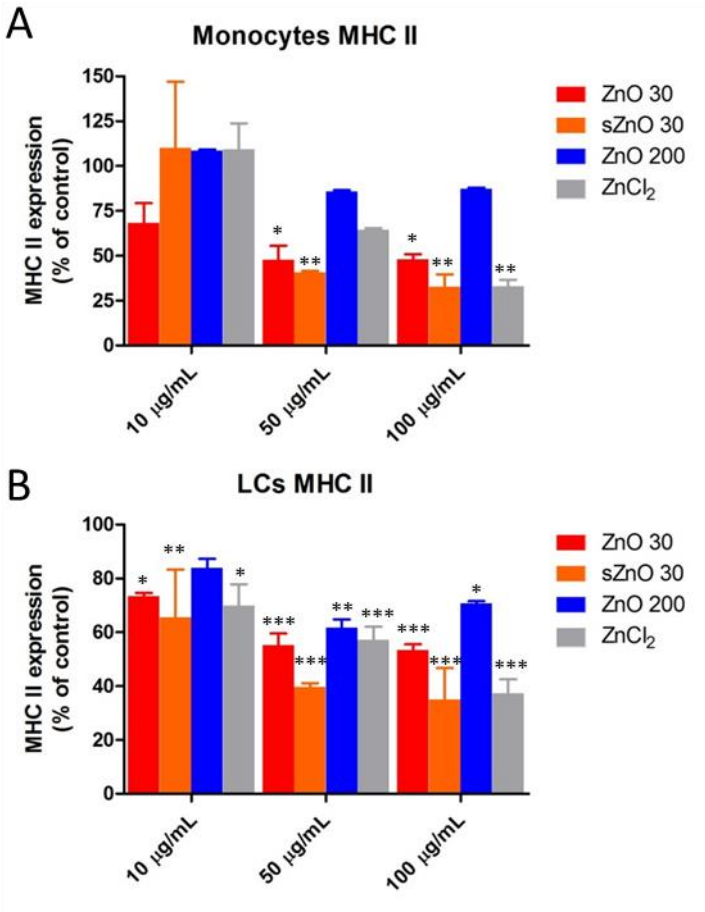

Figure 5.3 MHC II expression of human MUTZ-3 monocytes (A) and Langerhans cells (B) after 24 hr exposure to pristine or surfactant dispersed (s) ZnO NPs or $ZnCl_2$ (zinc ion control) (mean ± SEM, n=2 experiments). Concentrations marked with stars were significantly different from untreated control cells (* $p<0.05$, ** $p < 0.01$, *** $p<0.001$).

5.3.3 Lymphocyte Proliferation Assay

In this study, we have developed a lymphocyte proliferation assay, in which THP-1 macrophages pre-exposed to ZnO NPs were examined for their ability to stimulate proliferation of blood lymphocytes. Preliminary data from these experiments has shown the potential for zinc to cause a dose-dependent stimulation of immune proliferation, measured as an increased metabolic conversion of MTS (Figure 5.4).

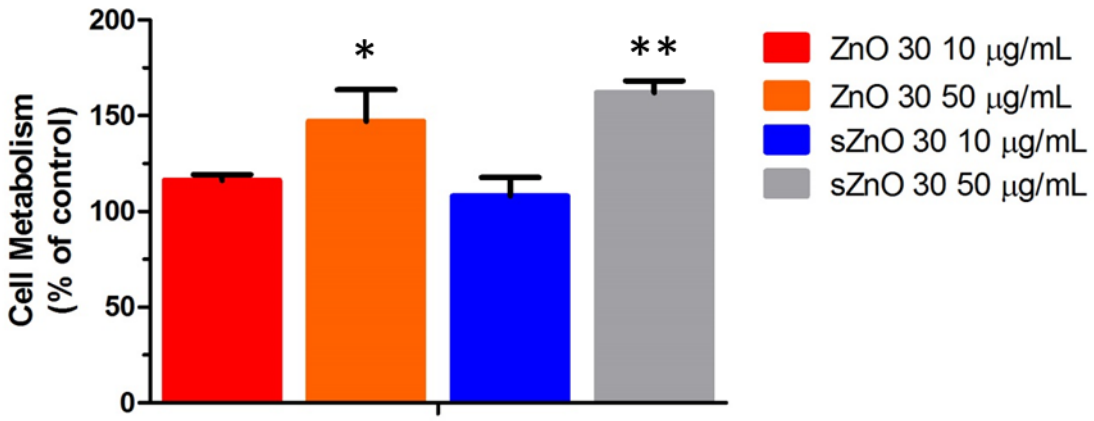

Figure 5.4 Lymphocyte proliferative response induced from THP-1 macrophages exposed to ZnO NPs. Both sub-toxic and cytotoxic concentrations of ZnO NPs were able to elicit a lymphocyte response (mean ± SEM, n=3 replicates). Concentrations marked with stars were significantly different from untreated control cells (* $p<0.05$, ** $p < 0.01$).

5.3.4 Cytokine profiling

In this study, we also examined the cytokine profiles of ZnO NP-exposed MUTZ-3 monocytes and LCs. We employed a fluorescent bead-based high-throughput multiplex kit and screened 13 different inflammatory cytokines by flow cytometry. The cytokines measured included: Th1 characteristic cytokines, IL-12 p70, IFN-γ, and IL-2; Th2 characteristic cytokines, IL-4, IL-5, IL-6, IL-10 and IL-13; Th9-related pro inflammatory cytokine, IL-9; Th17-related pro-inflammatory cytokine, IL-17A; Th22-related pro-inflammatory cytokine, IL-22; and pro-inflammatory cytokines IL-1β and TNF-α. Cells were exposed to ZnO NPs or $ZnCl_2$ at two concentrations, i.e. the sub-toxic dose of 10 μg/mL (Figure 5.5) and the higher dose of 50 μg/mL (Figure 5.6), which approximated the cytotoxicity EC50 value of sZnO 30 NPs in the LCs. We can see from these cytokine profiles that the various zinc-related exposures had different effects on the cytokines investigated. The expression of some cytokines was suppressed, while other cytokines were stimulated. For example, the Th1 cytokine IL-2 expression was suppressed in LCs exposed to ZnO NPs

(both 10 and 50 µg/mL), while, the Th2 cytokine IL-13 is stimulated in ZnO NP-exposed LCs.

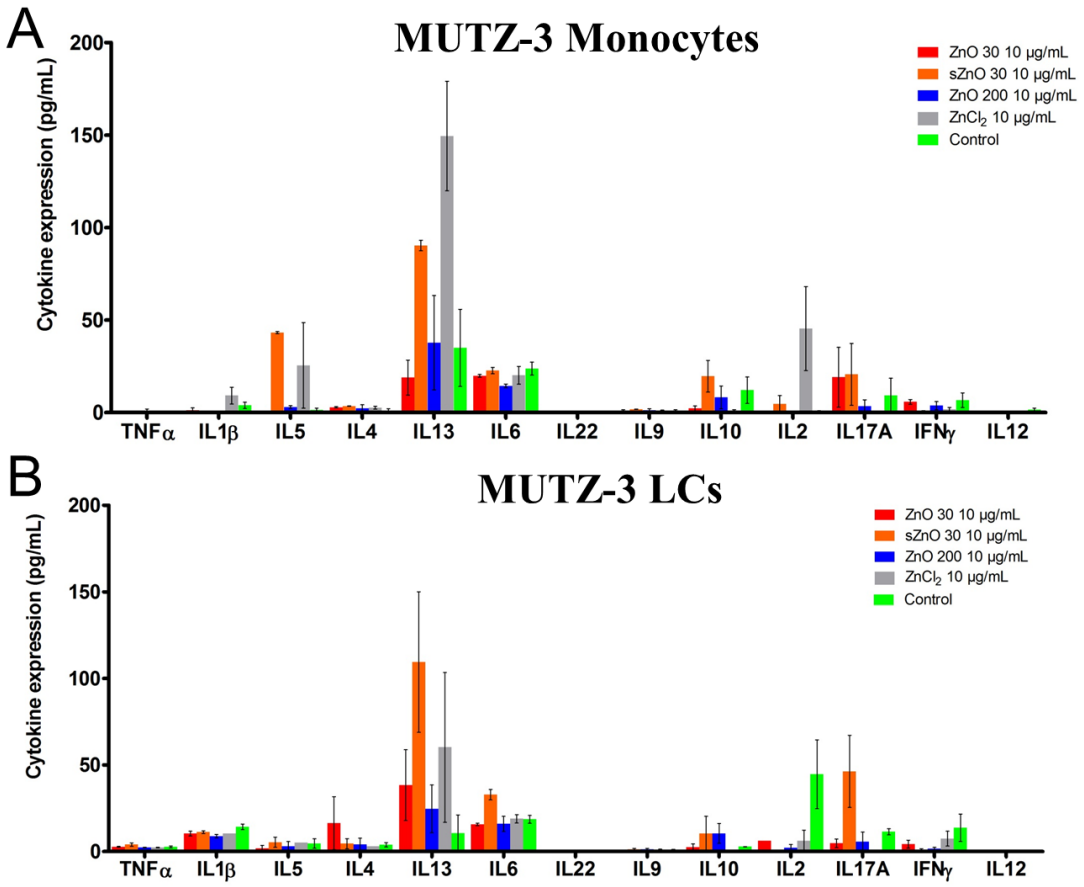

Figure 5.5 Multiplex cytokine profile of MUTZ-3 monocytes (A) and LCs (B) after 20 hr exposure to 10 µg/mL ZnO 30 nm surfactant-dispersed (sZnO) nanoparticles, ZnO 200 or zinc chloride ($ZnCl_2$) (mean ± SEM, n=3 replicates).

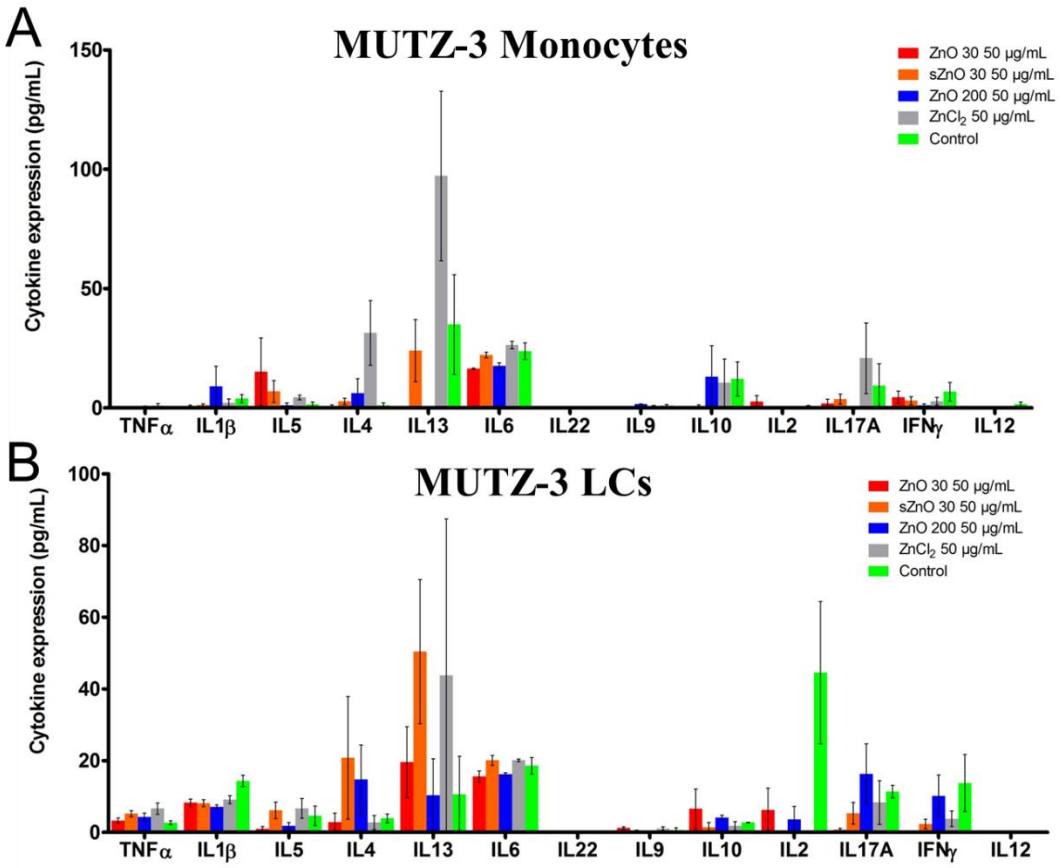

Figure 5.6 Multiplex cytokine profile of MUTZ-3 monocytes (A) and LCs (B) after 20 hr exposure to 50 µg/mL ZnO 30 nm surfactant-dispersed (sZnO) nanoparticles, ZnO 200 or zinc chloride ($ZnCl_2$) (mean ± SEM, n=3 replicates).

In this study, we also employed the ELISA method to examine IL-8 release in more detail, as this method is more precise in quantitating individual cytokine levels than the multiplex assay. We observed that at the sub-toxic dose, IL-8 expression increased with increasing ZnO dose, while at toxic doses the IL-8 expression was decreased due to the low viable cell number (Figure 5.7). It should be noted that sub-toxic and toxic doses were different between the particles and cell lines. ZnO 30 and ZnO 200 are sub-toxic in both monocytes and LCs over the whole dose range we used in this study. However, for monocytes the sZnO 30 and $ZnCl_2$ treatments were sub-toxic at 10 and 50 µg/mL, and cytotoxic at 100 µg/mL. Whereas, for LCs the sZnO 30 and $ZnCl_2$ treatments were only sub-toxic at 10 µg/mL, but were cytotoxic at 50 and 100 µg/mL.

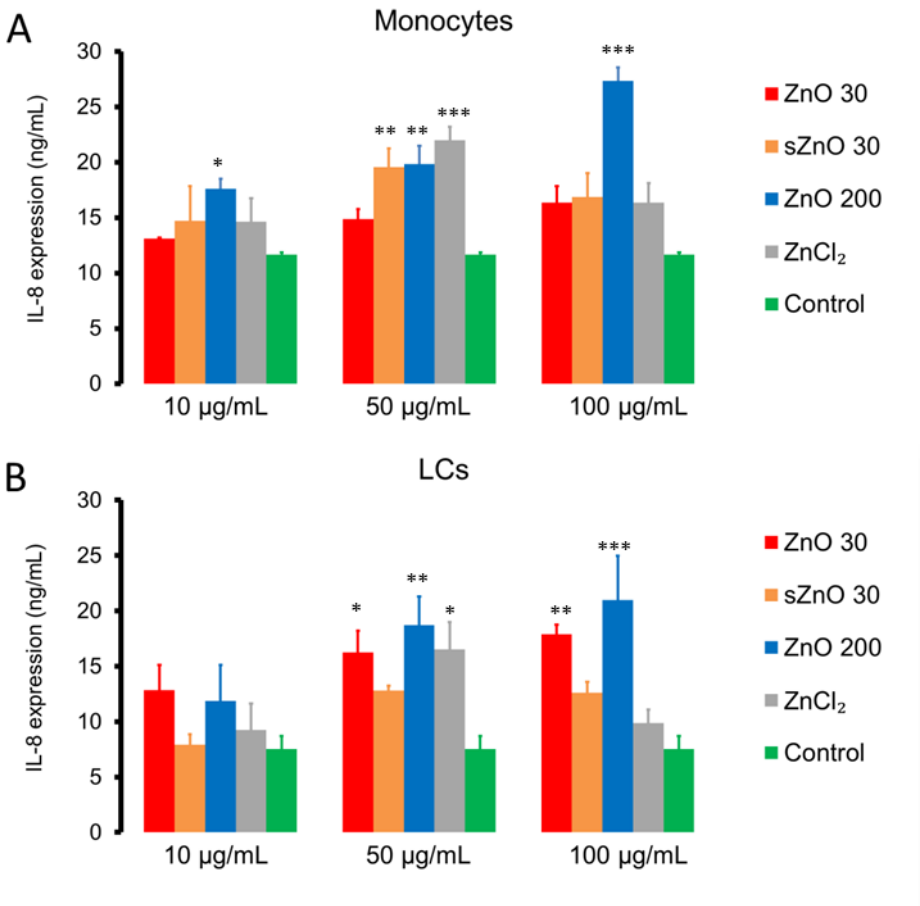

Figure 5.7 IL-8 expression of human MUTZ-3 monocytes (A) and Langerhans cells (B) after 24 hr exposure to pristine or surfactant-dispersed (s) ZnO NPs or $ZnCl_2$ (zinc ion control) (mean ± SEM, n=3 experiments). Concentrations marked with stars were significantly different from untreated control cells (* $p<0.05$, ** $p < 0.01$, *** $p<0.001$).

5.4 Discussion

ZnO NPs are widely formulated as UV filters in sunscreens, but the effects of ZnO NPs on the function of cellular elements of the innate immune system are not well characterised. LCs are the only dendritic cells of the epidermis and constitute the first immunological barrier against NPs (Merad, *et al.*, 2008). In this study, we investigated the effect of ZnO NPs on the

function of MUTZ-3 derived LCs. We used this system to assess whether the antigen presentation of these cells has been affected by ZnO NP exposure.

In this preliminary study, we investigated the cytotoxicity profile of ZnO NPs on human LCs. We found that the cytotoxicity profile data in the LC exposure system (Figure 5.1) was very similar to that seen in the THP-1 cell exposure system (Figure 3.5). That is, surfactant-dispersed ZnO 30 is more cytotoxic than pristine ZnO 30. The main difference from the THP-1 cell exposure system is that the cytotoxicity of ZnO 30 in this MUTZ-3 cell exposure system is very similar to that of ZnO bulk particulate. This suggests that even for the same NP, the cytotoxicity profile can be different between immune cell types and exposure systems. These different cytotoxicity profiles generated from different cell lines make it difficult for interpreting, and extrapolating from, *in vitro* exposure studies. From the cytotoxicity data we also found that the $ZnCl_2$ control was more cytotoxic to LCs than pristine ZnO NPs and bulk ZnO. As has been suggested by many studies that Zn^{2+} is related to the cytotoxicity of ZnO NPs (Muller *et al.*, 2010; Sasidharan *et al.*, 2011; Xia *et al.*, 2011), the findings here also suggest that zinc ions may be the main contributor for the cytotoxicity of ZnO particulates.

Antigen processing and presentation of immune cells is very important to the body. If cells are attacked by intracellular pathogens, the surface proteins on the pathogen released into the cytosol would stimulate the production of MHC I. In this study, we have observed suppression of MHC I expression after 24 hr exposure of MUTZ-3 monocytes and LCs to ZnO or $ZnCl_2$ (Figure 5.2). This result demonstrates that the cells do not respond to ZnO NPs as if they are antigens. It should be noted that in this *in vitro* exposure system, NPs are incubated in media with FBS, which can adsorb onto the particles and form the "protein corona" (Deng *et al.*, 2009; Lundqvist, *et al.*, 2008), which could potentially cause the NPs

to interact with other proteins and receptors on the surface of cells. In addition, the dissolution of ZnO NP will happen intracellularly (Turney, *et al.*, 2012), and zinc ions released from ZnO dissolution will complex with many intracellular proteins. Whilst this zinc ion binding to proteins could potentially alter some protein-ligand binding or enzyme functions, which could possibly mimic intracellular antigen release by a virus, the data suggests that this is not the case for these NPs. On the contrary, the observed down-regulation of MHC I suggested a level of immunosuppression, attributable to zinc ion interaction with intracellular components, which may indicate that high levels of intracellular zinc, if sustained, could suppress MHC I and create a potential vulnerability to viruses or tumours.

At 50 μg/mL there was substantial reduction in monocyte MHC I expression without a loss of cell viability (Figure 5.1). This suggests that the cell viability cannot entirely explain this drop of MHC I expression. The suppression of MHC I may instead relate to the up-regulation of metallothionein (MT). It has been reported that MT can reduce the expression of MHC I in lymphocytes (Youn *et al.*, 1999). It has been reported that ZnO NPs can significantly induce MT expression levels (Hanagata *et al.*, 2010), which then cause suppression of MHC I.

The MHC II expression data exhibited a very similar profile to MHC I. As the ZnO NP dose increased, the MHC II expression decreased. These data indicate that zinc particles have immunosuppressive properties. Also, both bulk and nanoparticulate forms of ZnO suppressed MHC levels, which suggests that the observed effects were due to zinc ion release, rather than any specific properties of zinc-containing nanomaterials. MHC II is presented on the cell surface after antigen processing by phagocytosis, and results in presentation of antigen fragments to T-cells and the initiation of an immune response. In our *in vitro* cell exposure system the LCs represent typical antigen presenting cells in the skin epidermis. The

suppression of the MHC II expression by ZnO particles could indicate that exposed LCs would not stimulate the T-cells to initiate an immune response. However, we observed a different phenomenon in the lymphocyte proliferation system. This multi-cellular indirect stimulation approach is more similar to the *in vivo* exposure scenario, in which exposed antigen-presenting cells travel to local lymph nodes, where they could potentially stimulate the production of lymphocytes and therefore generate an inflammatory response. In this preliminary study, we have shown that ZnO NPs can stimulate cell proliferation in primary human T cells. Altogether, these data indicate that ZnO NPs can simultaneously cause some pro-inflammatory and anti-inflammatory effects, which is consistent with our previous findings (Feltis, *et al.*, 2012). It should also be noted that zinc is used clinically as a mild anti-inflammatory – it might be that this simultaneous stimulation prevents it from having stronger anti-inflammatory properties.

To investigate the cytokine profile following *in vitro* ZnO NP exposure, we employed a multiplex cytokine assay. We have demonstrated that ZnO NPs can simultaneously cause pro-inflammatory effects from the cytokine profile, in contrast to the anti-inflammatory effects. It has been reported that Interleukin-8 (IL-8) is associated with zinc exposure and bacterial infection (Hirao *et al.*, 2000; Kim *et al.*, 2006). After detecting elevated IL-8 in NP-exposed macrophages, we employed the ELISA method to examine IL-8 in more detail, as it is more sensitive than the multiplex assay. We observed that at sub-toxic doses, IL-8 expression increased with increasing ZnO dose, while at cytotoxic concentrations the IL-8 expression was decreased, due to the low number of viable cells (Figure 5.7). From the ZnO NP cytotoxicity data (Figure 5.1), we can see that ZnO 30 and 200 NPs are not that toxic compared with sZnO NPs and $ZnCl_2$. At a dose of 100 μg/mL, ZnO 30 and 200 NP-treated cells still had cell viabilities around 80% of the control incubation. This is why we can still

see the increased IL-8 expression for ZnO 30 and 200 NPs at the highest dose (Figure 5.7). While, for sZnO 30 and $ZnCl_2$, the reduced cell viability at the highest dose results in only a small viable cell population to contribute to cytokine production, thus we see that IL-8 expression decreased for sZnO 30 and $ZnCl_2$ at this high dose (Figure 5.7).

In summary of the third part of this project, the effect of ZnO NPs on the function of LCs was investigated, as these dendritic cells are present in the epidermis and constitute the first immunological barrier against NPs. We found that ZnO NPs can simultaneously cause pro-inflammatory effects (as increased IL-8 and lymphocyte proliferation) and anti-inflammatory effects (as decreased MHC I and II expression in these antigen presenting cells). This study indicates that ZnO NPs may modulate antigen presentation processes, which could help to explain its anti-allergic properties.

Chapter 6 General discussion and conclusions

6.1 General discussion

Despite increasing use of new transparent sunscreens containing NPs of photoactive ZnO and TiO_2, the effect of these nanomaterials on innate immunity was previously unknown. This is particularly important as tissue resident immune cells are a first point of contact where NPs can be actively sequestered by cells. The aim of this project was to investigate the interactions between human immune cells and sunscreen NPs in an *in vitro* exposure system. In this project, the NP treatment doses used were likely to be higher than would be expected for topical exposure, as there is negligible penetration of NPs through human skin. These relatively higher doses amplify the effects of NPs in the *in vitro* exposure system, and enable us to see the differences in cellular responses between the NP treatments of different size and surface coating. Although the NP exposure dose in my project is higher than for topical exposure, this may not necessarily be the case for high levels of inhalational exposure, where respiratory immune cells like macrophages and DCs may encounter high direct amounts of NPs. Therefore, the findings of my project are also relevant to other exposure routes.

Generally, ZnO NPs are more directly cytotoxic than TiO_2 NPs, which is mainly due to the dissolution properties of ZnO in certain biological conditions. The relationships between the cytotoxicity of ZnO NPs, intracellular Zn^{2+} level and ROS production were addressed and quantified in this project. In addition, extracellular dissolution of ZnO NPs in cell culture media has been shown not to be sufficient to cause cytotoxicity, indicating a lack of soluble bioavailable zinc within the cell culture environment. Most of the Zn^{2+} released extracellularly from ZnO NPs interacted with PO_4^{3-} or CO_3^{2-} in the cell culture media to form zinc salt precipitates (Turney, *et al.*, 2012). In a related study by Xu and coworkers, the ZnO NPs were removed from the supernatant by high speed centrifugation (Xu *et al.,* 2013). They

then compared the cytotoxicity of the supernatant (containing zinc ions released from ZnO NP dissolution) with a ZnO NP suspension in a human A549 lung epithelial cell exposure system. These investigators estimated that the toxic contribution of extracellular zinc ions to the A549 cell lines was only about 10%. Although this contribution was greater than that seen in this project, it is likely due to methodological differences (where NPs spend a longer period in the supernatant liquid during the centrifugation step), and is consistent overall with the findings of my project. Therefore, the soluble extracellular [Zn^{2+}] released from ZnO NPs in the cell culture environment is not toxic to the cells. Whilst intracellular ROS is strongly related to cytotoxicity, it can also be modulated by antioxidant treatment without altering the cell viability – suggesting the standing premise that "ROS induces cytotoxicity" may be an oversimplification of a more complex series of events. Organelles like mitochondria also leak electrons and are a major source of intracellular ROS. Other possible sources of mitochondrial ROS may occur indirectly, e.g. generated by zinc ions fully occupying the divalent metal ion binding sites of oxidative stress defense macromolecules, such as metallothionein. When excessive zinc ion levels released from ZnO NP bind with these proteins, they could compete with, and displace, other transition metal ions, such as Fe and Cu, that would then be freely available to catalyze Fenton-type reactions and generate ROS.

The relatively low cytotoxicity of zinc and its intracellular dissolution could find application in therapeutic drug delivery. It has been reported recently that NPs can be engineered to deliver drugs to specific sites of inflammation using biocompatible polymers that degrade in the presence of peroxide (de Gracia Lux *et al.*, 2012). It follows that a ZnO nanoshell could be designed to only deliver its core payload after endocytosis, when the localized pH in endosomes was sufficiently acidic to dissolve ZnO. By extension, other NPs could be engineered to degrade at very specific points along the endocytic or phagocytic pathways.

While there is a promising future for the application of NPs in medical therapy, their safety must be considered first, and a mechanistic understanding of how these materials interact with living cells will greatly assist this process.

One important aim of this study was to attempt to understand the possible mechanism of sunscreen NP effects on human immune cells and develop more effective, less allergenic sunscreen NPs. The currently understood paradigm for ZnO NP cytotoxicity is that in human immune cells, ZnO NPs first undergo endocytosis to enter the cells, then dissolve into bioavailable zinc and increase oxidative stress, which then causes cytotoxicity. Based on this mechanism, we modified the surface of ZnO NP with PEG coating and successfully reduced the cytotoxicity of ZnO NPs. It has been reported that PEGylation of NPs is very effective in inhibiting their nonspecific binding to blood proteins and macrophages (Karakoti *et al*., 2011). In this study, uptake of PEGylated ZnO NPs was significantly reduced, which mainly contributed to the reduced cytotoxicity of ZnO NPs. This preliminary study provides us a new strategy in the safety-by-design approach to develop safer ZnO NPs in the future.

As ZnO and TiO_2 NPs are widely formulated in sunscreens, in this project we also investigated the effects of these metal oxide NPs on human immune cells in the presence of UVA. Although some ROS generation occurs in cells exposed to ZnO and TiO_2 NPs in the absence of UV light (Shen, *et al.*, 2013), it is unknown to what extent this ROS generation is altered with UVA co-exposure, which is more relevant to actual sunscreen usage. In order to determine the relative hazard potential of UVA co-exposure with nanosunscreen NPs, ROS generation was investigated in human THP-1 monocyte immune cells co-exposed to UVA and ZnO or TiO_2 NPs. This study confirmed that ROS generation from nanosunscreens, such as ZnO and rutile TiO_2 NPs, does not contribute significantly to the overall hazard associated

with oxidative stress from UVA exposure itself. Therefore, excessive UV light is a well-known and greater risk for skin damage and cancer compared to a perceived risk from using nanosunscreen that is not supported by our findings or the scientific literature. It is crucial that people do not stop using the most effective broad spectrum sunscreens as part of their sun protection measures. It should also be noted that ROS generated by UVA alone did not cause cytotoxicity in this test system. In contrast, many literature reports have suggested that ZnO NPs are supposed to cause cytotoxicity by generating ROS (Hanley *et al.,* 2009; Lin *et al.,* 2009; Xia, *et al.,* 2008). These two points are contradictory, but in this project, I have shown that antioxidants can modulate ROS production by ZnO NPs, without altering the resultant cell viability. This suggests that ROS may not be the main cause for the cytotoxicity of ZnO NPs.

In this project, the effects of ZnO NPs on antigen processing and presentation were also investigated. LCs were employed as a typical and relevant APC type for this study. LCs are usually found in the epidermal layer of the skin, and form a cellular network that surveys the epidermis for foreign invaders. If ZnO NPs penetrated the skin sufficiently to reach viable cells, the first immune cells they would encounter are LCs, and could therefore potentially alter the antigen presentation functions of these cells. In this project, we have shown that MHC I & II expression are suppressed by ZnO NP exposure. However, we have also seen that ZnO NPs have potential to stimulate immune cell proliferation in a multi-cellular indirect stimulation approach. We have also examined the release of bioactive molecules by screening for alterations in cytokine profiles following ZnO NP exposure. It was shown that the expression of some cytokines was suppressed, while others were stimulated. These findings indicate that ZnO NPs can simultaneously cause pro-inflammatory and anti-inflammatory effects in these antigen presenting cells.

6.2 Conclusions

In conclusion, sunscreen ZnO and TiO_2 NPs are well tolerated by skin immune cells, with only ZnO causing cytotoxicity at very high concentrations. Also, ZnO NPs possess immunomodulatory effects that provide further evidence of the mode of action in the therapeutic topical use of zinc.

We have demonstrated that the intracellular dissolution of ZnO NPs, with subsequent release of bioavailable Zn, is the main determinant of cytotoxicity for ZnO NPs. Moreover, these factors both correlate strongly with each other and with intracellular reactive oxygen generation, providing strong evidence that both of these determinants are required for ZnO NP cytotoxicity in human immune cells. Whilst dissolution of ZnO NPs may occur to some extent extracellularly, the extracellular concentration of bioavailable Zn released from ZnO NPs is insufficient to induce cytotoxicity, even with extremely high starting concentrations of NPs. Adding further complexity, intracellular superoxide levels can be slightly reduced without altering cytotoxicity, suggesting that part of the mitochondrial superoxide signal is likely to be the result of intracellular damage, and therefore ROS is not the sole cause of ZnO NP-induced cytotoxicity in this test system.

In this project, we also investigated intracellular peroxide and mitochondrial superoxide generation of sunscreen NP-exposed THP-1 monocytes in the presence and absence of UVA. These cells, as accumulators of particulates in body fluids and tissues, would be expected to have higher levels of NP exposure and thus should be the primary focus for ROS induced by UVA and NP co-exposure in the skin. We demonstrated that, with the exception of anatase TiO_2, ROS generation in these human immune cells following sunscreen NP and UVA co-

exposure is less than or equal to cellular ROS produced by UVA alone. The implications of this observation are that, whilst chemically it may be possible to demonstrate significant ROS activity in these materials over extended periods of UV exposure (such as with painted metal surfaces), at a biological level the quantity of ROS these NPs produce even in the presence of UV is insignificant compared with normal environmental stimuli (i.e. UV light itself). For sunscreen formulations, photocatalytic ROS generation induced by ZnO NPs and TiO_2 NPs of low anatase content appear to be of very low toxicological concern.

In this project, we also investigated effect of ZnO NPs on the antigen processing and presentation of MUTZ-3 monocytes and LCs. This range of responses suggests that ZnO NPs can cause simultaneous pro-inflammatory and anti-inflammatory effects in antigen presenting cells. This study indicates that ZnO NPs may modulate antigen presentation processes that can lead to allergic reactions.

6.3 Future directions

Preliminary work was performed in this project to modulate the cytotoxicity of ZnO NPs by surface modification with PEG coating. The uptake of PEGylated ZnO NPs was investigated by measuring the total cell-associated zinc using ICP-MS. In future work, the effects of different coatings on particle uptake and dissolution should be investigated. One may also examine why such coatings don't affect some aspects of NP bioactivity. All of these studies would help us gain a better understanding of the cellular responses of immune cells exposed to sunscreen metal-oxide NPs that will help in the safety evaluation of these products, as well as in the safety-by-design approach to developing more effective, hypoallergenic sunscreen NPs.

In the epidermis layer, keratinocytes constitute more than 90% of epidermal cells, while LCs represent 3-5% of epidermal cells. It should be noted that although LCs only constitute a small percentage of epidermal cells, these cells still account for the majority of immune cells in the epidermis layer. Therefore, co-culture of keratinocyte and LCs in an *in vitro* exposure system may be used to better mimic the *in vivo* responses of the epidermis. Thus, future research could involve exposing this *in vitro* co-culture system to NPs and UVA or UVB, further reproducing a more *in vivo*-like scenario. Also raising cells the cultured keratinocyte cell layer to an air interface to allow the formation of a keratinised layer would more easily enable the testing of sunscreen formulations, applied to the uppermost surface.

Finally, as we investigated the antigen processing and presentation of ZnO NP-exposed MUTZ-3 monocytes and LCs, primarily through changes in MHC I & II expression, future studies could examine whether ZnO NPs affect the presentation of viral, bacterial and tumour

antigens. One may also use the *in vitro* exposure methodologies developed in this project to study the effects of ZnO NPs on tumour surveillance by immune effector cells, such as natural killer cells and cytotoxic T lymphocytes.

In this project, we have obtained important information on the cellular responses of innate immune cells exposed to sunscreen NPs. To extend and validate the findings further, it would be desirable to investigate the effect of these NPs in an animal model.

Consequently, this project has provided an important foundation from which to conduct future mechanistic investigations and screening assays of the skin effects of metal oxide NPs used in sunscreens and industry.

References

Therapeutic Goods Administration (2013). Literature review on the safety of titanium dioxide and zinc oxide nanoparticles in sunscreens. Australian Government Department of Health and Ageing. In http://www.tga.gov.au/pdf/sunscreens-nanoparticles-review-2013.pdf, Accession date Feb. 3, 2014.

Akira, S., Uematsu, S., Takeuchi, O. (2006). Pathogen Recognition and Innate Immunity. *Cell*. **124**, 783–801.

Allen, N. S., Edge, M., Sandoval, G., Verran, J., Stratton, J., and Maltby, J. (2005). Photocatalytic coatings for environmental applications. *Photochem. Photobiol.* **81**, 279-90.

Banchereau, J., and Steinman, R. M. (1998). Dendritic cells and the control of immunity. *Nature* **392**, 245-252.

Barker, J. N., Mitra, R. S., Griffiths, C. E., Dixit, V. M. Nickoloff BJ. (1991). Keratinocytes as initiators of inflammation. *Lancet*. **26**, 211-214.

Beissert, S., Mohammad, T., Torri, H., Lonati, A., Yan, Z., Morrison, H., and Granstein, R. D. (1997). Regulation of tumor antigen presentation by urocanic acid. *J. Immunol.* **159**, 92-96.

Bennat, C., and Muller-Goymann, C. C. (2000). Skin penetration and stabilization of formulations containing microfine titanium dioxide as physical UV filter. *Int. J. Cosmetic. Sci.* **22**, 271-283.

Bos, J., and Luiten, R. (2009). Skin Immune System. In *Skin Cancer after Organ Transplantation* (E. Stockfleth, and C. Ulrich, Eds.), **146**, 45-62. Springer US.

Bos, J. D. (2005). *Skin Immune System (SIS): Cutaneous Immunology and Clinical Immunodermatology*. CRC Press.

Bos, J. D., and Kapsenberg, M. L. (1986). The skin immune system: its cellular constituents and their interactions. *Immunol. Today* **7**, 235-240.

Braydich-Stolle, L. K., Schaeublin, N. M., Murdock, R. C., Jiang, J., Biswas, P., Schlager, J. J., and Hussain, S. M. (2009). Crystal structure mediates mode of cell death in TiO_2 nanotoxicity. *J. Nanopart. Res.* **11**, 1361-1374.

Brinker, C. J. (2012). Nanoparticle immunotherapy: Combo combat. *Nat. Mat.* **11**, 831–832.

Campos, M. A., Gazzinelli, R. T. (2004). Trypanosoma cruzi and its components as exogenous mediators of inflammation recognized through Toll-like receptors. *Mediators Inflamm.* **13**, 139-143.

Carpenter, L. R., Moy, J. N., and Roebuck, K. A. (2002). Respiratory syncytial virus and TNF alpha induction of chemokine gene expression involves differential activation of Rel A and NF-kappa B1. *BMC Infect. Dis.* **2**, 5.

Casey, J. R., Grinstein, S., and Orlowski, J. (2010). Sensors and regulators of intracellular pH. *Nat. Rev. Mol. Cell Biol.* **11**, 50-61.

Casey, P. S., Rossouw, C. J., Boskovic, S., Lawrence, K. A., and Turney, T. W. (2006). Incorporation of dopants into the lattice of ZnO nanoparticles to control photoactivity. *Superlattices Microstruct.* **39**, 97-106.

Chan, K., and Kan, Y. W. (1999). Nrf2 is essential for protection against acute pulmonary injury in mice. *Proceedings of the National Academy of Sciences of the United States of America* **96**, 12731-12736.

Cherukuri, P., Bachilo, S. M., Litovsky, S. H., Weisman, R. B. (2004). Near-Infrared fluorescence microscopy of single-walled carbon nanotubes in phagocytic cells. *J. Am. Chem. Soc.* **126**, 15638–15639.

Chevion, M. (1988). A site-specific mechanism for free radical induced biological damage: the essential role of redox-active transition metals. *Free Radic. Biol. Med.* **5**, 27-37.

Cho, H. Y., Jedlicka, A. E., Reddy, S. P., Kensler, T. W., Yamamoto, M., Zhang, L. Y., and Kleeberger, S. R. (2002). Role of NRF2 in protection against hyperoxic lung injury in mice. *Am. J. Respir. Cell Mol. Biol.* **26**, 175-82.

Cho, H. Y., Reddy, S. P., and Kleeberger, S. R. (2006). Nrf2 defends the lung from oxidative stress. *Antioxid. Redox Signaling* **8**, 76-87.

Cho, W. S., Duffin, R., Howie, S. E., Scotton, C. J., Wallace, W. A., MacNee, W., Bradley, M., Megson, I. L., and Donaldson, K. (2011). Progressive severe lung injury by zinc oxide nanoparticles; the role of Zn^{2+} dissolution inside lysosomes. *Part. Fibre Toxicol.* **8**, 27.

Cho, W. S., Duffin, R., Poland, C. A., Duschl, A., Oostingh, G. J., MacNee, W., Bradley, M., Megson, I. L., and Donaldson, K. (2012). Differential pro-inflammatory effects of metal oxide nanoparticles and their soluble ions *in vitro* and *in vivo*; zinc and copper nanoparticles, but not their ions, recruit eosinophils to the lungs. *Nanotoxicology* **6**, 22-35.

Clydesdale, G. J., Dandie, G. W., and Muller, H. K. (2001). Ultraviolet light induced injury: immunological and inflammatory effects. *Immunol. Cell Biol.* **79**, 547-568.

Colognato, R., Bonelli, A., Ponti, J., Farina, M., Bergamaschi, E., Sabbioni, E., and Migliore, L. (2008). Comparative genotoxicity of cobalt nanoparticles and ions on human peripheral leukocytes in vitro. *Mutagenesis* **23**, 377-382.

Coyle, P., Zalewski, P. D., Philcox, J. C., Forbes, I. J., Ward, A. D., Lincoln, S. F., Mahadevan, I., and Rofe, A. M. (1994). Measurement of zinc in hepatocytes by using a fluorescent probe, zinquin: relationship to metallothionein and intracellular zinc. *Biochem. J.* **303**, 781-786.

Damian, D. L., Halliday, G. M., and Barnetson, R. S. (1997). Broad-spectrum sunscreens provide greater protection against ultraviolet-radiation-induced suppression of contact hypersensitivity to a recall antigen in humans. *J. Invest. Dermatol.* **109**, 146-151.

Dang, L. H., Lien, L. L., Benacerraf, B., and Rock, K. L. (1993). A mutant antigen-presenting cell defective in antigen presentation expresses class II MHC molecules with an altered conformation. *J. Immunol.* **150**, 4206-4217.

Darzynkiewicz, Z., Bruno, S., Del Bino, G., Gorczyca, W., Hotz, M. A., Lassota, P., and Traganos, F. (1992). Features of apoptotic cells measured by flow cytometry. *Cytometry* **13**, 795-808.

David, F., Farley, J., Huang, H., Lavoie, J. P., and Laverty, S. (2007). Cytokine and chemokine gene expression of IL-1beta stimulated equine articular chondrocytes. *Vet. Surg.* **36**, 221-227.

Dawson, K. A., Salvati, A., and Lynch, I. (2009). Nanotoxicology: nanoparticles reconstruct lipids. *Nat. Nanotechnol.* **4**, 84-85.

de Gracia Lux, C., Joshi-Barr, S., Nguyen, T., Mahmoud, E., Schopf, E., Fomina, N., and Almutairi, A. (2012). Biocompatible polymeric nanoparticles degrade and release cargo in response to biologically relevant levels of hydrogen peroxide. *J. Am. Chem. Soc.* **134**, 15758-15764.

Deng, Z. J., Mortimer, G., Schiller, T., Musumeci, A., Martin, D., and Minchin, R. F. (2009). Differential plasma protein binding to metal oxide nanoparticles. *Nanotechnology* **20**, 455101.

Dhawan, A., Sharma, V., and Parmar, D. (2009). Nanomaterials: A challenge for toxicologists. *Nanotoxicology* **3**, 1-9.

Dinarello, C. A. (2000). Proinflammatory cytokines. *Chest J.* **118**, 503-508.

Dobrovolskaia, M. A., and McNeil, S. E. (2007). Immunological properties of engineered nanomaterials. *Nat. Nanotechnology* **2**, 469-78.

Donaldson, K., and Tran, C. L. (2002). Inflammation caused by particles and fibers. *Inhal. Toxicol.* **14**, 5-27.

Dowlati, Y., Herrmann, N., Swardfager, W., Liu, H., Sham, L., Reim, E. K., and Lanctot, K. L. (2010). A meta-analysis of cytokines in major depression. *Biol. Psychiatry* **67**, 446-457.

Dwivedi, P. D., Misra, A., Shanker, R., and Das, M. (2009). Are nanomaterials a threat to the immune system? *Nanotoxicology* **3**, 19-26.

FoE, Friends of the Earth. (2006). Nanomaterials, sunscreens, and cosmetics: Small ingredients, big risks. In

http://nano.foe.org.au/sites/default/files/FoEA%20nano%20cosmetics%20report%202MB.pdf, Accession date Feb. 3, 2014.

FoE, Friends of the Earth. (2013) Sunscreens Exposed: Stripping away the gloss. In http://nano.foe.org.au/sunscreens-exposed-stripping-away-gloss, Accession date Feb. 3, 2014.

Elder, A., Vidyasagar, S., and DeLouise, L. (2009). Physicochemical factors that affect metal and metal oxide nanoparticle passage across epithelial barriers. *Wiley Interdiscip. Rev. Nanomed. Nanobiotechnol.* **1**, 434-450.

Elsabahy, M., and Wooley, K. L. (2013). Cytokines as biomarkers of nanoparticle immunotoxicity. *Chem. Soc. Rev.* **42**, 5552-5276.

Euvrard, S., Kanitakis, J., and Claudy, A. (2003). Skin cancers after organ transplantation. *N. Engl. J. Med.* **348**, 1681-1691.

Feltis, B. N., O'Keefe, S. J., Harford, A. J., Piva, T. J., Turney, T. W., and Wright, P. F. (2012). Independent cytotoxic and inflammatory responses to zinc oxide nanoparticles in human monocytes and macrophages. *Nanotoxicology* **6**, 757-765.

Fosmire, G. J. (1990). Zinc toxicity. *Am. J. Clin. Nutr.* **51**, 225-227.

Furuyama, A., Kanno, S., Kobayashi, T., and Hirano, S. (2009). Extrapulmonary translocation of intratracheally instilled fine and ultrafine particles via direct and alveolar macrophage-associated routes. *Arch. Toxicol.* **83**, 429-437.

Goettsch, W., Garssen, J., Slob, W., de Gruijl, F. R., and Van Loveren, H. (1998). Risk assessment for the harmful effects of UVB radiation on the immunological resistance to infectious diseases. *Environ. Health Perspect.* **106**, 71-77.

Goodman, D. W. (2008). Chemistry: Precious little catalyst. *Nature* **454**, 948-949.

Grasset, F., Saito, N., Li, D., Park, D., Sakaguchi, I., Ohashi, N., Haneda, H., Roisnel, T., Mornet, S., and Duguet, E. (2003). Surface modification of zinc oxide nanoparticles by aminopropyltriethoxysilane. *J. Alloys Compd.* **360**, 298-311.

Gulson, B., McCall, M., Korsch, M., Gomez, L., Casey, P., Oytam, Y., Taylor, A., McCulloch, M., Trotter, J., Kinsley, L., *et al.* (2010). Small Amounts of Zinc from Zinc Oxide Particles in Sunscreens Applied Outdoors Are Absorbed through Human Skin. *Toxicol. Sci.* **118**, 140-149.

Halliday, G. M., Damian, D. L., Rana, S., and Byrne, S. N. (2012). The suppressive effects of ultraviolet radiation on immunity in the skin and internal organs: implications for autoimmunity. *J. Dermatol. Sci.* **66**, 176-182.

Halliwell, B., and Gutteridge, J. (2007). *Free Radicals in Biology and Medicine.* Oxford University Press.

Hambidge, K. M., and Krebs, N. F. (2007). Zinc deficiency: a special challenge. *J. Nutr.* **137**, 1101-1105.

Hanagata, N., Xu M., Takemura, T., Zhuang, F. (2010) Cellular Response to ZnO Nanoparticle Toxicity Inferred from Global Gene Expression Profiles. *Nano Biomed.* **2**, 153-169.

Hanley, C., Thurber, A., Hanna, C., Punnoose, A., Zhang, J., and Wingett, D. G. (2009). The Influences of Cell Type and ZnO Nanoparticle Size on Immune Cell Cytotoxicity and Cytokine Induction. *Nanoscale Res. Lett.* **4**, 1409-1420.

Hanson, K. M., Gratton, E., and Bardeen, C. J. (2006). Sunscreen enhancement of UV-induced reactive oxygen species in the skin. *Free Radic. Biol. Med.* **41**, 1205-1212.

He, Q., Zhang, J., Shi, J., Zhu, Z., Zhang, L., Bu, W., Guo, L., and Chen, Y. (2010). The effect of PEGylation of mesoporous silica nanoparticles on nonspecific binding of serum proteins and cellular responses. *Biomaterials* **31**, 1085-1092.

Hirao, Y., Kanda, T., Aso, Y., Mitsuhashi, M., and Kobayashi, I. (2000). Interleukin-8 — An Early Marker for Bacterial Infection. *Lab Medicine* **31**, 39-44.

Hiura, T. S., Li, N., Kaplan, R., Horwitz, M., Seagrave, J. C., and Nel, A. E. (2000). The role of a mitochondrial pathway in the induction of apoptosis by chemicals extracted from diesel exhaust particles. *J. Immunol.* **165**, 2703-2711.

Hu, Z. B., Ma, W., Zaborski, M., MacLeod, R., Quentmeier, H., and Drexler, H. G. (1996). Establishment and characterization of two novel cytokine-responsive acute myeloid and monocytic leukemia cell lines, MUTZ-2 and MUTZ-3. *Leukemia* **10**, 1025-1040.

Ichihashi, M., Ueda, M., Budiyanto, A., Bito, T., Oka, M., Fukunaga, M., Tsuru, K., and Horikawa, T. (2003). UV-induced skin damage. *Toxicology* **189**, 21-39.

ISO (2010). Nanotechnologies -- Model taxonomic framework for use in developing vocabularies -- Core concepts. *International Organisation for Standardisation (ISO)*.

Jackson, N., Lopata, A., Elms, T., and Wright, P. (2009). *Engineered Nanomaterials: Evidence on the effectiveness of workplace controls to prevent exposure*, Safe Work Australia, Commonwealth of Australia publication. ISBN 978-0-642-33100-7.

Jan, E., Byrne, S. J., Cuddihy, M., Davies, A. M., Volkov, Y., Gun'ko, Y. K., and Kotov, N. A. (2008). High-content screening as a universal tool for fingerprinting of cytotoxicity of nanoparticles. *ACS Nano* **2**, 928-938.

Jeevan, A., and Kripke, M. L. (1989). Effect of a single exposure to ultraviolet radiation on Mycobacterium bovis bacillus Calmette-Guerin infection in mice. *J. Immunol.* **143**, 2837-2843.

Jeevan, A., and Kripke, M. L. (1990). Alteration of the immune response to Mycobacterium bovis BCG in mice exposed chronically to low doses of UV radiation. *Cellular Immunol.* **130**, 32-41.

John, A. E., Lukacs, N. W., Berlin, A. A., Palecanda, A., Bargatze, R. F., Stoolman, L. M., and Nagy, J. O. (2003). Discovery of a potent nanoparticle P-selectin antagonist with anti-inflammatory effects in allergic airway disease. *FASEB J.* **17**, 2296-2298.

Karakoti, A. S., Das, S., Thevuthasan, S., and Seal, S. (2011). PEGylated Inorganic Nanoparticles. *Angew. Chem. Int. Ed.* **50**, 1980-1994.

Karlsson, H. L., Cronholm, P., Gustafsson, J., and Moller, L. (2008). Copper oxide nanoparticles are highly toxic: a comparison between metal oxide nanoparticles and carbon nanotubes. *Chem. Res. Toxicol.* **21**, 1726-1732.

Kawai, T., and Akira, S. (2006). Innate immune recognition of viral infection. *Nat. Immunol.* **7**, 131-137.

Kedmi, R., Ben-Arie, N., Peer, D. (2010).The systemic toxicity of positively charged lipid nanoparticles and the role of Toll-like receptor 4 in immune activation. *Biomaterials*. **31**, 6867-6875.

Kim, Y. M., Reed, W., Wu, W., Bromberg, P. A., Graves, L. M., and Samet, J. M. (2006). Zn^{2+}-induced IL-8 expression involves AP-1, JNK, and ERK activities in human airway epithelial cells. *Am. J. Physiol. Lung Cell Mol. Physiol.* **290**, 1028-1035.

Kisin, E. R., Murray, A. R., Keane, M. J., Shi, X. C., Schwegler-Berry, D., Gorelik, O., Arepalli, S., Castranova, V., Wallace, W. E., Kagan, V. E., *et al.* (2007). Single-

walled carbon nanotubes: geno- and cytotoxic effects in lung fibroblast V79 cells. *J. Toxicol. Environ. Health Part A* **70**, 2071-2079.

Kitamura, H., Morikawa, H., Kamon, H., Iguchi, M., Hojyo, S., Fukada, T., Yamashita, S., Kaisho, T., Akira, S., Murakami, M., *et al.* (2006). Toll-like receptor-mediated regulation of zinc homeostasis influences dendritic cell function. *Nat. Immunol.* **7**, 971-977.

Kocbek, P., Teskac, K., Kreft, M. E., and Kristl, J. (2010). Toxicological aspects of long-term treatment of keratinocytes with ZnO and TiO_2 nanoparticles. *Small* **6**, 1908-1917.

Kondo, S., Sauder, D. N., McKenzie, R. C., Fujisawa, H., Shivji, G. M., El-Ghorr, A., and Norval, M. (1995). The role of cis-urocanic acid in UVB-induced suppression of contact hypersensitivity. *Immunol. Lett.* **48**, 181-186.

Krezel, A., Hao, Q., and Maret, W. (2007). The zinc/thiolate redox biochemistry of metallothionein and the control of zinc ion fluctuations in cell signaling. *Arch. Biochem. Biophys.* **463**, 188-200.

Kripke, M. L., Cox, P. A., Alas, L. G., and Yarosh, D. B. (1992). Pyrimidine dimers in DNA initiate systemic immunosuppression in UV-irradiated mice. *Proceedings of the National Academy of Sciences of the United States of America* **89**, 7516-7520.

Kuchel, J. M., Barnetson, R. S. C., and Halliday, G. M. (2002). Ultraviolet a augments solar-simulated ultraviolet radiation-induced local suppression of recall responses in humans. *J. Invest. Dermatol.* **118**, 1032-1037.

Kupper, T. S., and Fuhlbrigge, R. C. (2004). Immune surveillance in the skin: mechanisms and clinical consequences. *Nat. Rev. Immunol.* **4**, 211-222.

Lam, C. W., James, J. T., McCluskey, R., and Hunter, R. L. (2004). Pulmonary toxicity of single-wall carbon nanotubes in mice 7 and 90 days after intratracheal instillation. *Toxicol. Sci.* **77**, 126-134.

Lee, J. H., Huh, Y. M., Jun, Y. W., Seo, J. W., Jang, J. T., Song, H. T., Kim, S., Cho, E. J., Yoon, H. G., Suh, J. S., *et al.* (2007a). Artificially engineered magnetic nanoparticles for ultra-sensitive molecular imaging. *Nat. Med.* **13**, 95-99.

Lee, W. A., Pernodet, N., Li, B., Lin, C. H., Hatchwell, E., and Rafailovich, M. H. (2007b). Multicomponent polymer coating to block photocatalytic activity of TiO_2 nanoparticles. *Chem. Commun.* **45**, 4815-4817.

Leitzmann, M. F., Stampfer, M. J., Wu, K., Colditz, G. A., Willett, W. C., and Giovannucci, E. L. (2003). Zinc supplement use and risk of prostate cancer. *J. Natl. Cancer Inst.* **95**, 1004-1007.

Ley, R. D., Applegate, L. A., Fry, R. J., and Sanchez, A. B. (1991). Photoreactivation of ultraviolet radiation-induced skin and eye tumors of Monodelphis domestica. *Cancer Res.* **51**, 6539-6542.

Li, N., Hao, M., Phalen, R. F., Hinds, W. C., and Nel, A. E. (2003). Particulate air pollutants and asthma. A paradigm for the role of oxidative stress in PM-induced adverse health effects. *Clin. Immunol.* **109**, 250-265.

Li, N., Kim, S., Wang, M., Froines, J., Sioutas, C., and Nel, A. (2002). Use of a stratified oxidative stress model to study the biological effects of ambient concentrated and diesel exhaust particulate matter. *Inhal. Toxicol.* **14**, 459-486.

Li, N., and Nel, A. E. (2006). Role of the Nrf2-mediated signaling pathway as a negative regulator of inflammation: implications for the impact of particulate pollutants on asthma. *Antioxid. Redox Signaling* **8**, 88-98.

Lin, W. S., Xu, Y., Huang, C. C., Ma, Y. F., Shannon, K. B., Chen, D. R., and Huang, Y. W. (2009). Toxicity of nano- and micro-sized ZnO particles in human lung epithelial cells. *J. Nanopart. Res.* **11**, 25-39.

Lindberg, H. K., Falck, G. C., Suhonen, S., Vippola, M., Vanhala, E., Catalan, J., Savolainen, K., and Norppa, H. (2009). Genotoxicity of nanomaterials: DNA damage and micronuclei induced by carbon nanotubes and graphite nanofibres in human bronchial epithelial cells *in vitro*. *Toxicol. lett.* **186**, 166-173.

Liu, H., Ma, L., Zhao, J., Liu, J., Yan, J., Ruan, J., Hong, F. (2009). Biochemical toxicity of nano-anatase TiO_2 particles in mice. *Biol. Trace. Elem. Res.* **129**,170-180.

Locksley, R. M., Killeen, N., and Lenardo, M. J. (2001). The TNF and TNF receptor superfamilies: integrating mammalian biology. *Cell* **104**, 487-501.

Lombi, E., Donner, E., Tavakkoli, E., Turney, T. W., Naidu, R., Miller, B. W., and Scheckel, K. G. (2012). Fate of Zinc Oxide Nanoparticles during Anaerobic Digestion of Wastewater and Post-Treatment Processing of Sewage Sludge. *Environ. Sci. Technol.* **46**, 9089-9096.

Lucarelli, M., A.M., G., Savarino, G., Ouattroni, P., Martinelli, L., Monari, E., and Boraschi, D. (2004). Innate defence functions of macrophages can be biased by nano-sized ceramic and metallic particles. *Eur. Cytokine Netw.* **15**, 339-346.

Lundqvist, M., Stigler, J., Elia, G., Lynch, I., Cedervall, T., and Dawson, K. A. (2008). Nanoparticle size and surface properties determine the protein corona with possible implications for biological impacts. *Proc. Natl. Acad. Sci. USA* **105**, 14265-14270.

Male, D., Brostoff, J., Roth, D., and Roitt, I. (2013). *Immunology, 8th Edition*. Elsevier. ISBN-9780323080583.

Martinez, G. R., Loureiro, A. P., Marques, S. A., Miyamoto, S., Yamaguchi, L. F., Onuki, J., Almeida, E. A., Garcia, C. C., Barbosa, L. F., Medeiros, M. H., *et al.* (2003). Oxidative and alkylating damage in DNA. *Mutat. Res.* **544**, 115-127.

Masterson, A. J., Sombroek, C. C., De Gruijl, T. D., Graus, Y. M., van der Vliet, H. J., Lougheed, S. M., van den Eertwegh, A. J., Pinedo, H. M., and Scheper, R. J. (2002). MUTZ-3, a human cell line model for the cytokine-induced differentiation of dendritic cells from CD34+ precursors. *Blood* **100**, 701-703.

Matthews, Y. J., Halliday, G. M., Phan, T. A., Damian, D .L. (2010a). Wavelength dependency for UVA-induced suppression of recall immunity in humans. *J. Dermatol. Sci*. **59**, 192-197.

Matthews Y. J., Halliday G. M., Phan T. A., Damian, D .L. (2010b). A UVB wavelength dependency for local suppression of recall immunity in humans demonstrates a peak at 300 nm. *J. Invest. Dermatol.* **130**, 1680-1684.

Merad, M., Ginhoux, F., and Collin, M. (2008). Origin, homeostasis and function of Langerhans cells and other langerin-expressing dendritic cells. *Nat. Rev. Immunol.* **8**, 935-47.

Muller, J., Decordier, I., Hoet, P. H., Lombaert, N., Thomassen, L., Huaux, F., Lison, D., and Kirsch-Volders, M. (2008). Clastogenic and aneugenic effects of multi-wall carbon nanotubes in epithelial cells. *Carcinogenesis* **29**, 427-433.

Muller, K. H., Kulkarni, J., Motskin, M., Goode, A., Winship, P., Skepper, J. N., Ryan, M. P., and Porter, A. E. (2010). pH-dependent toxicity of high aspect ratio ZnO nanowires in macrophages due to intracellular dissolution. *ACS Nano* **4**, 6767-6779.

Musatov, A., and Robinson, N. C. (2012). Susceptibility of mitochondrial electron-transport complexes to oxidative damage. Focus on cytochrome c oxidase. *Free Radical Res.* **46**, 1313-1326.

Nel, A., Xia, T., Madler, L., and Li, N. (2006). Toxic potential of materials at the nanolevel. *Science* **311**, 622-627.

Nemmar, A., Hoet, P. H. M., Vanquickenborne, B., Dinsdale, D., Thomeer, M., Hoylaerts, M. F., Vanbilloen, H., Mortelmans, L., and Nemery, B. (2002). Passage of Inhaled Particles Into the Blood Circulation in Humans. *Circulation* **105**, 411-414.

Nickoloff, B. J., and Turka, L. A. (1994). Immunological functions of non-professional antigen-presenting cells: new insights from studies of T-cell interactions with keratinocytes. *Immunol. Today* **15**, 464-469.

NNI, National Nanotechnology Initiative (2013). What is Nanotechnology. In http://www.nano.gov/nanotech-101/what/definition, Accession date Dec. 23, 2013.

Norval, M., Gibbs, N. K., and Gilmour, J. (1995). The role of urocanic acid in UV-induced immunosuppression: recent advances (1992-1994). *Photochem. Photobiol.* **62**, 209-217.

Nurkiewicz, T. R., Porter, D. W., Barger, M., Castranova, V., and Boegehold, M. A. (2004). Particulate matter exposure impairs systemic microvascular endothelium-dependent dilation. *Environ. Health Perspect.* **112**, 1299-1306.

Nurkiewicz, T. R., Porter, D. W., Barger, M., Millecchia, L., Rao, K. M., Marvar, P. J., Hubbs, A. F., Castranova, V., and Boegehold, M. A. (2006). Systemic microvascular dysfunction and inflammation after pulmonary particulate matter exposure. *Environ. Health Perspect.* **114**, 412-419.

Oberdorster, G., Ferin, J., and Lehnert, B. E. (1994). Correlation between particle size, in vivo particle persistence, and lung injury. *Environ. Health Perspect.* **102 Suppl 5**, 173-9.

Oberdorster, G., Oberdorster, E., and Oberdorster, J. (2005). Nanotoxicology: an emerging discipline evolving from studies of ultrafine particles. *Environ. Health Perspect.* **113**, 823-839.

Opal, S. M., and DePalo, V. A. (2000). Anti-inflammatory cytokines. *Chest J.* **117**, 1162-1172.

Pacurari, M., Yin, X. J., Zhao, J., Ding, M., Leonard, S. S., Schwegler-Berry, D., Ducatman, B. S., Sbarra, D., Hoover, M. D., Castranova, V., *et al.* (2008). Raw single-wall carbon nanotubes induce oxidative stress and activate MAPKs, AP-1, NF-kappaB, and Akt in normal and malignant human mesothelial cells. *Environ. Health Perspect.* **116**, 1211-1217.

Paris, C., Lhiaubet-Vallet, V., Jimenez, O., Trullas, C., and Miranda, M. A. (2009). A Blocked Diketo Form of Avobenzone: Photostability, Photosensitizing Properties and Triplet Quenching by a Triazine-derived UVB-filter. *Photochem. Photobiol.* **85**, 178-184.

Paterson, D., de Jonge, M. D., Howard, D. L., Lewis, W., McKinlay, J., Starritt, A., Kusel, M., Ryan, C. G., Kirkham, R., Moorhead, G., *et al.* (2010). The X-ray Fluorescence Microscopy Beamline at the Australian Synchrotron. In *10th International Conference on X-Ray Microscopy (XRM2010) Proceedings*. Chicago, IL, USA.

Perelshtein, I., Applerot, G., Perkas, N., Wehrschetz-Sigl, E., Hasmann, A., Guebitz, G. M., and Gedanken, A. (2009). Antibacterial Properties of an In Situ Generated and Simultaneously Deposited Nanocrystalline ZnO on Fabrics. *ACS Appl. Mater. Interfaces* **1**, 363-366.

Petrarca, C., Perrone, A., Verna, N., Verginelli, F., Ponti, J., Sabbioni, E., Di Giampaolo, L., Dadorante, V., Schiavone, C., Boscolo, P., *et al.* (2006). Cobalt nano-particles modulate cytokine in vitro release by human mononuclear cells mimicking autoimmune disease. *Int. J. Immunopathol. Pharmacol.* **19**, 11-14.

Pinnell, S. R. (2003). Cutaneous photodamage, oxidative stress, and topical antioxidant protection. *J. Am. Acad. Dermatol.* **48**, 1-19.

Pompella, A., Visvikis, A., Paolicchi, A., De Tata, V., and Casini, A. F. (2003). The changing faces of glutathione, a cellular protagonist. *Biochem. Pharm.* **66**, 1499-1503.

Prasad, A. S. (2003). Zinc deficiency. *BMJ* **326**, 409-410.

Promega (2009). *CellTiter 96® AQueous Non-Radioactive Cell Proliferation Assay Technical Bulletin*.

Puzyr, A. P., Tarskikh, S. V., Makarskaya, G. V., Chiganova, G. A., Larionova, I. S., Detkov, P. Y., and Bondar, V. S. (2002). Damaging effect of detonation diamonds on human white and red blood cells in vitro. *Dokl. Biochem. Biophys.* **385**, 201-204.

Rink, L., and Gabriel, P. (2000). Zinc and the immune system. *Proc. Nutr. Soc.* **59**, 541-552.

Rizzo-Padoin, N., Farina, A., Le Pen, C., Dute, M., Mundler, O., and Leverge, R. (2001). A comparison of radiopharmaceutical agents used for the diagnosis of pulmonary embolism. *Nuclear Medicine Communications* **22**, 375-381.

Roduner, E. (2006). Size matters: why nanomaterials are different. *Chem. Soc. Rev.* **35**, 583-592.

Romani, N., Gruner, S., Brang, D., Kampgen, E., Lenz, A., Trockenbacher, B., Konwalinka, G., Fritsch, P. O., Steinman, R. M., and Schuler, G. (1994). Proliferating dendritic cell progenitors in human blood. *J. Exp. Med.* **180**, 83-93.

Rossi, E. M., Pylkkanen, L., Koivisto, A. J., Vippola, M., Jensen, K. A., Miettinen, M., Sirola, K., Nykasenoja, H., Karisola, P., Stjernvall, T., *et al.* (2010). Airway exposure to

silica-coated TiO_2 nanoparticles induces pulmonary neutrophilia in mice. *Toxicol. Sci.* **113**, 422-433.

Sadrieh, N., Wokovich, A. M., Gopee, N. V., Zheng, J., Haines, D., Parmiter, D., Siitonen, P. H., Cozart, C. R., Patri, A. K., McNeil, S. E., *et al.* (2010). Lack of significant dermal penetration of titanium dioxide from sunscreen formulations containing nano- and submicron-size TiO_2 particles. *Toxicol. Sci.* **115**, 156-166.

Sakamoto, Y., Nakae, D., Fukumori, N., Tayama, K., Maekawa, A., Imai, K., Hirose, A., Nishimura, T., Ohashi, N., and Ogata, A. (2009). Induction of mesothelioma by a single intrascrotal administration of multi-wall carbon nanotube in intact male Fischer 344 rats. *J. Toxicol. Sci.* **34**, 65-76.

Santegoets, S. J., Masterson, A. J., van der Sluis, P. C., Lougheed, S. M., Fluitsma, D. M., van den Eertwegh, A. J., Pinedo, H. M., Scheper, R. J., and de Gruijl, T. D. (2006). A CD34(+) human cell line model of myeloid dendritic cell differentiation: evidence for a CD14(+)CD11b(+) Langerhans cell precursor. *J. Leukoc. Biol.* **80**, 1337-1344.

Sasidharan, A., Chandran, P., Menon, D., Raman, S., Nair, S., and Koyakutty, M. (2011). Rapid dissolution of ZnO nanocrystals in acidic cancer microenvironment leading to preferential apoptosis. *Nanoscale* **3**, 3657-3669.

Scharffetter-Kochanek, K., Wlaschek, M., Brenneisen, P., Schauen, M., Blaudschun, R., and Wenk, J. (1997). UV-induced reactive oxygen species in photocarcinogenesis and photoaging. *Biol. Chem.* **378**, 1247-1257.

Schrand, A. M., Huang, H., Carlson, C., Schlager, J. J., Omacr Sawa, E., Hussain, S. M., and Dai, L. (2007). Are diamond nanoparticles cytotoxic? *J. Phys. Chem. B* **111**, 2-7.

Schwarz, T. (2008). 25 years of UV-induced immunosuppression mediated by T cells-from disregarded T suppressor cells to highly respected regulatory T cells. *Photochem. Photobiol.* **84**, 10-18.

Semmler-Behnke, M., Kreyling, W. G., Lipka, J., Fertsch, S., Wenk, A., Takenaka, S., Schmid, G., and Brandau, W. (2008). Biodistribution of 1.4- and 18-nm gold particles in rats. *Small* **4**, 2108-2111.

Shaw, S. Y., Westly, E. C., Pittet, M. J., Subramanian, A., Schreiber, S. L., and Weissleder, R. (2008). Perturbational profiling of nanomaterial biologic activity. *Proc. Natl. Acad. Sci. USA* **105**, 7387-7392.

Shen, C., James, S. A., deJonge, M. D., Turney, T. W., Wright, P. F. A., and Feltis, B. N. (2013). Relating cytotoxicity, zinc ions and reactive oxygen in ZnO nanoparticle exposed human immune cells. *Toxicol Sci*. **136**, 120-130.

Shvedova, A. A., Kisin, E., Murray, A. R., Johnson, V. J., Gorelik, O., Arepalli, S., Hubbs, A. F., Mercer, R. R., Keohavong, P., Sussman, N., *et al.* (2008). Inhalation vs. aspiration of single-walled carbon nanotubes in C57BL/6 mice: inflammation, fibrosis, oxidative stress, and mutagenesis. *Am. J. Physiol. Lung Cell Mol. Physiol.* **295**, 552-565.

Shvedova, A. A., Kisin, E. R., Mercer, R., Murray, A. R., Johnson, V. J., Potapovich, A. I., Tyurina, Y. Y., Gorelik, O., Arepalli, S., Schwegler-Berry, D., *et al.* (2005). Unusual inflammatory and fibrogenic pulmonary responses to single-walled carbon nanotubes in mice. *Am. J. Physiol. Lung Cell Mol. Physiol.* **289**, 698-708.

Shvedova, A. A., Kisin, E. R., Porter, D., Schulte, P., Kagan, V. E., Fadeel, B., and Castranova, V. (2009). Mechanisms of pulmonary toxicity and medical applications of carbon nanotubes: Two faces of Janus? *Pharmacol. Ther.* **121**, 192-204.

Song, M. F., Li, Y. S., Kasai, H., and Kawai, K. (2012). Metal nanoparticle-induced micronuclei and oxidative DNA damage in mice. *J. Clin. Biochem. Nutr.* **50**, 211-216.

Song, W., Zhang, J., Guo, J., Ding, F., Li, L., and Sun, Z. (2010). Role of the dissolved zinc ion and reactive oxygen species in cytotoxicity of ZnO nanoparticles. *Toxicol. Lett.* **199**, 389-397.

Steinman, R. M. (1991). The dendritic cell system and its role in immunogenicity. *Annu. Rev. Immunol.* **9**, 271-296.

Stoimenov, P. K., Klinger, R. L., Marchin, G. L., and Klabunde, K. J. (2002). Metal oxide nanoparticles as bactericidal agents. *Langmuir* **18**, 6679-6686.

Strober, W. (2001). Trypan blue exclusion test of cell viability. *Current protocols in immunology*, Appendix 3B.

Strobl, H., Riedl, E., Scheinecker, C., Bello-Fernandez, C., Pickl, W. F., Rappersberger, K., Majdic, O., and Knapp, W. (1996). TGF-beta 1 promotes in vitro development of dendritic cells from CD34+ hemopoietic progenitors. *J. Immunol.* **157**, 1499-1507.

Surjana, D., Halliday, G. M., and Damian, D. L. (2013). Nicotinamide enhances repair of ultraviolet radiation-induced DNA damage in human keratinocytes and ex vivo skin. *Carcinogenesis* **34**, 1144-1149.

Swardfager, W., Lanctot, K., Rothenburg, L., Wong, A., Cappell, J., and Herrmann, N. (2010). A meta-analysis of cytokines in Alzheimer's disease. *Biol. Psychiatry* **68**, 930-941.

Takagi, A., Hirose, A., Nishimura, T., Fukumori, N., Ogata, A., Ohashi, N., Kitajima, S., and Kanno, J. (2008). Induction of mesothelioma in p53+/- mouse by intraperitoneal application of multi-wall carbon nanotube. *J. Tox. Sci.* **33**, 105-116.

Tian, B., Nowak, D. E., and Brasier, A. R. (2005). A TNF-induced gene expression program under oscillatory NF-kappaB control. *BMC Genomics* **6**, 137.

Tie, C., Golomb, C., Taylor, J. R., and Streilein, J. W. (1995). Suppressive and enhancing effects of ultraviolet B radiation on expression of contact hypersensitivity in man. *J. Invest. Dermatol.* **104**, 18-22.

Toews, G. B., Bergstresser, P. R., and Streilein, J. W. (1980). Epidermal Langerhans cell density determines whether contact hypersensitivity or unresponsiveness follows skin painting with DNFB. *J. Immunol.* **124**, 445-453.

Toyokuni, S. (1998). Oxidative stress and cancer: the role of redox regulation. *Biotherapy* **11**, 147-154.

Tran, D. T., and Salmon, R. (2011). Potential photocarcinogenic effects of nanoparticle sunscreens. *Australas J. Dermatol.* **52**, 1-6.

Truong-Tran, A. Q., Carter, J., Ruffin, R. E., and Zalewski, P. D. (2001). The role of zinc in caspase activation and apoptotic cell death. *Biometals* **14**, 315-330.

Turney, T. W., Duriska, M. B., Jayaratne, V. N., Elbaz, A., O'Keefe, S. J., Hastings, A. S., Piva, T. J., Wright, P., and Feltis, B. N. (2012). Formation of Zinc-Containing Nanoparticles from Zn^{2+} Ions in Cell Culture Media: Implications for the Nanotoxicology of ZnO. *Chem. Res. Toxicol.* **25**, 2057-2066.

Ullrich, S. E. (2005). Mechanisms underlying UV-induced immune suppression. *Mutat. Res.* **571**, 185-205.

Unfried, K., Albrecht, C., Klotz, L. Mikecz, A. V., Grether-Beck S., Schins, R. P. F. (2007). Cellular responses to nanoparticles: Target structures and mechanisms. *Nanotoxicology*. **1**, 52-71.

United Nations Environment Programme, E. E. A. P., Andrady, A. L., Aucamp, P. J., Austin, A. T., Bais, A. F., Ballare, C. L., Bjorn, L. O., Bornman, J. F., Caldwell, M., Cullen, A. P., *et al.* (2012). Environmental effects of ozone depletion and its interactions with climate change: progress report, 2011. *Photochem. Photobiol. Sci.* **11**, 13-27.

van der Mei, I. A., Ponsonby, A. L., Engelsen, O., Pasco, J. A., McGrath, J. J., Eyles, D. W., Blizzard, L., Dwyer, T., Lucas, R., and Jones, G. (2007). The high prevalence of vitamin D insufficiency across Australian populations is only partly explained by season and latitude. *Environ. Health Perspect* **115**, 1132-1139.

Vevers, W. F., and Jha, A. N. (2008). Genotoxic and cytotoxic potential of titanium dioxide (TiO_2) nanoparticles on fish cells in vitro. *Ecotoxicol.* **17**, 410-420.

Vlahopoulos, S., Boldogh, I., Casola, A., and Brasier, A. R. (1999). Nuclear factor-kappaB-dependent induction of interleukin-8 gene expression by tumor necrosis factor alpha: evidence for an antioxidant sensitive activating pathway distinct from nuclear translocation. *Blood* **94**, 1878-1889.

Vogt, S. (2003). MAPS: A set of software tools for analysis and visualization of 3D X-ray fluorescence data sets. *J. Phys. IV France* **104**, 635-638.

Waiblinger, F., Keck, J., Stein, M., Fluegge, A. P., Kramer, H. E. A., Leppard, David. (2000). Light-Induced Opening of the Intramolecular Hydrogen Bond of UV Absorbers of the 2-(2-Hydroxyphenyl)-1,3,5-triazine and the 2-(2-Hydroxyphenyl)benzotriazole Type. *J. Phys. Chem. A.* **104**, 1100–1106.

Wakefield, G., Lipscomb, S., Holland, E., and Knowland, J. (2004). The effects of manganese doping on UVA absorption and free radical generation of micronised titanium dioxide and its consequences for the photostability of UVA absorbing organic sunscreen components. *Photochem. Photobiol. Sci.* **3**, 648-652.

Wang, J. J., Sanderson, B. J., and Wang, H. (2007). Cytotoxicity and genotoxicity of ultrafine crystalline SiO2 particulate in cultured human lymphoblastoid cells. *Environ. Mol. Mutagen.* **48**, 151-157.

Wapnir, R. A. (1990). *Protein nutrition and mineral absorption*. CRC Press, Boca Raton, FL, USA.

Webster, N., and Galley, H. (2003). Inflammation and immunity. *BJA CEPD Rev.* **3**, 54-58.

Xia, T., Korge, P., Weiss, J. N., Li, N., Venkatesen, M. I., Sioutas, C., and Nel, A. (2004). Quinones and aromatic chemical compounds in particulate matter induce mitochondrial dysfunction: implications for ultrafine particle toxicity. *Environ. Health Perspect* **112**, 1347-1358.

Xia, T., Kovochich, M., Brant, J., Hotze, M., Sempf, J., Oberley, T., Sioutas, C., Yeh, J. I., Wiesner, M. R., and Nel, A. E. (2006). Comparison of the abilities of ambient and manufactured nanoparticles to induce cellular toxicity according to an oxidative stress paradigm. *Nano Lett.* **6**, 1794-1807.

Xia, T., Kovochich, M., Liong, M., Madler, L., Gilbert, B., Shi, H., Yeh, J. I., Zink, J. I., and Nel, A. E. (2008). Comparison of the mechanism of toxicity of zinc oxide and cerium oxide nanoparticles based on dissolution and oxidative stress properties. *ACS Nano* **2**, 2121-2134.

Xia, T., Zhao, Y., Sager, T., George, S., Pokhrel, S., Li, N., Schoenfeld, D., Meng, H., Lin, S., Wang, X., *et al.* (2011). Decreased dissolution of ZnO by iron doping yields nanoparticles with reduced toxicity in the rodent lung and zebrafish embryos. *ACS Nano* **5**, 1223-1235.

Xiao, B. G., Huang, Y. M., and Link, H. (2006). Tolerogenic dendritic cells: the ins and outs of outcome. *J. Immunother.* **29**, 465-471.

Xiao, G. G., Wang, M., Li, N., Loo, J. A., and Nel, A. E. (2003). Use of proteomics to demonstrate a hierarchical oxidative stress response to diesel exhaust particle chemicals in a macrophage cell line. *J. Biol. Chem.* **278**, 50781-5090.

Youn, J., Lynes, M. A. (1999). Metallothionein-induced suppression of cytotoxic T lymphocyte function: an important immunoregulatory control. *Toxicol. Sci.* **52**, 199-208.

Zak, A. K., Razali, R., Majid, W. H., and Darroudi, M. (2011). Synthesis and characterization of a narrow size distribution of zinc oxide nanoparticles. *Int. J. Nanomed.* **6**, 1399-1403.

Zhang, L., Gu, F. X., Chan, J. M., Wang, A. Z., Langer, R. S., and Farokhzad, O. C. (2008a). Nanoparticles in medicine: therapeutic applications and developments. *Clin. Pharmacol. Ther.* **83**, 761-769.

Zhang, L. W., Yu, W. W., Colvin, V. L., and Monteiro-Riviere, N. A. (2008b). Biological interactions of quantum dot nanoparticles in skin and in human epidermal keratinocytes. *Toxicol. Appl. Pharmacol.* **228**, 200-211.

Zhou, J., Xu, N. S., and Wang, Z. L. (2006). Dissolving behavior and stability of ZnO wires in biofluids: A study on biodegradability and biocompatibility of ZnO nanostructures. *Adv. Mater.* **18**, 2432-2435.

Zhu, L., Chang, D. W., Dai, L., and Hong, Y. (2007). DNA damage induced by multiwalled carbon nanotubes in mouse embryonic stem cells. *Nano Lett.* **7**, 3592-3597.

Zolnik, B. S., González-Fernández, A., Sadrieh, N., Dobrovolskaia M. A. (2010). Nanoparticles and the Immune System. *Endocrinol.* **151**, 458-465.

Zvyagin, A. V., Zhao, X., Gierden, A., Sanchez, W., Ross, J. A., and Roberts, M. S. (2008). Imaging of zinc oxide nanoparticle penetration in human skin *in vitro* and *in vivo*. *J. Biomed. Opt.* **13**, 064031.